Cytoplasmic CPSF6 and Cyclophilin A Modulate HIV-1 Trafficking

by

Zhou Zhong

BS, University of Wisconsin Madison, 2012

Submitted to the Graduate Faculty of the

School of Medicine in partial fulfillment

of the requirements for the degree of

Doctor of Medicine

University of Pittsburgh

2020

UNIVERSITY OF PITTSBURGH

SCHOOL OF MEDICINE

This dissertation was presented

by

Zhou Zhong

It was defended on

October 7, 2020

and approved by

Alan N. Engelman, PhD, Professor; Department of Cancer Immunology and Virology, Dana-Farber Cancer Institute

Paul R. Kinchington, PhD, Professor; Department of Ophthalmology and Molecular Microbiology and Genetics, University of Pittsburgh School of Medicine

Nicolas Sluis-Cremer, PhD, Professor; Division of Infectious Diseases, Department of Medicine, University of Pittsburgh School of Medicine

Simon C. Watkins, PhD, Distinguished Professor; Department of Cell Biology, University of Pittsburgh School of Medicine

Dissertation Director: Zandrea Ambrose, PhD, Associate Professor; Department of Microbiology and Molecular Genetics, University of Pittsburgh School of Medicine

CYTOPLASMIC CPSF6 AND CYCLOPHILIN A MODOULATE HIV-1 TRAFFICKING

Zhou Zhong, PhD

University of Pittsburgh, 2020

Human immunodeficiency virus type 1 (HIV-1) capsid binds to multiple host cell proteins after entry into a cell, including cyclophilin A (CypA) and cleavage and polyadenylation specificity factor 6 (CPSF6), which is expressed predominantly in the nucleus. As CPSF6 expression was observed in the cytoplasm, we examined the effect of CPSF6 on HIV-1 capsid and nucleic acid trafficking in the cytoplasm of HeLa cells and primary macrophages. High-speed live-cell microscopy was performed with fluorescently labeled wild-type (WT) HIV-1 and capsid (CA) mutants and cells expressing labeled CPSF6. Imaging data were complimented with infectivity assays in HeLa cells, primary CD4+ T lymphocytes, and primary macrophages and in vitro binding assays with CA tubular assemblies and purified full-length CPSF6 protein and CypA. In cells, CPSF6 forms higher order complexes in the cytoplasm upon infection with WT HIV-1 but not N74D HIV-1, which does not bind to CPSF6. CPSF6 complexes associate with WT HIV-1 capsid and traffic on microtubules. Full-length CPSF6 protein and CPSF6 lacking the R/S domain (CPSF6-358) form higher order complexes that bind to and disrupt WT CA assemblies but not N74D CA assemblies in vitro. CPSF6-capsid complex trafficking can be altered by mutations in HIV-1 CA (e.g. N74D) or mutations in or truncation of the C-terminus of CPSF6 (e.g. CPSF6-358), which is associated with decreased HIV-1 infection. In addition, disruption of HIV-1 capsid binding to CypA (e.g. cyclosporine A treatment or G89V mutation in CA) leads to increased CPSF6 binding to capsid in vivo and in vitro and altered capsid trafficking in HeLa cells and macrophages, resulting in reduced infectivity. Altered trafficking and reduced infectivity due to

capsid-CypA perturbation can be partially restored by depletion of CPSF6 in HeLa cells but not in macrophages. Our data suggest that both CPSF6 and CypA are important for proper HIV-1 cytoplasmic capsid trafficking and infection. We propose that CypA prevents HIV-1 capsid from premature binding to cytoplasmic CPSF6. Differences in CypA cellular localization and type I interferon responses may explain cell-specific variations in HIV-1 capsid trafficking and uncoating as well as subsequent infectivity.

Table of Contents

List of Figures

Preface

Throughout the work of my thesis dissertation, I have received a great deal of support and assistance from many people.

I would first like to thank my supervisor, Dr. Zandrea Ambrose, whose patience, expertise, and guidance are invaluable to me. Her insightful and critical feedback pushed me to sharpen my thinking and brought my scientific work to a higher level. Her support as a mentor allows me to explore the world of science freely and grow as a scientist confidently.

I would also like to acknowledge my dissertation committee members, who kindly offered me priceless feedback and advice. Without them, I certainly could not get this far. Particularly, Dr. Simon Watkins kindly provided me the opportunity to attend the Quantitative Fluorescent Imaging training at MDI Biological Laboratory and opened the door of biological imaging for me.

Next, I am grateful to the past and present members of the Ambrose Lab: Emerson Boggs, Douglas Fischer, Christopher Kline, Isabel Miller, and Chandra Roy. Outside the Ambrose Lab, I would like to thank Mike Calderon, Greg Gibson, Sizun Jiang, Jiying Ning, Stephanie Mutchler, Callen Wallace, and Yinzhou Zhu, who helped me tremendously in my experiments, coursework, and related projects. I would also like to acknowledge the amazing staff members in the Center for Biologic Imaging, who kindly provided me training, expertise, and help for my projects.

Last but not least, I would like to thank my wife, Ruiqi Pu. Without her conditional support and love, it would never be possible for me to complete this journey.

1.0 Chapter 1: Introduction

1.1 HIV-1 Pathogenesis and Human Health

1.1.1 Retroviruses and HIV-1

Before the discovery of retroviruses and the mechanism of reverse transcription, there was a unidirectional central dogma of biological information flow: genetic information encoded in DNA was transcribed to RNA, and the RNA was then translated into protein. This central dogma stood as the "gold standard" for years due to the limitation of model systems and available tools at the time [1]. It was not until the discovery of reverse transcriptase, a retroviral enzyme that catalyzes the "reverse" flow of the genetic information from RNA to DNA, demonstrated that genetic information flow was not unidirectional [2,3]. A retrovirus is an RNA virus that is able to produce viral DNA from RNA by reverse transcription during infection of host cells. Thus, this RNA-to-DNA pattern leads to the name retro (backward).

With the continuous development of biological tools, such as culturing of CD4+ T lymphocytes and detection of RT in the 1970s [2,4–6], human retroviruses were discovered. Two human T-lymphotropic viruses (HTLV-I and HTLV-2) were isolated from cutaneous T cell lymphoma patients and hairy cell T-cell leukemia patients, respectively [7–9]. HTLV-1 has been implicated in aggressive adult T-cell lymphoma (ATL), HTLV-I-associated myelopathy, uveitis, and *Strongyloides stercoralis* hyper-infection [10]. HTLV-2 shares approximately 70% genomic homology [11]. However, HTLV-2 infection generally causes no signs or symptoms [12]. The

discovery of HTLV-1 and HTLV-2 along with the developments in biological tools laid the foundation for the subsequent discovery of human immunodeficiency virus (HIV).

In June 1981, five young homosexual men in Los Angeles contracted *Pneumocystis* pneumonia (PCP), an infection that is normally limited to severely immunosuppressed individuals [13]. These patients showed abnormally low blood CD4+ T cell counts and decreased *in vitro* lymphocyte proliferation responses [13]. Soon after this report, another group documented 26 homosexual male patients with PCP or Kaposi sarcoma (KS), a rare disease normally found in immunosuppressed individuals or in older men of Mediterranean or Middle Eastern descent [14]. In response, the U.S. Centers for Disease Control and Prevention (CDC) formed a task force to investigate this new disease. In 1982, the CDC published their first report, documenting 159 cases with PCP, KS, and other opportunistic infections [15]. Later that year, the CDC issued an update of a new illness, describing an acquired immunodeficiency disease associated with defects in cellular immunity and the occurrence of opportunistic infections or malignant neoplasms, which they termed acquired immunodeficiency syndrome (AIDS) [16]. Two years later, a new human retrovirus was successfully isolated from a 33-year-old homosexual French individual with symptoms that preceded AIDS, which was named lymphadenopathy-associated virus (LAV), HTLV-3, or AIDS-related virus (ARV) [17,18], now known as HIV [19,20].

HIV was shown to be the causative agent of AIDS [18]. Primarily, HIV type 1 (HIV-1), which originated from multiple zoonotic transmissions from wild chimpanzees (*Pan troglodytes troglodytes*) or gorillas (*Gorilla gorilla gorilla)* infected with simian immunodeficiency viruses (SIV) to humans in west-central Africa, contributes to the majority of human infections today [21–26]. HIV type 2 (HIV-2) originated from the transmission of SIV infecting sooty mangabeys to humans and is less prevalent and less pathogenic compared to HIV-1 [27,28].

1.1.2 HIV-1 Pathogenesis

It was estimated that 38 million people worldwide were living with HIV-1 in 2019 [29]. Of these, 36.2 million were adults and 1.8 million were children less than 15 years old [29]. Although AIDS-related deaths have reduced by 60% to 690,000 since 2004, an estimated 1.7 million individuals became newly infected in 2019 [29], which is still alarming.

HIV-1 transmission usually occurs from exposure to infectious bodily fluids containing virus, such as blood, breast milk, or sexual fluids [17,18,21]. There is a brief period upon exposure, called the eclipse phase, lasting 1 – 2 weeks, in which infected individuals do not experience many symptoms. During this time, the virus replicates at the site of initial exposure and starts to spread to the lymphatic system [30,31]. As the virus continues to replicate and disseminate, an infected individual starts to experience flu-like symptoms, such as fever, headache, joint pain, and rash [32,33]. While infected individuals mount an adaptive immune response against HIV-1, detection of neutralizing antibodies does not occur until at least three months after infection [34]. This is followed by the systematic spread of HIV-1, leading to chronic immune activation and the rapid depletion of CD4+ T cells [35–40]. When CD4+ T cells drop to 200 cells/μl or less (healthy individuals typically have 500-1500 cells/μl), an HIV-infected individual is diagnosed with AIDS [38]. People with AIDS have limited immune responses to most opportunistic infections, which lead to high morbidity and mortality. In the absence of therapeutic intervention, the average survival rate of individuals with AIDS is 18% in 6 years, in comparison to 78% for individuals on antiretroviral therapy [41].

1.1.3 Current Treatment

When left untreated, HIV-1 replicates in the body and causes damage to the immune system, eventually leading to AIDS. The treatment for HIV-1 is called antiretroviral therapy (ART) and consists of a combination of HIV medications, usually 3 drugs from at least 2 different classes. There are multiple enzymatic processes and host-viral interactions that occur during HIV-1 replication (discussed in more detail in Section 1.2). Disruption of any of these processes or interactions can lead to inhibition or potent restriction of viral replication. As HIV-1 contains multiple essential enzymes required for infection, most antiretroviral drugs target these viral proteins to avoid interference of host processes or enzymes (Figure 1).

Most of the first antiretroviral drugs inhibited reverse transcription. Nucleoside/nucleotide reverse transcriptase inhibitors (NRTIs) were the first class of drugs used against HIV-1 infection [42–44]. NRTIs, by mimicking a nucleotide but missing a 3'-hydroxyl group on the 2'-deoxyribosyl sugar to form 3'-5'-phosphodiester bond with subsequent dNTP, compete with dNTPs for incorporation into the reverse transcribed DNA and act as chain terminators [45]. Non-nucleoside reverse transcriptase inhibitors (NNRTIs) also target HIV-1 reverse transcription, but they bind to RT in a hydrophobic pocket, known as NNRTI-binding pocket, adjacent to the catalytic active site of the enzyme, resulting in a conformational change and inhibition of RT activity [42,46]

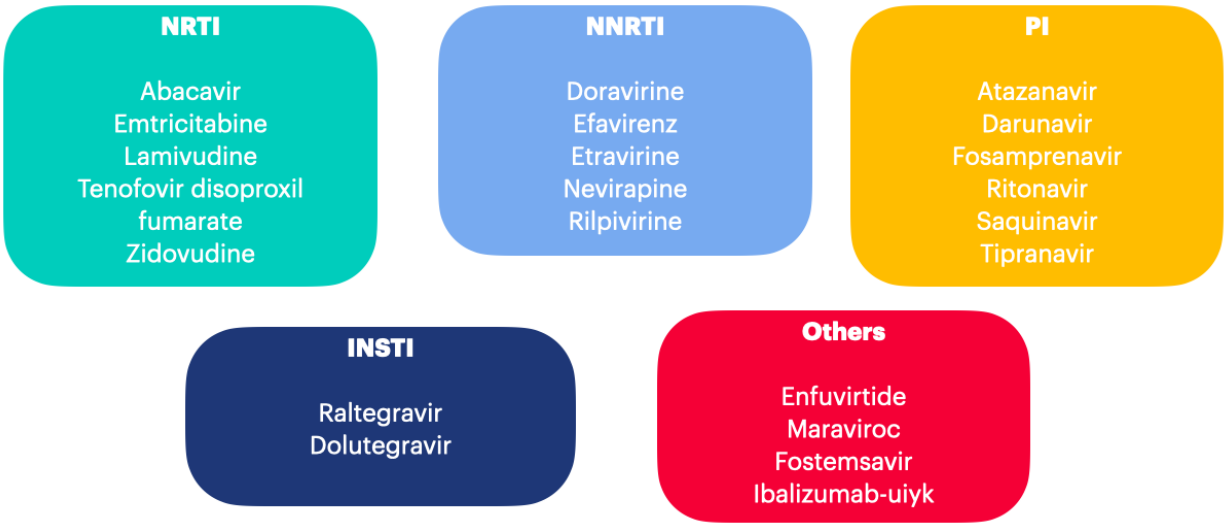

Figure 1. Current FDA-approved drugs in use to target HIV-1 replication: Nucleoside/nucleotide reverse transcriptase inhibitors (NRTIs), non-nucleoside reverse transcriptase inhibitors (NNRTIs), protease inhibitors (PIs), integrase strand transfer inhibitors (INSTIs), fusion inhibitor (Enfuvirtide), CCR5 antagonist (Maraviroc), attachment inhibitor (Fostemsavir), and post-attachment inhibitor (Ibalizumab-uiyk).

Protease inhibitors (PIs) were developed to target the catalytic domain of viral protease (PR) and prevent viral Gag and Gag-Pol polyprotein cleavage, which is necessary for HIV-1 maturation [47]. Most PIs directly interact with catalytic aspartic acid residues of HIV-1 PR [48,49]. These drugs act on the late stage of HIV-1 infection after reverse transcription and integration occur (described in more detail in Section 1.2 below).

Integrase strand transfer inhibitors (INSTIs) are a newer class of drugs that target one of the essential viral enzymes, integrase (IN), to prevent infection (described in more detail in Section 1.2.4.3) [50,51]. INSTIs bind to HIV-1 IN to prevent the strand transfer of viral DNA into host chromosomes [50,52]. Due to the potency and tolerability of INSTIs, they are recommended as first-line HIV-1 therapy in combination with two NRTIs in the U.S. [48].

Other FDA approved drugs in use include fusion inhibitor (enfuvirtide), CCR5 antagonist (maraviroc), attachment inhibitor (fostemsavir), and post-attachment inhibitor (ibalizumab-uiyk).

Although multiple classes of antiretrovirals are available, it is worth noting that HIV-1 can generate drug-resistant mutations quickly due to its intrinsic high rate of mutagenesis [53] and/or if an infected individual does not adhere to an ART regimen [54]. In addition, replicating HIV-1 in a population exists as a quasi-species, a "swarm" of viruses that are genetically diverse but collectively behave as a single species [55]. Therefore, treatment failure can result from preexisting resistant viral populations [53]. In addition, poor adherence to regimens or transmission of drug-resistant strains also contributes to treatment failure [56]. To make the situation worse, some drug resistance mutations can lead to cross-resistance to multiple drugs, sometimes leading to resistance to multiple inhibitors in the same class [46], requiring switching to a regimen with a different class of drugs. Therefore, there is a great need to understand the biology of HIV-1 better to develop new drugs.

ART is administered to HIV-1 positive individuals to inhibit virus replication. An ART regimen consists of two or more classes of drugs targeting at least two different viral molecules to create a much higher mutational barrier for developing drug resistance mutations [57]. Currently, the standard ART regimen is a combination of two nucleoside reverse transcriptase inhibitors plus one NNRTI, PI, or INSTI [58].

1.2 HIV-1 General Biology

1.2.1 HIV-1 Genome Structure

HIV-1 contains two copies of the 9.1 kb genomic RNA (gRNA) in each virion (Figure 2) [59,60]. The 5' end of the gRNA is composed of R and U5 elements and the 3' end is consisted of U3 and R elements. These elements are important for transcription and reverse transcription [61–65]. The gRNA also encodes three genes that are consistent in most retroviruses: *gag*, *pol*, and *env*. Translation of HIV-1 *env* results in the production of gp160, the precursor glycoprotein of the post-cleavage products gp120 (the surface subunit) and gp41 (the transmembrane subunit) together which form surface heterotrimers on the virus membrane that bind to the receptor CD4 discussed below in Section 1.2.3.1 [66,67]. Gag-Pol is translated by a ribosomal shift to the -1 reading frame at the 3' site of the *gag* open reading frame. This leads to the production of the Gag and Gag-Pol polyproteins at a ratio of 20:1 [68]. Gag-Pol and Gag polyproteins assemble with gp160 and other viral proteins at the cell membrane. After HIV-1 buds from the cell membrane, PR cleaves Gag into p17 matrix (MA), p24 capsid (CA), p7 nucleocapsid (NC), and p6 [69] and Gag-Pol into the same products plus enzymes RT, IN, and PR [47,49,70], in a process known as proteolysis. HIV-1 maturation leads to a morphological change of Gag from a spherical shape to a conical core consisting of CA (Figure 3) [71–73]. The gRNA contains sequences that are important for replication, such as the primer binding site (PBS), a packaging signal (Psi, ψ), the Rev response element (RRE), and a polypurine tract (PPT) [74,75].

Compared to simple retroviruses, the HIV-1 genome also encodes accessory proteins for optimal replication in host cells (Figure 2). These accessory proteins include virion infectivity factor (Vif), virus protein R (Vpr), virus protein U (Vpu), and negative regulatory factor (Nef)[76–

[79], which are mainly involved *in vivo* pathogenesis. In addition, trans-activator of transcription (Tat) and regulator of virion (Rev) are also encoded for efficient viral protein expression and viral RNA export, respectively [76,80,81]. Their functions will be further discussed in Section 1.2.3 and Section 1.2.4.

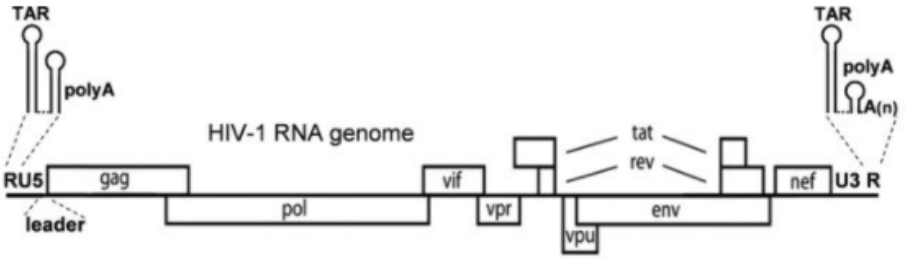

Figure 2 Structure of the HIV-1 genome. Adapted from [82] with permission from Oxford University Press.

1.2.2 HIV-1 Structure

A mature HIV-1 virion consists of an outer spherical lipid bilayer and an inner conical-shaped core (Figure 3). The outer lipid bilayer is derived from the host cell membrane with viral Env glycoprotein (gp120 and gp41 heterotrimers) on the surface. The inner membrane portion of gp41 is anchored with MA [83]. The conical-shaped core, known as the capsid, is made of roughly 1,200 copies of CA protein that form hexamers and pentamers [73]. Within the capsid, two copies of positive-sense gRNA are bound with NC, along with RT, IN, and host proteins [84,85]. The conical-shaped core is crucial for viral infectivity, as mutations in CA may result in aberrant capsid formation, leading to immature virus particles or eccentric cores and reduced infectivity[86,87].

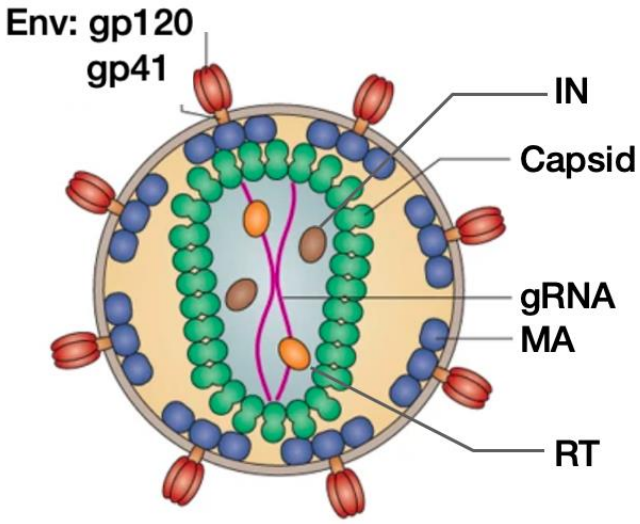

Figure 3 Illustration of HIV-1 virion. Adapted from [102], with permission from Springer Nature.

1.2.3 HIV-1 Infection of Cells

HIV-1 infection is a multiple-step process that requires an orchestra of viral enzymatic activities and interactions with host proteins.

1.2.3.1 HIV-1 Entry

As an enveloped virus, HIV-1 infects target cells by fusion after HIV-1 gp120 on the virus binds to the cell surface CD4 receptor [66,67]. HIV-1 Env is a trimeric heterodimer composed of gp120 and gp41 subunits. After binding to CD4, HIV-1 gp120 undergoes a conformational change that allows the recruitment of the co-receptors (CCR5 for macrophage-tropic or CXCR4 for T cell-tropic). This leads to the subsequent conformational change of gp41 to initiate fusion by bringing the membrane between HIV-1 envelope and the target cell membrane together [67]. Then gp41 extends the transmembrane peptide from the viral membrane into the target cell membrane to complete fusion.

1.2.3.2 Reverse Transcription and Capsid Uncoating

The functional HIV-1 RT enzyme is a heterodimer made of p66 and p51 subunits. The p51 subunit is a cleaved product of the p66 molecule that lacks the C-terminal ribonuclease H (RNase H) domain [43,88,89]. Viral DNA synthesis starts with a primer, tRNALys3 packaged from the cell, binding to the gRNA template at the PBS [90]. DNA synthesis proceeds for a short distance towards the 5'end of gRNA, where the first strand transfer occurs and in which RT translocates to the 3' end of the gRNA [70]. After the first strand transfer, DNA synthesis continues, while RNase H from the p66 subunit degrades the RNA template intermittently, leaving several short RNA fragments on the newly synthesized DNA, specifically at two polypurine tracts (PPTs) located in the central (cPPT) and 3' (3'PPT) portions of the genome [70]. These RNA fragments serve as primers for the synthesis of the complementary DNA strand [90]. Further DNA synthesis in the complementary strand leads to the second strand transfer and completion of reverse transcription [90].

Reverse transcription can initiate after the formation of mature virion [91,92]. However, due to the limited pool of dNTPs inside the virion, reverse transcription will not complete until after infection of a cell [90,93]. Reverse transcription continues to proceed after virus entry, forming the reverse transcription complex (RTC), and viral DNA can be detected within hours of infection [94]. The rate of DNA synthesis varies depending on the target cell type [95,96]. For instance, reverse transcription in macrophages, which have lower cytosolic dNTP pools, is much slower compared to CD4+ T cells [97].

HIV-1 CA, the capsid protein monomer, consists of two independently folded domains, the N terminal domain (NTD), comprising seven α-helices and a β-hairpin, and the C terminal domain (CTD), comprising four α-helices connected with a flexible linker [73,85,98]. Upon virus maturation, HIV-1 CA is cleaved from Gag. Cleaved CA multimerizes into hexameric or

pentameric forms *in vitro* (Figures 4A and 4B) [99]. The original estimation of the virus capsid was that it contained approximately 1,500 CA molecules [71]. Higher-resolution structures and structural modeling updated the number to be approximately 1,200 CA molecules [73]. Together the 216 hexamers and 12 pentamers form the capsid with a size of 119 x 60 nm (Figure 4C) [73,85,98]. The location of the pentamers dictates the overall shape of the core [73]. Five pentamers are located at one end and seven at the other end, resulting in the asymmetrical cone-shaped HIV-1 capsid [73]. It has been shown that some cellular components can facilitate the formation of the hexamers. For example, inositol hexakisphosphate (IP6), a highly negatively-charged compound present in all mammalian cells at concentrations of 10–40 μM without well-defined physiological functions, has been shown to promote the formation of hexamers [99,100].

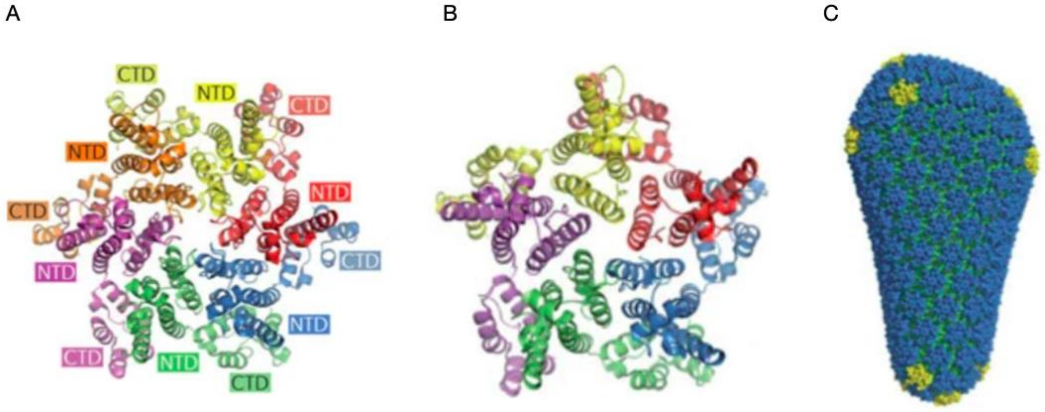

Figure 4 HIV-1 Capsid Structure. A. The crystal structure of the hexameric full-length HIV-1 capsid (CA) protein assembly (Protein Data Bank, PDB 3H47). B. The crystal structure of the pentameric full-length HIV-1 CA assembly (PDB 3P05). C. The model view for the complete HIV-1 capsid based on crystal structures. NTDs of the hexameric and pentameric CA units are shown in blue and yellow, respectively, and CTDs are shown in green. Adapted from [101] with permission from Springer Nature.

It has been demonstrated that reverse transcription is coupled with a process called capsid uncoating, a controlled disassembly of viral CA from capsid [94,102]. However, the mechanism of

capsid uncoating remains controversial in the field. There are several proposed uncoating models: 1) rapid dissociation of CA molecules from the capsid in the cytoplasm (Figure 5A) [103–106]; 2) continuous loss of CA while capsid traffics towards the nucleus (Figure 5B) [107,108]; 3) CA molecules remain associated with the RTC and capsid dissociates at the nuclear pore complex (Figure 5C) [105], and 4) the majority of CA remains associated with the RTC in the cytoplasm and capsid dissociates after nuclear import (Figure 5D) [109,110].

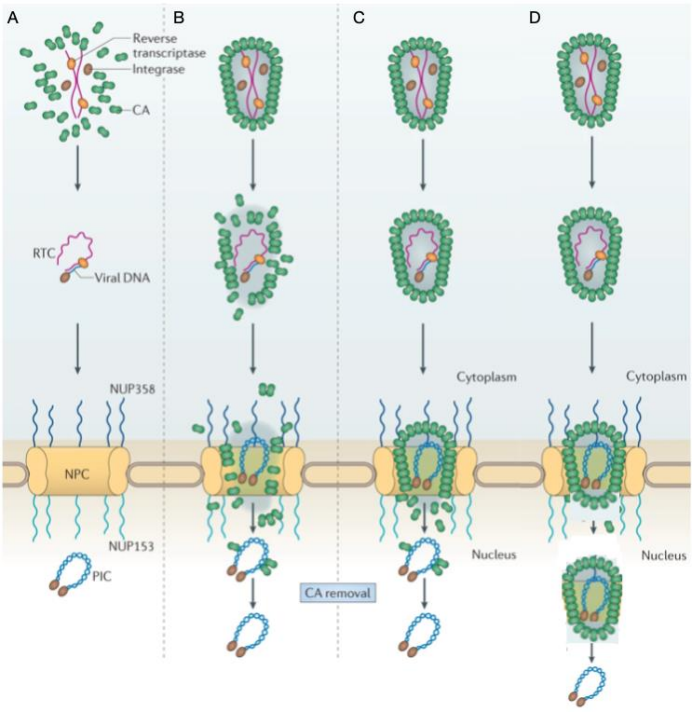

Figure 5 Schematic of different uncoating models. Adapted from [102] with permission from Springer Nature.

The uncoating of HIV-1 capsid can be affected by multiple factors. CA mutations can directly affect the stability of capsid, which can lead to a hyperstable or a hypostable capsid and reduced infectivity [111]. While it was previously thought that HIV-1 capsid uncoating and reverse transcription initiated in the cytoplasm, recently it has been proposed that newly synthesized double-stranded viral DNA is more rigid than the single-stranded RNA genome, which leads to an

increase of pressure inside the capsid during reverse transcription [112–114]. The size of the capsid is estimated to be ~60nm in diameter, which is too large to pass through the nuclear pore complex [72,85]. However, recent studies demonstrated that reverse transcription completes in the nucleus and uncoating may also occur in the nucleus [106,109,110]. Moreover, capsid interaction with host cell factors can also affect its stability. Some of these host factors, such as TRIM5α and cleavage and polyadenylation specificity factor 6 (CPSF6), can destabilize capsid, whereas others such as cyclophilin A (CypA), may stabilize the capsid [115–118]. The interaction between host factors and the stability of HIV-1 capsid is still actively investigated.

1.2.3.3 Nuclear Import and Integration

Some retroviruses, such as murine leukemia virus (MLV), require cell division and the dissolution of the nuclear membrane during cell division for successful infection [119]. In contrast, lentiviruses, including HIV-1, can integrate into host chromatin in both dividing and non-dividing cells due to its ability to hijack host factors for active nuclear import [120–122]. This ability to infect non-dividing cells, such as resting CD4+ T cells and terminally differentiated macrophages, has been proposed to be a major contribution of the HIV-1 reservoir, as these cell types have a much longer half-life compared to activated CD4+ T cells [123].

It was previously proposed that HIV-1 viral components, such as the DNA flap (a triple stranded HIV cDNA intermediate of reverse transcription), Vpr, MA, and IN, contain nuclear localization signals (NLSs) and drive nuclear import[124–131]. However, subsequent studies have refuted these models [125,132–137]and demonstrated that CA is the primary determinant for HIV-1 nuclear import to infect non-dividing cells [119,138]. In 2008, several RNA interference screens identified multiple nucleoporins (Nups), such as Nup358 (or RANBP2) and Nup153 [120–122], that were shown subsequently to play important roles in HIV-1 nuclear import [139,140]. Meanwhile,

transportin-3 (TNPO3) depletion experiments have shown TNPO3 to be crucial for HIV-1 nuclear import [120]. Subsequently, expression of a truncated form of CPSF6 (CPSF6-358) was demonstrated to potently restrict HIV-1 at the step of nuclear import [141,142]. Later, it was shown that CPSF6-358 blocks HIV-1 due to the truncation of its C terminal arginine/serine-rich (R/S) domain, which is needed for its interaction with TNPO3 for nuclear import [143–145]. The dependency on these host factors has been mapped to CA, specifically to a binding pocket defined by helix 4 on one side and by helices 3 and 5, and the helix 5/6 turn on the other side [144]. A CPSF6 peptide containing the CA binding motif can directly interact with CA at this pocket [144]. CA mutations in this binding pocket, such as N74D (most commonly used in the field and mainly used in this thesis study), A105T, N57A/S, A77V, R132K/L136M, M66F, Q67A, K70A, and/or T107A, render HIV-1 less sensitive or insensitive to depletion of Nup358, Nup153 and TNPO3 and restriction by CPSF6-358 [144,146,147].

Following successful nuclear import, HIV-1 IN catalyzes the integration of the viral DNA genome into the host genome, called the provirus [148]. Initially, a terminal dinucleotide from each end of the cDNA is removed (3′ processing) by IN [149]. Then the viral DNA is inserted into host chromosome DNA (strand transfer) catalyzed by IN [150]. Later, host DNA repair machineries fix the gap of the inserted viral DNA [151]. The sites of HIV-1 integration are not random and favor gene bodies, actively transcribing genes, and gene dense regions [140]. This integration pattern has been mapped to CA interaction with CPSF6 and IN interaction with lens epithelium-derived growth factor (LEDGF/p75) [152,153]. LEDGF/p75 acts as a tethering factor for IN and protects IN from degradation[154].

1.2.3.4 HIV-1 Transcription and Translation

After integration, the viral DNA is transcribed similarly to host genes by recruiting RNA Pol II to its 5' long terminal repeat (LTR), which serves as the promotor [155]. However, initial RNA transcripts are generally short as RNA Pol II dissociates from viral DNA often [156]. This process is improved by the HIV-1 accessory protein Tat [155]. Tat recruits the positive transcription elongation factor b (P-TEFb) and enhances the processivity of RNA Pol II for more efficient and longer transcription [155]. In the case of unspliced and incompletely spliced RNAs, another viral protein, Rev, promotes the export of these RNAs by binding to the RRE [75]. Viral mRNAs are translated like host mRNAs to produce viral proteins.

1.2.3.5 HIV-1 Packaging and Assembly

During Env translation, the precursor gp160 is translocated into the endoplasmic reticulum (ER), where it undergoes glycosylation, cleavage into gp120 and gp41, and formation of trimers, before trafficking to the plasma membrane [157]. Gag and Gag-Pro-Pol have a myristylation signal at the N-terminus of the MA domain, which targets the polyproteins to the plasma membrane [158]. Two copies of HIV-1 gRNA are noncovalently dimerized at their 5' untranslated region (UTR). The viral packaging signal Ψ interacts with NC within Gag or Gag-Pol for its encapsulation [159,160]. After forming the spherical shaped bud with all the viral components and host proteins, virus budding is facilitated by the host ESCRT machinery [159,161,162].

1.2.4 Evasion of Innate Restriction Factors

There has been a long ongoing battle between viral infection and the host immune response during evolution. In this battle, several host innate restriction factors are at the frontline. For HIV-1, these host factors include apolipoprotein B mRNA editing enzyme, catalytic polypeptide-like family proteins (APOBEC), sterile alpha motif and histidine aspartate domain-containing protein 1 (SAMHD1), tetherin, and tripartite motif (TRIM) family proteins. They act on different stages of HIV-1 life cycle [163].

It is estimated that a substantial proportion of proviruses in HIV-infected individuals are defective, likely due to G-to-A hypermutations during reverse transcription or mutations mediated by APOBEC3G (A3G) and APOBEC3F (A3F) [164–166]. A3G and A3F belong to the APOBEC superfamily, which is a group of cytidine deaminase enzymes. A3G and A3F are present in abundance in the cytosol of immune cells and can be incorporated into the budding virion [166,167]. During reverse transcription, A3G and A3F catalyze cytosine-to-uracil deamination in the nascent viral DNA, resulting in G-to-A hypermutation and potentially defective provirus [165,168]. HIV-1 has evolved to encode Vif to antagonize A3G and A3F activity by recruiting cullin-5 E3 ubiquitin ligase, which results in ubiquitination and subsequent proteasomal degradation of A3G and A3F [164–166].

SAMHD1 is a deoxynucleotide triphosphohydrolase that impairs HIV-1 reverse transcription by depleting the dNTP pool in cells [169]. As mentioned above, reverse transcription requires dNTPs. SAMHD1 hydrolyzes dNTPs to deoxynucleosides and inorganic phosphate [169–171]. As a consequence, in some cells, such as macrophages, a high level of SAMHD1 expression reduces available dNTP pools and slows reverse transcription and HIV-1 replication [171]. Therefore, HIV-1 infects macrophages less efficiently than CD4+ T cells. HIV-2 and some SIVs encode an

accessory protein, Vpx, to overcome SAMHD1 restriction [169–171]. Vpx interacts with the C-terminal domain of SAMHD1 and recruits the cullin-4 E3 ubiquitin ligase complex, which leads to poly-ubiquitination and proteasomal degradation of SAMHD1 [169–172].

Tetherin/BST-2 (Bone marrow stromal antigen 2) is an interferon stimulated gene (ISG), which functions as a transmembrane protein that potently blocks the release of HIV-1 by holding the budding viral particles on the surface of infected cells [173]. Tetherin has an N-terminal transmembrane domain and a C-terminal glycosyl-phosphatidylinositol group. Therefore, tetherin is able to attach one end to the plasma membrane and the other to the viral envelope. The unreleased virions are later internalized and degraded via the endosomal/lysosomal pathway. HIV-1 encodes the accessory protein Vpu to overcome tetherin restriction [173,174]. It has been shown that Vpu can promote the poly-ubiquitination of tetherin transmembrane domain, inducing the subsequent proteasomal degradation [173,175]. Vpu can also downregulate tetherin concentration on the cell surface [173].

TRIM proteins constitute a large family of E3 ligases. There are approximately 100 known *TRIM* genes in humans. TRIM5α is a cytosolic protein that restricts retrovirus infection in a species-specific fashion [117]. TRIM5α from Old World monkeys restricts HIV-1 and HIV-2 potently [176]. TRIM5α contains the SPRY domain at the C terminus, which is important for the recognition of capsid hexameric lattice [177–179]. The coiled-coil domain of TRIM5α is required for its proper function to form homodimer and heterodimer [163]. Human TRIM5α was shown to potently restrict MLV and EIAV but not HIV-1 [180]. Recently, the importance of human TRIM5α has been re-evaluated due to the host factor CypA. CypA, which is a host protein that catalyzes the isomerization of peptide bonds to facilitate protein folding [181], binds to capsid [116,182,183].

Recently, CypA has been shown to protect the capsid from human TRIM5α recognition and restriction [184,185].

Besides these known restriction factors, additional host restriction factors have been discovered, including SERINC3/5, MX-2, IFITMs, MARCH2/8, and Schlafen 11 [163]. It is worth noting that there is a constant battle between the host defense mechanism and viral infection. A better understanding of the restriction factors would help identify new strategies to inhibit HIV-1 replication.

1.2.5 Capsid Trafficking to the Nucleus

After fusion, capsid is released into the cell cytoplasm. HIV-1 uses cytoplasmic trafficking to get to the nucleus. Depending on the cell type, this journey can be longer or shorter. For instance, a T cell has a diameter of approximately 5–7 μm and macrophages are 20–30μm in diameter [186,187]. The distance from the plasma cell membrane to the nucleus is longer in macrophages compared to CD4+ T cells. However, HIV-1 movement towards the nucleus is unlikely to be due to random motion, as the cytoplasm is crowded with cellular organelles and cytoskeleton components, imposing barriers and limiting free diffusion. Studies performing fluorescence recovery after photobleaching (FRAP) on fluorescently labeled dextran particles demonstrated that particles with > 20 nm diameters are unlikely to move through the cytoplasm by random diffusion [188,189].

To move large cargos, cells use their own highways to achieve this goal. Microtubules, which are hollow tubular structures approximately 25 nm in diameter [190], are one of the cellular cytoskeleton components involved in trafficking. Microtubules undergo constant disassembly and assembly, known as dynamic instability [191]. This is an important characteristic of microtubules for their structural and trafficking roles [192,193]. Microtubule-dependent trafficking requires the cargo

to contain a signal that is recognized by a motor adapter protein [108,194,195]. Once the motor adapter protein binds the cargo and activates the motor protein, the motor protein hydrolyzes ATP and initiates movement of the cargo [191].

Depending on the direction of the movement, motor proteins can be classified into two categories: dyneins, retrograde motors that move towards the minus end of microtubules; and kinesins, anterograde motors that traffic towards the plus end of microtubules. Both dyneins and kinesins are involved in HIV-1 trafficking, affecting subsequent infection [108,194,195]. Until recently, several motor adapter proteins were determined to directly interact with HIV-1 CA and facilitate the trafficking of HIV-1 capsid: FEZ1, BICD-2, and KIF5B [108,194,195]. The depletion of any of these factors results in reduced trafficking of HIV-1 complexes in the cells and restricted HIV-1 infection [108,194,195]. Mutations in CA (e.g., N74D or P90A) can abolish the restriction posed by KIF5B depletion [108]. Direct *in vitro* binding to HIV-1 CA has been shown for FEZ1 and BICD-2 [194,195]. As both dynein and kinesin are important in HIV-1 trafficking, it is proposed that bidirectional trafficking is important for HIV-1 infection [196].

HIV-1 CA has been shown to be the dominant determinant for infection of non-dividing cells and nuclear import [119,141]. Specifically, its ability to interact with CPSF6 to mediate nuclear import and targeted integration has been carefully examined in the past few years [141,153,197]. CPSF6 is part of the cleavage factor I mammalian (CFIm) complex, which is mainly nuclear and is involved in cellular pre-mRNA processing and polyadenylation [198]. Mutations and mutation-induced fusion of CPSF6 with other host proteins have been implicated in various human cancers such as breast cancer and leukemia [199–203]. However, it is still elusive where and when HIV-1 capsid initiates contact with CPSF6. It is possible that CPSF6 may access the HIV-1 capsid outside

the nucleus. It is also of interest to understand the effect of CPSF6 binding to HIV-1 capsid and its role in HIV-1 capsid uncoating.

1.3 Imaging HIV-1 Trafficking to the Nucleus

As HIV-1 protein or complex trafficking is an important step of its early life cycle, multiple research groups have developed imaging assays and technologies to study this process [107,108,194,195,204–206]. Initial approaches heavily relied on fixed cell laser scanning confocal imaging at different time points after HIV-1 infection [107,108,194]. These imaging experiments provided a series of snapshots of HIV-1 localization in cells. However, due to the inability to follow individual virus particles over time, most readouts require averaging of multiple virus complexes over time. This can provide helpful insights into trafficking of the overall population. However, this approach lacks accurate spatial and temporal information of individual HIV-1 particles over time, which are likely heterogeneous.

Live-cell imaging has been the Holy Grail to study HIV-1 trafficking. Currently, most imaging methods are based on spinning-disk confocal microscopy. Compared to scanning confocal imaging, data generated from spinning-disk confocal imaging provide researchers the ability to follow individual viruses for a duration of time, with only 2-10 minute intervals due to photobleaching [109,204,207]. Unfortunately, each virus has limited space to package fluorescently labeled molecules. For this limited pool of fluorescent molecules, longer and higher intensities of exposure to the excitation laser lead to faster photobleaching. However, the pin hole inside the spinning-disk confocal microscope requires high excitation laser intensity and long exposure time to visualize small objects, leading to limited temporal resolution. This results in laborious data

analysis for HIV-1 tracking, normally requiring pinpointing particle location manually due to the "jumpy" trajectories. This limitation makes spinning-disk confocal microscopy unsuitable to study microtubule-dependent movement, as cargos on microtubules can move as fast as 1 μm/s [208]. Within minutes, the particle may have traveled a relatively far distance across the cell.

We have implemented highly inclined and laminated optical sheet (HILO) imaging for studying HIV-1 trafficking [209]. HILO is based on total internal reflection fluorescence microscopy (TIRF) [210]. TIRF utilizes evanescent energy transfer instead of direct laser exposure to excite the fluorophore [211]. The design of TIRF grants a high signal to noise ratio during imaging. It allows real-time single molecule imaging with minimal photobleaching. However, TIRF is limited to surface imaging and unable to penetrate deep enough to image HIV-1 trafficking after entry into cells [212]. HILO overcomes this limitation by positioning the incident laser beam at a higher inclined angle at the large refraction surface compared to TIRF. This results in the formation of a highly inclined and laminated thin optical sheet above the coverslip, penetrating through the imaging sample [209]. HILO imaging allows deeper penetration into samples (>10 μm) while maintaining a high signal/noise ratio and low photobleaching [209]. Using HILO, along with synchronizable fast excitation laser filter wheel, we are able to capture HIV-1 trafficking on microtubules with two different fluorophores at 2 frames per second (FPS) for at least 10 minutes with minimal observed photobleaching. Data acquired by HILO imaging allow us to investigate HIV-1 trafficking in high resolution, including speed, direction, and track length of individual viral particles. The high spatial and temporal precision allows HIV-1 trafficking data analysis to be streamlined and automated.

1.4 Specific Aims

Aim 1: Determine whether HIV-1 complexes interact with CPSF6 in the cytoplasm and whether disruption of CPSF6 localization affects HIV-1 cytoplasmic trafficking

CPSF6, as part of the CFIm complex, is conventionally considered a nuclear protein. CPSF6 is important for HIV-1 nuclear import and it is also a cargo of TNPO3. Specifically, the nuclear localization of CPSF6 mediated by TNPO3 is crucial for HIV-1 nuclear import and subsequent integration and infection. However, the exact location and timing of where and when CPSF6 and TNPO3 interact with HIV-1 remain elusive.

Hypothesis: HIV-1 interacts with CPSF6 in the cytoplasm. Disruption of CPSF6 localization will affect HIV-1 cytoplasmic trafficking, uncoating, and subsequent infection.

Aim 2: Determine how depletion of CPSF6 alters HIV-1 trafficking and infection in primary cells

CPSF6 has been shown to be a host factor that helps HIV-1 evade innate immune sensing. Both depletion of CPSF6 or defects in capsid binding to CPSF6 result in restriction of HIV-1 infection and induction of interferon production in primary cells. However, the exact mechanism of this restriction is unknown. In addition, the effect of CPSF6 depletion on HIV-1 trafficking also remains elusive.

Hypothesis: HIV-1 trafficking and infection in primary peripheral blood mononuclear cells (PBMC) and macrophages will be altered by depletion of CPSF6. Depletion of CPSF6 will prevent HIV-1 evasion from a type I interferon response.

Aim 3. Investigate the role of CypA in HIV-1 trafficking and how disruption of CypA binding alters HIV-1 capsid interaction with CPSF6

CypA has been shown as one of the most important host factors required for HIV-1 early infection in certain cell types but not others. Moreover, recent studies have shown that CypA protects HIV-1 in the cytoplasm from other restriction factors. However, little is known whether CypA will affect the interaction between HIV-1 capsid and CPSF6.

Hypothesis: Disruption of the interaction between CypA and HIV-1 capsid will affect HIV-1 interaction with CPSF6, trafficking, and infection. Additionally, disruption of CypA binding to HIV-1 capsid will lead to an enhanced type I interferon response after infection.

2.0 Chapter 2: HIV-1 Complexes Interact with CPSF6 in the Cytoplasm and Disruption of CPSF6 Localization Affects HIV-1 Cytoplasmic Trafficking

2.1 Project Summary

This chapter is comprised of results and data adapted from the following manuscripts:

Ning J*, **Zhong Z***, Fischer DK, Harris G, Watkins SC, Ambrose Z, Zhang P. Truncated CPSF6 Forms Higher-Order Complexes That Bind and Disrupt HIV-1 Capsid. J Virol. 2018 Jun 13;92(13):e00368-18. doi: 10.1128/JVI.00368-18. PMID: 29643241; PMCID: PMC6002704. * authors contributed equally

Zhong Z, Ning J, Boggs EA, Jang S, Wallace C, Telmer C, Bruchez M., Ahn J, Engelman AN, Zhang P, Watkins SC, Ambrose Z. Cytoplasmic CPSF6 regulates HIV-1 capsid trafficking and infection in a cyclophilin A dependent manner, submitted.

For this Aim, I performed experiments to show that CPSF6 is expressed in the cytoplasm, CPSF6 traffics on microtubules, disruption of CPSF6 localization alters HIV-1 trafficking and infection, and > 90% of VSV-G pseudotyped HIV-1 virions completed fusion into the cytoplasm by 1 h post-infection. Jiying Ning performed the purification of CPSF6 and CPSF6-358 and *in vitro* CA binding assays. Douglas Fischer conducted the capsid permeablization assays. Sooin Jang made the CPSF6-4Glu mutant. Cheryl Telmer made the GPI-FAP construct.

2.2 Introduction

Unlike other retroviruses, HIV-1 can infect non-dividing cells, such as resting CD4+ T cells and terminally differentiated macrophages, due to its ability to transport its genome across the nuclear membrane without cell division [97]. The HIV-1 RTC is estimated to have a diameter of approximately 56 nm, which is too large to pass the nuclear envelope via passive diffusion [85]. Thus, HIV-1 exploits host factors for nuclear import. As stated in Chapter 1, HIV-1 CA was shown to be the determinant for HIV-1 nuclear import, in which the CA coding region of HIV-1 was replaced with MLV CA [119]. This chimeric virus showed significantly reduced replication in growth-arrested cells compared to WT HIV-1 or MLV with HIV-1 CA. Moreover, the MLV/ HIV-1 chimeric virus was used to show that HIV-1 CA, not IN, is responsible for restriction by TNPO3 depletion [139].

CPSF6 present in target cells plays an important role in HIV-1 infection. Expression of CPSF6 truncated at the 358th residue, CPSF6-358, potently blocked HIV-1 at the step of nuclear import [141]. The pocket formed by helices 3 and 4 of the N-terminal domain of CA was shown to be key to this restriction, as multiple mutations in this pocket (residues N57, Q67, K70, N74, A105, T107, and S109) resulted in reduced restriction by depletion of TNPO3 or expression of CPSF6-358 [144]. Binding experiments also showed a direct interaction between a CPSF6 peptide and this pocket at low affinity (362 μM) [144]. CPSF6 was also shown to be imported into and maintained in the nucleus by the cellular karyopherin TNPO3 [143,145]. Depletion of TNPO3 resulted in cytoplasmic mislocalization of CPSF6, which is believed to cause restriction of HIV-1 nuclear import similar to expression of CPSF6-358 [145]. Moreover, the restriction due to TNPO3 depletion was relieved by CPSF6 siRNA knockdown, suggesting that CPSF6 is necessary for the HIV-1 restriction posed by TNPO3 depletion [213]. More recently, structural data showed that the C-terminal serine and

arginine-rich domain (RS domain) of CPSF6 interacts with TNPO3 [143]. Mutations in or truncation of this region significantly reduced the interaction between CPSF6 and TNPO3 [143,144,213].

For this Aim, we investigated whether HIV-1 capsid interacts with CPSF6 in the host cell cytoplasm and whether this interaction affects capsid trafficking and subsequent virus infectivity. Using live-cell microscopy, we visualized WT HIV-1 complexes colocalized with cytoplasmic CPSF6 that trafficked together on microtubules. By negative-stain transmission electron microscopy (TEM), we show that purified CPSF6-358 and CPSF6 protein form oligomers that bind and disrupt CA tubular assemblies.

2.3 Results

2.3.1 Cytoplasmic CPSF6 Traffics on Microtubules

Previous studies have shown strong nuclear localization of CPSF6 in cells [145]. Due to its role in HIV-1 nuclear import, we examined whether CPSF6 was expressed in the cell cytoplasm. Antibody staining of endogenous CPSF6 or expression of green fluorescent protein tagged CPSF6 (CPSF6-GFP) in HeLa cells showed mostly nuclear expression as well as punctate cytoplasmic expression mainly near the nuclear membrane, which may indicate higher-order complex formation (Figure 6A). HILO live-cell microscopy showed that perinuclear CPSF6-GFP puncta were dynamic in cells and were colocalized with microtubules (Figure 6B). Inhibition of microtubule polymerization with nocodazole inhibited CPSF6-GFP movement in cells, suggesting that CPSF6 traffics on microtubules (Figure 6C).

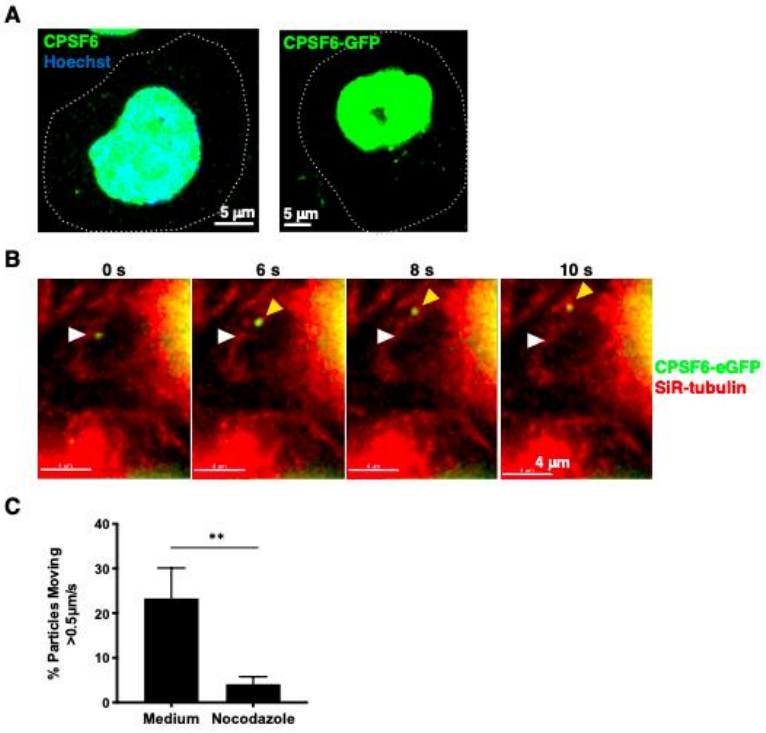

Figure 6 CPSF6 puncta are detected in the perinuclear region and traffic on microtubules. (A) Endogenous CPSF6 or expression of CPSF6-GFP in HeLa cells (dotted lines, cell outlines).CPSF6 is expressed as two different isoforms composed of 551 or 588 amino acid residues [214]; exogenously expressed proteins throughout this study were based on the 588 isoform. (B) Movement of a CPSF6-GFP higher order complex (green) is shown in a HeLa cell stained with SiR-tubulin (red) by HILO live-cell imaging. The white arrow indicates the location of the complex at the first time point and the yellow arrow indicates the location at subsequent time points. (C) The percentage of cytoplasmic CPSF6-GFP complexes is shown that trafficked > 0.5 µm/s in HeLa cells treated with or without nocodazole. Error bars indicate STDEV of n ≥ 185 complexes.

To visualize HIV-1 particles, we labeled the contents of the capsid by generating a fluorescently tagged integrase (IN), since direct labeling of CA is not ideal, as tags on the protein may impact capsid stability and/or interactions with other host factors. Specifically, the fluorescent protein tagRFP or mRuby3 [215,216] was introduced between Vpr and IN in a previously described fusion construct [217], called Vpr-mRuby3-IN or Vpr-tagRFP-IN, and was expressed during HIV-1

production in trans (Figure 7A). The labeled IN was determined to be functional, as it was able to rescue the infectivity of HIV-1 containing an IN active site mutation, D116N [218] (Figure 7B). mRuby3-IN allowed visualization of virus particles prior to (Figure 7C) and after (Figure 7D) infection of HeLa cells and was colocalized with HIV-1 RNA after the infection of cells (Figure 7D), suggesting that it is present within capsids and reverse transcription complex (RTC) or pre-integration complex (PIC).

As HIV-1 RTCs also traffic on microtubules [219], we examined the association of fluorescently labeled HIV-1 particles with cytoplasmic CPSF6- GFP in cells. To investigate whether this cytoplasmic interaction between HIV-1 and CPSF6 is HIV-1 CA specific, vesicular stomatitis virus glycoprotein (VSV-G)-pseudotyped WT or N74D (does not bind to CPSF6) HIV-1 encoding firefly luciferase and labeled with Vpr-mRuby3-IN or Vpr-tagRFP-IN was used to infect cells expressing CPSF6-GFP. WT complexes were colocalized with perinuclear CPSF6-GFP, while N74D complexes were not (Figure 8A). Multiple WT or N74D virus particles that colocalized with CPSF6-GFP were assessed by live-cell imaging over time. The fluorescence intensity of WT HIV-1 complexes remained associated with CPSF6-GFP, whereas the fluorescence intensity of N74D viral particles did not (Figure 8B). This is consistent with a recent study showing WT HIV-1 particles associated with CPSF6 initially outside of the nucleus [109]. WT HIV-1 particles associated with CPSF6-GFP trafficked rapidly and linearly, suggestive of microtubule movement (Figure 8C). Consistent with this interpretation, trafficking of WT HIV-1 particles associated with CPSF6-GFP was inhibited with nocodazole treatment (Figure 8D). Finally, a HeLa cell line expressing CPSF6 tagged with iRFP670 and TNPO3 tagged with GFP respectively was made. Using live-cell imaging, we observed that CPSF6-iRFP trafficked towards

the nucleus with its TNPO3-GFP binding partner (Figure 8E). These results suggest that HIV-1 complexes traffic with CPSF6 on microtubules.

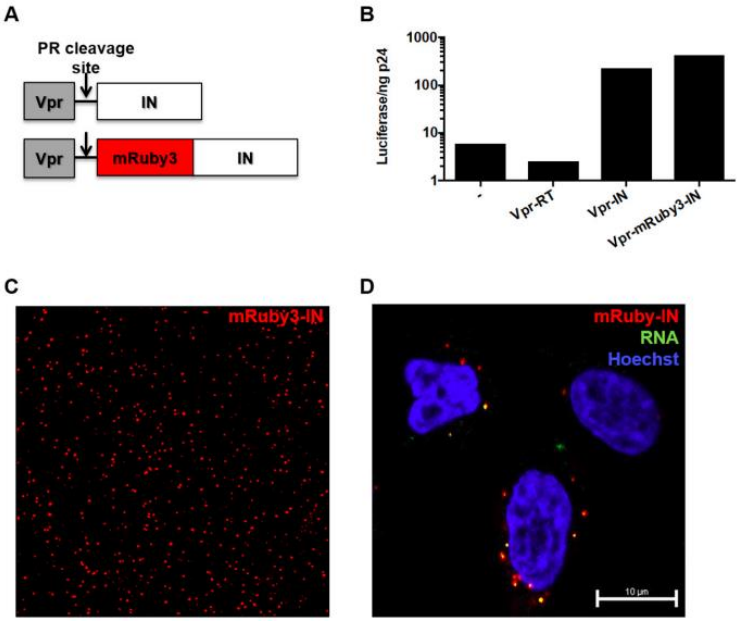

Figure 7 Generation of fluorescently labeled HIV-1. (A) The schematic design of the Vpr-mRuby3-IN construct used to label HIV-1 particles in trans. (B) Specific infectivity (luciferase per nanogram of p24) was measured for D116N HIV-1 complemented in trans with no plasmid, Vpr-RT, Vpr-IN, or Vpr-mRuby3-IN. (C) TIRF microscopy image of WT HIV-1 labeled with Vpr-mRuby3-IN. (D) Confocal image of HeLa cells synchronously infected with WT HIV-1 labeled with Vpr-mRuby3-IN and 5-ethynyl uridine and fixed 30 min post-infection.

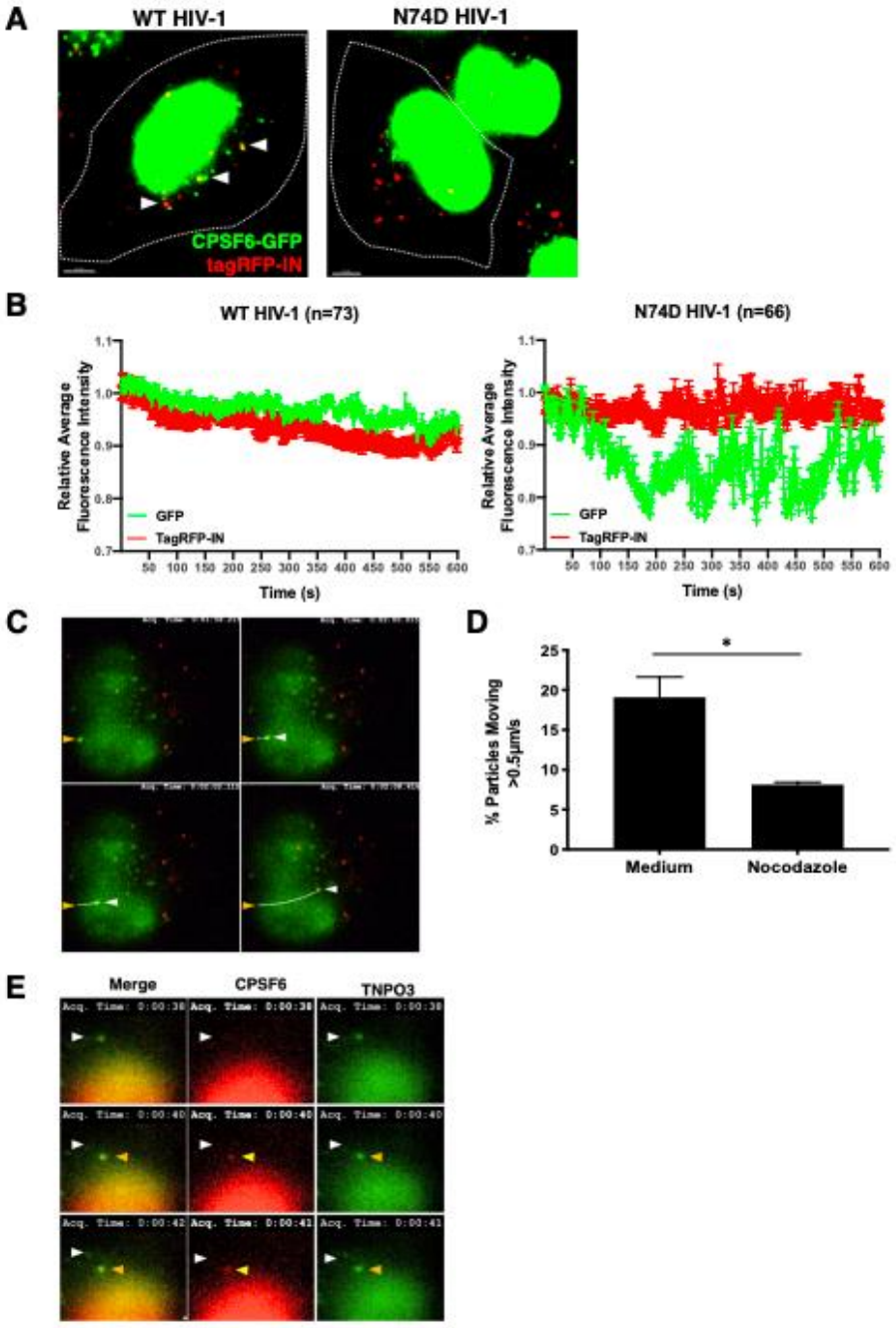

Figure 8 HIV-1 complexes associate with perinuclear CPSF6 and co-traffic on microtubules. (A) Confocal images of HeLa cells expressing CPSF6-GFP (green) are shown 60 min after infection with WT HIV-1 or N74D HIV-1 containing tagRFP-IN (red). The white arrow indicates tagRFP-IN particles colocalized with CPSF6-GFP (yellow). (B) The average intensities of cytoplasmic tagRFP-IN from WT or N74D virus complexes and CPSF6-GFP during HILO imaging were measured for 10 min, normalized to 1.0 at time 0, and graphed. Error bars indicate STDEV. (C) The track of a WT HIV-1 mRuby3-IN complex (red) colocalized with CPSF6-GFP

(green) is shown by HILO imaging in a HeLa cell over time. The yellow arrow indicates the location of the complex at the first time point and the white arrow indicates the location at subsequent time points. (D) The percentage of cytoplasmic CPSF6-GFP complexes colocalized with mRuby3-IN (n = 156-189) is shown that trafficked > 0.5 µm/s in HeLa cells treated with or without nocodazole. Error bars indicate standard errors of the mean (SEM). (E) A HeLa cell expressing GFP-TNPO3 (green) and CPSF6-iRFP (red) is shown. The white arrow indicates the location of a GFP-TNPO3 complex at the first time point that becomes colocalized with CPSF6-iRFP at subsequent time points (yellow arrow).

2.3.2 Changes in the CPSF6 RS Domain Alter WT HIV-1 Complex Trafficking

CPSF6-358, which lacks the RS domain, or alteration of four positively charged amino acids (K547, R549, R559, and R561) in the RS domain to glutamic acid (CPSF6-4Glu) (Figure 9A) leads to decreased nuclear localization of CPSF6 and restriction of WT HIV-1 infection at the step of nuclear entry [141,220]. Expression of iRFP670 tagged CPSF6-4Glu or CPSF6-358 led to increased cytoplasmic localization in cells, with the truncated protein showing a greater effect than the 4Glu mutant (Figure 9B). Similarly, the expression of CPSF6-358 resulted in a greater restriction of WT HIV-1 infection than the expression of CPSF6-4Glu (Figure 9C). N74D HIV-1, which does not bind to CPSF6, was not restricted by either mutant.

To determine if mislocalization of CPSF6 to the cytoplasm affects HIV-1 complex trafficking, live-cell imaging of WT and N74D HIV-1 complexes was performed in cells expressing fluorescently tagged CPSF6, CPSF6-4Glu, or CPSF6-358. To avoid imaging particles that have not yet fused out of endosomes into the cytoplasm, imaging was performed using mRuby3-IN labeled WT HIV-1 particles that were also labeled with the glycosylphosphatidylinositol targeting motif of decay-accelerating factor (normally anchored at the outer leaflet of plasma membrane) [221] tagged with fluorogen activating protein [222] (FAP-GPI)

to label the virus membrane. The loss of FAP-GPI signal from the mRuby3 signal signified that the HIV-1 membrane had fused with the endosome and the contents of the virus have been released into the cytoplasm. During synchronized infection, we observed that nearly all mRuby3 signals separated from the viral membrane by 50 min (Figure 10). Thus, for virus tracking experiments, the acquisition of images began at 60 min post-infection.

In HeLa cells expressing CPSF6-GFP, WT and N74D viral complexes had similar speeds, and track lengths but differed in track straightness (Figures 9D, 11). In contrast, WT HIV-1 particles increased in all three measurements when CPSF6-4Glu-iRFP670 or CPSF6-358-iRFP670 was expressed in cells (Figures 9D, 11). Little or no change in particle speed, track length, or track straightness was observed for N74D complexes in the presence of CPSF6-4Glu or CPSF6-358. Similar to the effect of increased CPSF6 cytoplasmic localization on WT HIV-1 infectivity, average WT virus particle speed and track length inversely correlated with the intensity of nuclear CPSF6 expression (Figure 9E). These data demonstrate that HIV-1 complex trafficking is altered in the cytoplasm via enhancing CPSF6 cytoplasmic localization. Furthermore, the altered/increased trafficking HIV-1 trafficking by mislocalized CPSF6 is associated with an infectivity defect. It is possible that the restriction of HIV-1 due to CPSF6 mislocalization may occur at the trafficking of HIV-1, which is earlier than nuclear import as previous studies have shown[141,145].

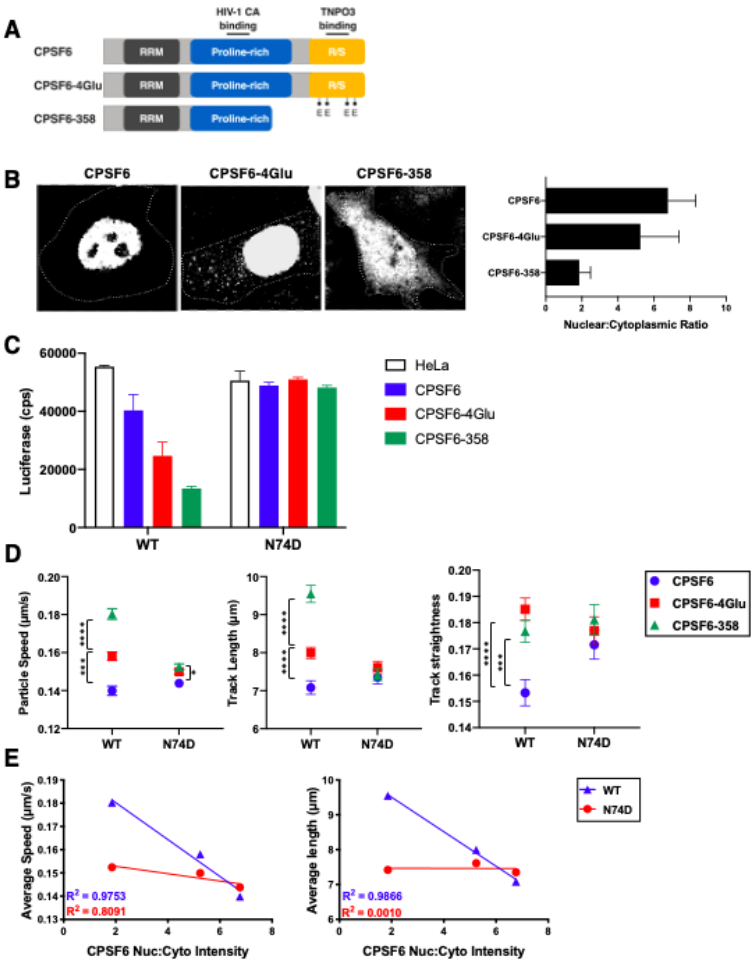

Figure 9 Alteration of the CPSF6 RS domain impacts HIV-1 trafficking. (A) CPSF6 protein domains and associated CPSF6-4Glu and CPSF6-358 changes. (B) Confocal microscopy images are shown of cells expressing CPSF6-iRFP, CPSF6-4Glu-iRFP, or CPSF6-358-iRFP. The cell periphery is indicated by dotted lines. The graph shows the nuclear to cytoplasmic ratio of CPSF6 for each. (C) Infection of WT and N74D HIV-1 in normal HeLa cells or HeLa cells expressing CPSF6-iRFP, CPSF6-4Glu-iRFP, or CPSF6-358-iRFP is shown as luciferase expression (counts per second, or cps) from a representative of 2 independent experiments. Error bars indicate STDEV of duplicates. (D) The average particle speeds, track lengths and track straightness of WT or N74D HIV-1 mRuby3-IN complexes in HeLa cells expressing CPSF6-iRFP, CPSF6-4Glu-iRFP, or CPSF6-358-iRFP are shown from one of 2 independent HILO live-cell imaging experiments. Error bars indicate SEM. (E) Correlations of the average particle speed or average track length and CPSF6 nuclear: cytoplasmic ratio are shown for WT and N74D HIV-1.

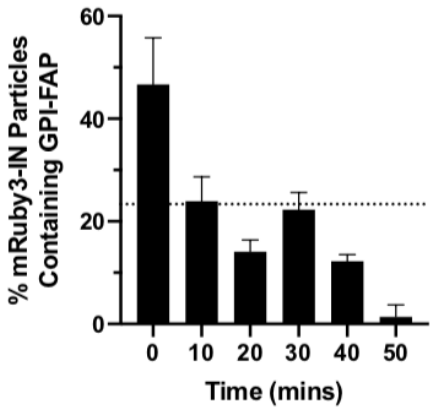

Figure 10 FAP-GPI membrane label on HIV-1 particles is lost over time after incubation on HeLa cells. HeLa cells were synchronously infected with WT HIV-1 produced with mRuby3-IN and FAP- GPI and imaged by live-cell microscopy. The average percentage of mRuby3-IN complexes still containing FAP-GPI was determined between 0 - 50 min from n ≥ 375 cells/experiment from two separate experiments. Error bars represent STDEV and the dotted line represents 50% of double-positive HIV-1 complexes at time 0.

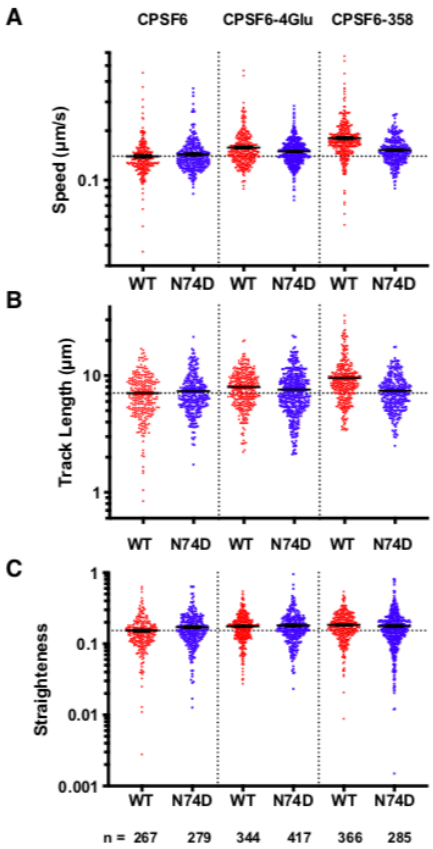

Figure 11 Mutation or truncation of the CPSF6 R/S domain alters HIV-1 trafficking. Results from HILO live-cell imaging are shown that were summarized in Figure 9D. Statistics are shown in Figure 9D. The particle speed (A), track length (B), and track straightness (C) of individual WT or N74D HIV-1 mRuby3-IN complexes in HeLa cells expressing CPSF6-iRFP, CPSF6-4Glu-iRFP, or CPSF6-358-iRFP are shown. Error bars indicate SEM. Dotted lines denote the mean of WT complexes in CPSF6-iRFP cells. The number (n) of mRuby3-IN complexes analyzed for each condition is listed at the bottom.

2.3.3 CPSF6-358 and CPSF6 Oligomerize and Disrupt Assembled WT CA

Detailed analysis of the direct interaction between HIV-1 capsid and CPSF6-358 has historically been hindered by the inability to express and purify high-quality and high-quantity yields of CPSF6-358 protein. To overcome this challenge, we attached a His6-albumin fusion tag to the N terminus of CPSF6-358 (His6-albumin–CPSF6-358) and expressed the protein in

mammalian cells. The albumin-fused protein was robustly expressed (Figure 12A) and subsequently purified using Ni-nitrilotriacetic acid (NTA) resin followed by a Superdex 200 26/60 gel filtration column. Two broad peaks were observed in the gel filtration profile of the tagged protein (Figure 12B, P1, and P2), both of which corresponded to His6-albumin–CPSF6-358, as confirmed by Western blotting with anti-His and antiCPSF6 antibodies (Figure 12A). The presence of two peaks suggests that the purified fusion protein may adopt different oligomeric states. Size exclusion chromatography coupled with in-line multiangle light scattering (SEC-MALS) further showed that the P1 protein contained primarily large oligomers with molecular masses around 2.1 MDa, whereas the P2 sample was a mixture of oligomeric states, with the majority around 260 kDa and 148 kDa and a small fraction similar to P1, around 2 MDa. Negative-stain electron microscopy (EM) revealed this to be the case, with the P1 peak showing linear strings of varying protein oligomer lengths (Figure 13C, left), while P2 contained a complex mixture of oligomeric species that were mostly shorter and thinner than those observed in P1 (Figure 12C, right).

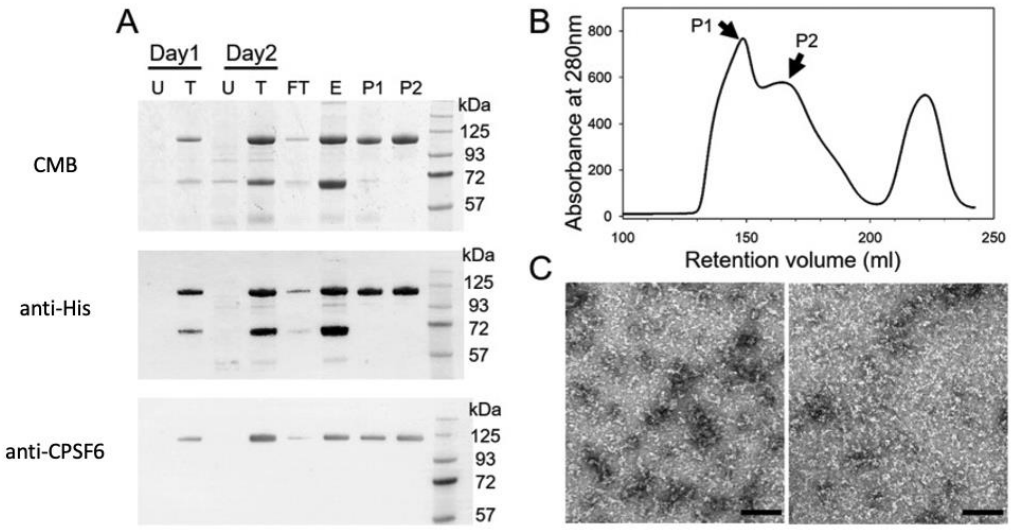

Figure 12 Purification of CPSF6-358 with an albumin tag from the mammalian secretory expression system. (A) SDS-PAGE and Western blot analysis of His6-albumin–CPSF6-358 expression and purification. Samples taken from untransfected cells (U), transfected cells (T), the flowthrough (FT) and elution (E) from Ni-NTA resin, and peaks (P1 and P2) from the Superdex 200 26/60 column (shown in panel B) were stained with Coomassie blue (top) or processed with anti-His (middle) or anti-CPSF6 (bottom) antibody, following Western blotting. (B) Gel filtration profile of the protein eluted from the Superdex 200 26/60 column. The two His6-albumin–CPSF6-358 peaks are labeled P1 and P2. (C) Representative EM images of negatively stained His6-albumin–CPSF6-358 samples from fractions P1 (left) and P2 (right), as shown in panel B. Scale bars, 100 nm.

Many studies have shown that CPSF6-358 is a potent inhibitor of HIV-1 infection and prevents HIV-1 nuclear entry and integration by targeting the viral capsid [94,141,142,223]. To investigate whether CPSF6-358 alters the capsid upon binding, we incubated preassembled WT HIV-1 CA tubes, generated in vitro from purified CA protein [71], with either His6-albumin–CPSF6-358 (P1 or P2) or untagged CPSF6-358 from P2. In all cases, the cosedimentation of the CPSF6-358 proteins with the CA tubes was observed (Figures 13A, B, and M, left). In contrast, binding of CPSF6-358 proteins to tubes assembled with N74D HIV-1 CA, a mutation previously shown to abolish CPSF6-358 binding and restriction [223], was negligible (Figures 13A and B). Binding of

assembled CA tubes by untagged CPSF6-358 was more efficient than that by the tagged protein, as almost all of the untagged CPSF6-358 came down with CA tubes, whereas only about 50% of the tagged protein cosedimented with CA (Figures 13A and B). Quantitative analysis of CPSF6-358 binding was performed by measuring the molar ratio of CA-bound CPSF6-358 over a range of CPSF6-358 concentrations. The dose-dependent binding was observed for both tagged CPSF6-358 (P1 and P2) and untagged CPSF6-358 (Figure 13M, left). To investigate the effect of CPSF6-358 binding on CA tubular assemblies, we examined the samples from our CPSF6-358/CA binding assays using TEM (Figures 13C to L). Remarkably, TEM micrographs showed a drastic structural disruption of WT CA tubes upon incubation with either His6-albumin–CPSF6-358 (P1 or P2) (Figures 13D and E) or untagged CPSF6-358 (Figure 13J), whereas N74D CA tubes remained intact (Figures 13G to H and L). Still, significant differences in the morphology of the breakdown products were evident in the presence of P1 protein compared to P2 protein. Binding of the large P1 oligomers resulted in dissolution of tubes and an appearance of distinctly curved capsid remnants (Figure 13D, arrows), whereas P2 protein and untagged CPSF6-358 derived from P2, consisting of mostly dimers, broke the tubes into short segments and a mixture of cones and spheres, respectively (Figures 13E and J). In all cases, CPSF6-358 densities around the CA tube fragments apparently remained bound to the surfaces of CA tube fragments (Figures 13D, E, and J). Intriguingly, the amount of pelletable capsid did not change upon tube breakdown (Figures 13A and B), suggesting that the predominant effect of CPSF6-358 is fragmentation without dissociation into soluble proteins. Quantitative analysis of CA tube fragmentation by CPSF6-358, by measuring tube numbers and lengths at different concentrations of CPSF6-358, revealed a dose-dependent reduction in both the number of long, unfragmented tubular assemblies and the lengths of

fragmentation products as the CPSF6-358 concentration increased (Figures 13M, middle and right).

To determine whether full-length CPSF6 had similar properties, it was purified and characterized with WT and N74D CA tubular assemblies. To obtain soluble CPSF6, an N-terminal maltose binding protein (MBP) fusion construct was expressed and purified, resulting in two peaks in size exclusion chromatography (Figure 14, labeled P1 and P2) that corresponded to the tagged full-length CPSF6, as confirmed by western blot (Figure 14B). This suggests that the purified fusion protein may adopt different oligomeric states similar to what was observed for CPSF6-358, which also displayed two peaks in a size exclusion chromatography profile with dimer and large oligomers. Removal of the MBP-tag with HRV-3C protease resulted in precipitation of CPSF6 from both P1 and P2 (Figure 14C). Therefore, MBP-tagged soluble MBP-His6-CPSF6-588 (denoted as "MBP-CPSF6" henceforth) was used for further binding experiments

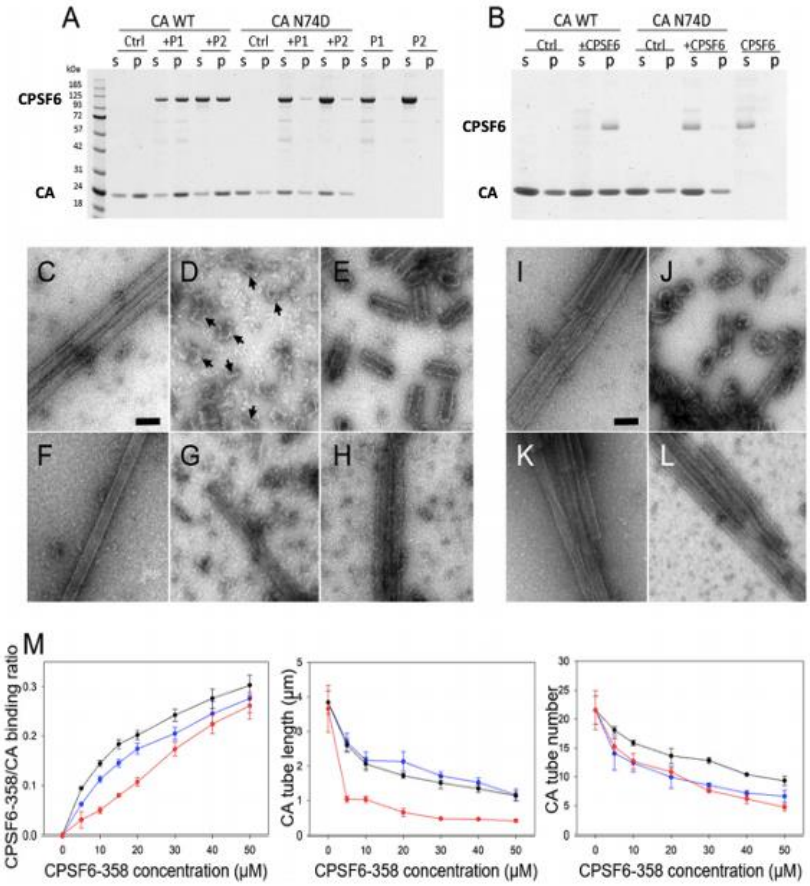

Figure 13 CPSF6-358 binds and disrupts WT CA tubular assemblies. (A) SDS-PAGE of WT and N74D CA assemblies, following incubation with His6-albumin–CPSF6-358, from P1 or P2 and centrifugation. The gel was Coomassie blue stained, with supernatant (s) and pellet (p) samples indicated. (B) SDS-PAGE of WT and N74D CA assemblies following incubation with untagged CPSF6-358 and centrifugation. (C to H) Representative negative-stain EM micrographs of the samples in panel A. (C to E) WT CA tubular assemblies alone (C) or with 30 μM P1 (D) or 30 μM P2 (E) His6-albumin–CPSF6-358. (F to H) CA N74D alone (F) or with 30 μM P1 (G) or 30 μM P2 (H) His6-albumin–CPSF6-358. The arrows indicate the capsid fragments. (I to L) Representative negative-stain EM micrographs of the samples in panel B. Shown are WT CA tubular assemblies alone (I) or with 30 μM CPSF6-358 (J) and CA N74D tubular assemblies alone (K) or with 30 μM CPSF6-358 (L). Scale bars, 100 nm. (M) Dose-dependent effect of CPSF6-358 on CA tubes. Shown is the binding of P1 (blue), P2 (black), and CPSF6-358 (red) to assembled WT CA tubes (left). The effects of P1 (blue), P2 (black), and CPSF6-358 (red) binding on the average length of tubes (middle) and on the number of remaining initial tubular assemblies (right) were measured. The error bars indicate the standard deviation of the values.

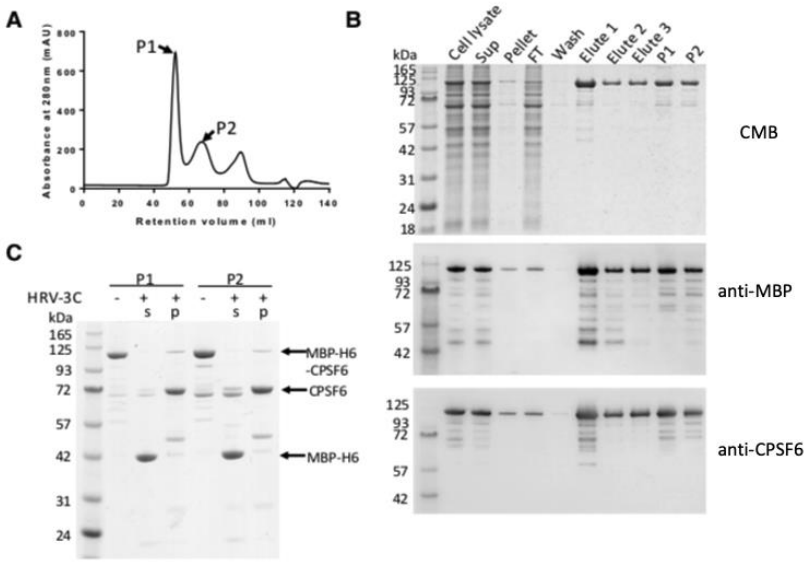

Figure 14 Purification of MBP-CPSF6 with an MBP tag from mammalian cell expression system. (A) Gel filtration profile of the protein eluted from the Superdex 200 16/60 column. The two MBP-CPSF6 peaks are labeled P1 and P2. (B) SDS-PAGE and Western blot analysis of MBP-CPSF6 purification. Samples taken from cell lysate, supernatant (sup), pellet, flowthrough (FT), wash, elute 1, 2, and 3 from Amylose resin, and peaks (P1 and P2) from the Superdex 200 16/60 column (showed in panel A) were stained with Coomassie blue (top) or processed with anti-MBP (middle) or anti-CPSF6 (bottom) antibody, following Western blotting. (C) MBP tag removal analysis, the uncleaved P1 and P2 was shown in lane 2 and 5, the supernatant (s) and pellet (p) of P1 and P2 after cleavage with HRV-3C protease were shown in lane 3, 4, 6, and 7, respectively. Samples were stained with Coomassie blue. Proteins are indicated by arrows on the right.

Incubation of in vitro preassembled WT HIV-1 CA tubes with MBP-CPSF6 (both P1 and P2) resulted in co-sedimentation of MBP-CPSF6/CA complexes in the pelleted fractions (Figure 15A). Negligible binding of MBP-CPSF6 to N74D HIV-1 CA tubes was observed under the same assay conditions. TEM of the negative stained samples showed a drastic structural disruption of capsid tubes when incubated with MBP-CPSF6 (P1 or P2), while N74D CA tubes remained intact (Figure 15C). MBP-CPSF6, by itself, formed protein oligomers for both P1 and P2 fractions in CA assembly buffer (Figure 15B). Binding of MBP-CPSF6 to WT CA tubes resulted in dissolution

of tubes and an appearance of distinctly curved capsid remnants associated with MBP-CPSF6 densities. Intriguingly, the amount of pelleted capsid did not change upon capsid disruption (Figure 15A), suggesting that the predominant effect of MBP-CPSF6 is HIV-1 capsid fragmentation without dissociation into soluble proteins. Dose-dependent binding of MBP-CPSF6 to CA tubes was observed for both MBP-CPSF6 P1 and P2 by TEM (Figure 16). This represents the first direct evidence of full-length CPSF6 binding to and disruption of WT CA tube assemblies. Overall, our *in vitro* binding data suggests that CPSF6 interacts with HIV-1 in a CA-specific manner. This interaction can result in the destabilization of HIV-1 capsid.

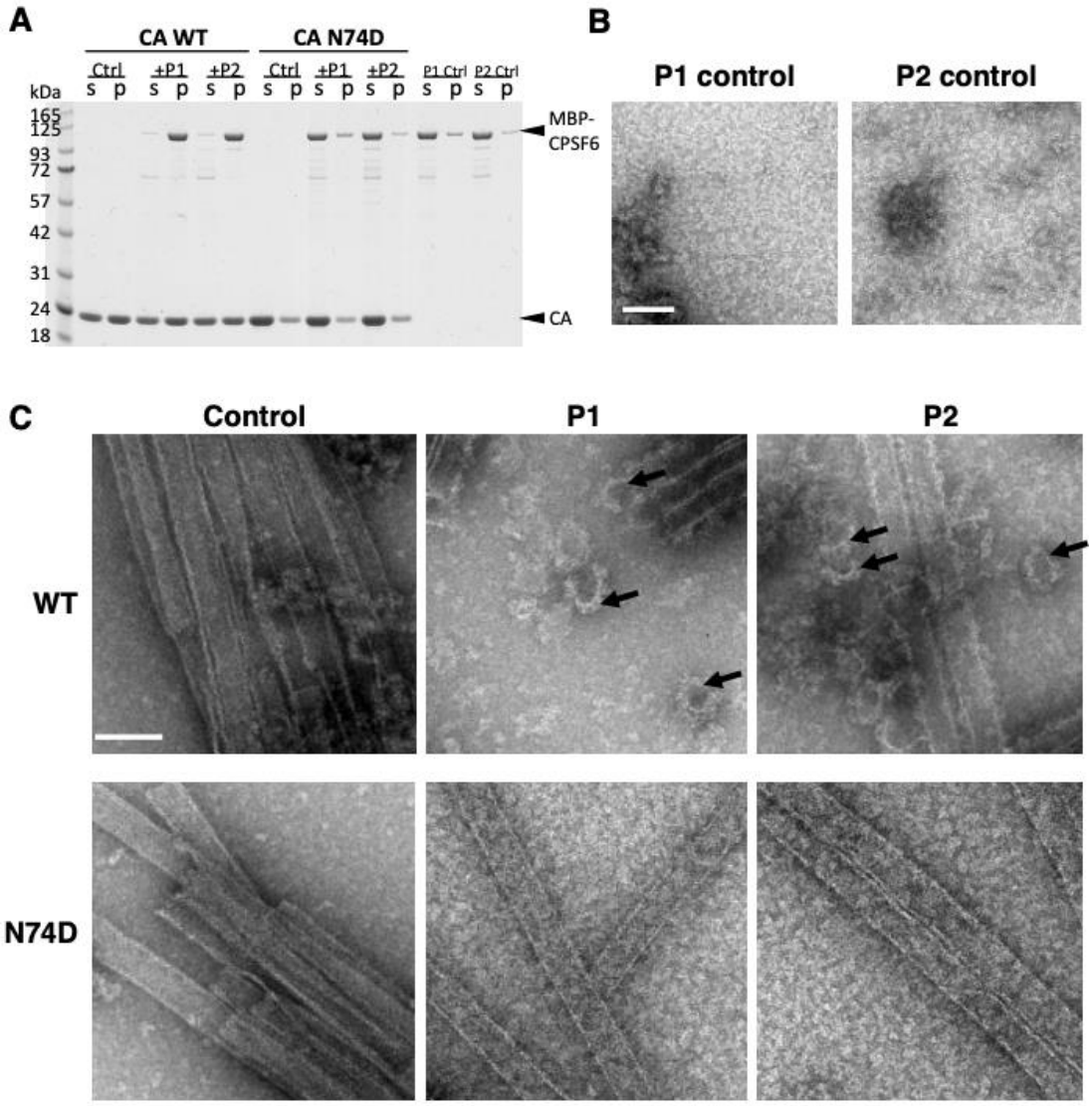

Figure 15 CPSF6 binds to and disrupts CA tubular assemblies. (A) SDS-PAGE analysis of WT and N74D CA assemblies following incubation with MBP-CPSF6 P1 or P2 and centrifugation. The gel was stained with Coomassie blue; supernatant (s) and pellet (p) samples are indicated. (B) Representative negative-stain EM micrographs are shown of P1 or P2 incubated in the buffer. (C) Representative negative-stain EM micrographs are shown of WT CA (top panel) and CA N74D (bottom panel) tubular assemblies alone (control) or with 9 µM MBP-CPSF6 P1 or P2. The arrows indicate capsid fragments. Scale bars, 100 nm.

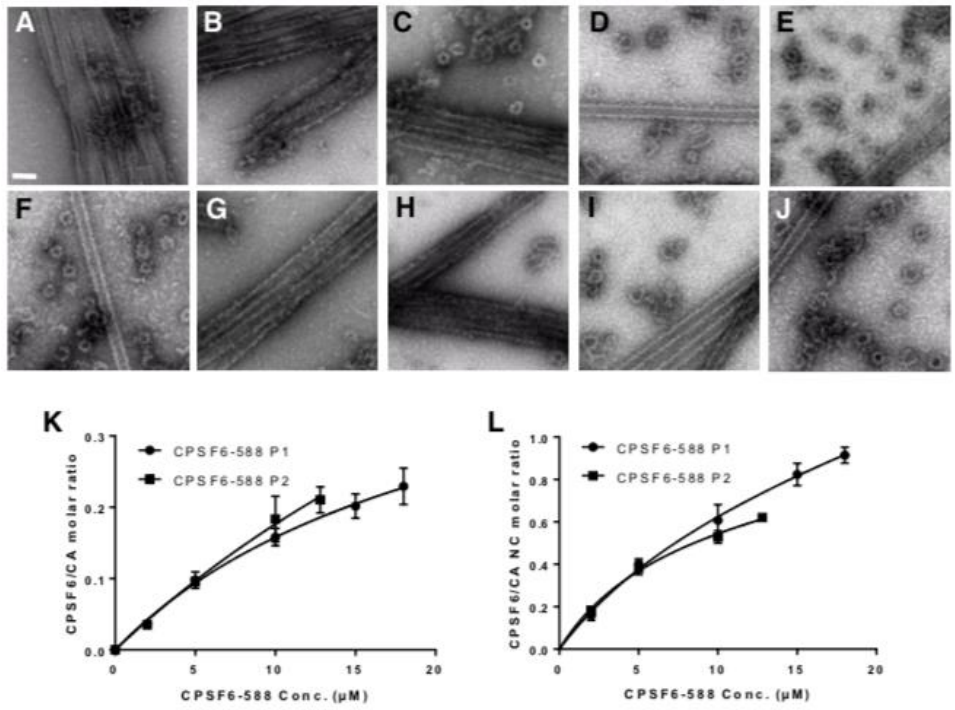

Figure 16 Dose-dependent effect of MBP-CPSF6 on HIV-1 capsid tubes. (A-J) Representative negative-stain EM micrographs of CA with different concentrations of MBP-CPSF6 P1 or P2. WT CA tubular assemblies alone (A) or with 2 μM (B), 5 μM (C), 10 μM (D), 15 μM (E), or 18 μM (F) of MBP-CPSF6 P1, or with 2 μM (G), 5 μM (H), 10 μM (I), or 12.8 μM (J) of MBP-CPSF6 P2. Scale bars, 100nm. (K&L) Dose-dependent effect of MBP-CPSF6 on CA tubes (K) or CA-NC tubes (L). Shown is the binding of P1 (circles) and P2 (squares) to assembled WT CA tubes or CA-NC tubes. The error bars indicate the standard deviation of the values.

2.3.4 CPSF6-358 Promotes WT HIV-1 Capsid Permeabilization after Infection of Cells

Our in vitro data suggest that multiple copies of CPSF6-358 and CPSF6 bind HIV-1 capsid and that binding induces capsid disassembly. It is possible that CPSF6-358 and CPSF6 disrupt HIV-1 capsid in cells as well. However, the amount of CPSF6 presented in the cytoplasm is limited compared to CPSF6-358 (Figure 9B). Therefore, CPSF6-358 is a good tool to test its effect on HIV-1 capsid stability in cells. To test our hypothesis, a capsid permeabilization assay was

performed on HeLa cells (express endogenous CPSF6) or HeLa cells expressing CPSF6-358-eGFP expression after WT HIV-1 infection. This approach allowed us to directly study the effect of CPSF6-358 binding on HIV-1 capsid. Previously, labeling of HIV-1 RNA with 5-ethynyl uridine (EU) during virus production could be detected by staining with an EU-specific dye only when the viral core was permeabilized, normally around 30 to 45 min post-infection of HeLa cells, consistent with capsid uncoating using other assays [107]. In this study, peak WT HIV-1 RNA staining in HeLa cells occurred at 30 min post-infection, whereas peak staining in cells expressing CPSF6-358-eGFP occurred at 20 min post-infection (Figure 17A). Viral RNA staining of N74D HIV-1 did not differ in HeLa cells with or without CPSF6-358-eGFP (Figure 17B). Collectively, these results suggest that premature access of CPSF6-358, and perhaps also full-length CPSF6, oligomerizes on WT HIV-1 capsid in cells and promotes capsid permeabilization.

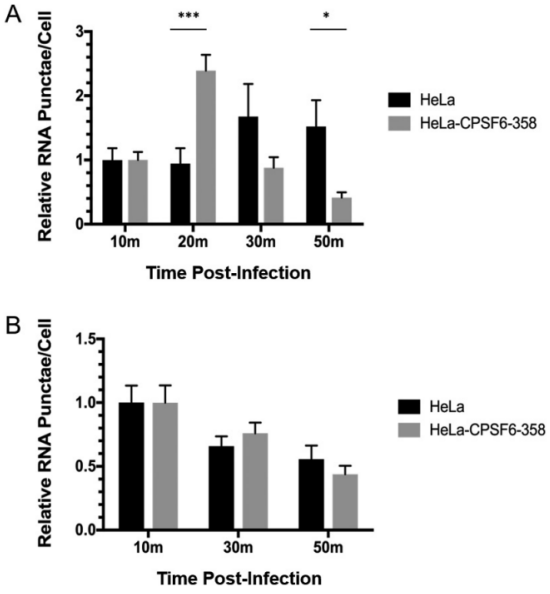

Figure 17 Capsid permeabilization of WT HIV-1 occurs more quickly in HeLa cells expressing CPSF6-358 – eGFP. HeLa cells and HeLa cells expressing CPSF6-358 – eGFP were infected with WT HIV-1 (A) or N74D HIV-1 (B) and stained for viral RNA at different times. The error bars represent SEM of two (WT) or one (N74D) independent experiments. *, P < 0.05; ***, P < 0.001.

2.4 Discussion

HIV-1 capsid has been shown to interact directly or indirectly with many host cell factors [224]. Included in this long list is CPSF6, which is involved in mRNA splicing and polyadenylation in the nucleus [141]. In this study, we detected cytoplasmic, punctate expression of endogenous CPSF6 and fluorescently tagged CPSF6 in the perinuclear region of cells. This is consistent with a recent study in which CPSF6 was associated with HIV-1 complexes in the cytoplasm prior to nuclear import [109].Our imaging data indicate that HIV-1 interacts with cytoplasmic CPSF6 and co-traffics on microtubules in a capsid-dependent manner. Removal or truncation of the CPSF6 RS domain leads to mislocalization of CPSF6 to the periphery of the cell due to loss of TNPO3 binding, and reduced HIV-1 nuclear import and infectivity [141,145,220]. In addition, virus complexes increase in speed in the presence of CPSF6 RS mutants or by introducing the CA N74D mutation that abolishes CPSF6 binding. Interestingly, increased microtubule trafficking of HIV-1 is associated with reduced infectivity. It is possible that faster or more efficient trafficking is due to the modulation of capsid integrity by CPSF6 binding to capsid, which may alter the accessibility of capsid to certain host proteins, such as microtubule motor proteins or motor adaptors. Previously it was shown that HIV-1 capsid traffics on microtubules on its way to the nucleus [108,195]. HIV-1 capsid uncoating is delayed by destabilization of microtubules or knockdown of microtubule motor proteins kinesin and dynein or NPC protein Nup358 [108,194,196], suggesting that microtubule trafficking and NPC binding is linked to capsid uncoating. Recent work from several groups suggests that the main uncoating event occurs at or inside the nucleus [105,106,109]. Here we demonstrate that HIV-1 capsid traffics with CPSF6 and TNPO3 on microtubules and that CPSF6 facilitates CA tubular disassembly.

Our in vitro binding data demonstrated that preassembled CA tubes have a high affinity to purified CPSF6-358, as we could detect substantial binding to CA tubular assemblies in pelleting assays. A similar pattern was seen with purified full-length CPSF6. Since both HIV-1 CA assemblies, CPSF6-358, and CPSF6 oligomerization are required for efficient interaction, CPSF6 and CPSF6-358 may have an intrinsic capsid lattice-sensing ability, similar to other capsid-interacting host factors, such as TRIM5α [117,118,225,226]. CPSF6 and CPSF6-358 oligomers achieve both recognition and disruption of viral capsid assemblies in vitro. In addition, our results show that WT HIV-1 capsid permeabilization occurs more rapidly in the presence of fluorescently labeled CPSF6-358 in cells, suggesting that CPSF6-358 may promote more rapid capsid uncoating. Together, CPSF6 may play a role in both HIV-1 capsid uncoating, which may initiate in the cytoplasm and during the nuclear import [227,228].

2.5 Materials and Methods

2.5.1 Plasmids

The replication-defective HIV-1 proviral plasmid pNLdE-luc (WT and mutants) has been described [141,142]. Viruses were pseudotyped with pL-VSV-G [229]. N74D was also introduced by PCR based mutagenesis in a replication-competent proviral plasmid pNL4-BAL (gift from Ned Landau). The cDNA encoding CPSF6 1 to 358 was amplified and cloned into pcDNA3.1(+) mammalian expression vectors (Thermo Fisher), which were modified to encode a 6×His tag at the N terminus, followed by albumin as a secretion signal protein, using EcoRI and XhoI sites

(modified pcDNA3.1(+) with a His_6-albumin tag was a gift from Troy Krzysiak, University of Pittsburgh) and with a TEV cleavage site immediately following the albumin sequence.

The protein was expressed in a suspension-adapted HEK293 cell line (Expi 293F, a human embryonic kidney cell line; Thermo Fisher). Cells growing in flasks were transfected at a density of 2.5×10^6/ml using ExpiFectamine 293 (Thermo Fisher) according to the manufacturer's instructions. Following transfection, the cells were grown at 37°C with shaking at 125 rpm in 8% CO_2 and 80% humidity for 2 days. The conditioned media, containing secreted protein, were harvested on day 2 by centrifugation at 5,000 rpm for 30 min. The clarified media were pooled and used for purification.

Lentiviral vectors were used to introduce tagged host proteins. Fluorescently tagged CPSF6 and related mutants were introduced into the pSICO vector using BamHI and NotI sites. pSICO-GFP-TNPO3 was created using same sites with GFP-TNPO3 (gift from Ned Landau). pLenti-FAP-GPI was created using the BamHI and NotI sites to move the FAP-GPI sequence from pcDNA-IgKappa-myc-dL5-2XG4S-GPI (Addgene 153308) into pLenti-puro (gift from Ie-Ming Shih; Addgene #39481). Lentiviral packaging plasmid psPAX2 (gift from Dr. Didier Trono, Addgene #109012) and pCMV-VSV-G were used to produce viruses.

The *CPSF6* gene and the MBP tag were amplified by PCR and subcloned into the pcDNA3.1(+) mammalian expression vector (Thermo Fisher Scientific) using the NEBuilder HiFi Assembly kit (New England Biolabs) after linearization with the restriction enzymes Eco RV and Xba I. The resulting insert, designated as MBP-His_6-CPSF6-588, has a leading Kozak sequence, an N-terminal MBP tag, followed by a hexahistidine tag (His_6). HIV-1 CA and CA-NC were previously described [71,230]. In brief, they were cloned from the cDNA of $Pr55^{Gag}$, which was obtained from the NIH AIDS Research and Reference Reagent Program, Division of AIDS,

NIAID, NIH. Briefly, CA and CA-NC regions were amplified and subcloned into pET21 (EMD Chemicals Inc.) using NdeI and XhoI sites. Proteins were expressed and purified as previously described for Gag ($MA_{15–100}$ p6) [73,231].

2.5.2 Cells

HeLa and HEK 293T cell lines were cultured in Dulbecco's modified Eagle medium (DMEM; Thermo Fisher Scientific) supplemented with 10% fetal bovine serum (FBS; Atlanta Biologicals), 100 U/ml penicillin, 100 g/ml streptomycin, and 2 mM L-glutamine (PSG; Thermo Fisher Scientific) at 37° C, 5% CO_2. Stable cell lines were made by transduction with lentiviruses expressing fluorescently tagged host proteins followed by fluorescence activated cell sorting. GHOST-R3/X4/R5 lentiviral reporter cells [232] were cultured in DMEM supplemented with 10% FBS, PSG, 100 g/ml Geneticin G418 (Thermo Fisher Scientific), 0.5 g/ml puromycin (Invitrogen), and 100 g/ml hygromycin B (Invitrogen).

2.5.3 Viruses

Replication-defective HIV-1_{NL4-3}-luciferase virus pseudotyped with VSV-G was produced by transfection of HEK 293T cells or HEK 293T cells stably expressing FAP-GPI with pNLdE-luc, pL-VSV-G, and pVpr-pcs-mRuby3-IN/pVpr-tagRFP-IN/CypA-DsRed at a weight ratio of 5:5:1. Replication-competent HIV-1 was produced by transfection of HEK 293T cells with the full-length proviral construct. Lentiviruses encoding fluorescent host proteins were produced by transfecting HEK 293T cells with lentiviral, packaging, and pCMV-VSV-G plasmids at a weight ratio of 4:3:1. Transfections were performed using Lipofectamine 2000 (Invitrogen).

Viruses were filtered through a 0.45 M filters, concentrated with Lenti-X (Takara Bio) following the manufacturer's protocol, and stored at -80° C. Viruses were quantified by p24 ELISA (XpressBio) and titered on GHOST-R3/X4/R5 cells. FAP-GPI, and mRuby3-IN, labeled viruses were assessed for labeling efficiency by TIRF imaging.

2.5.4 HIV-1 Infection Assays

HeLa cells and differentiated macrophages were seeded in 24-well plates for overnight incubation. Next day, cells were infected with equal p24 amounts of luciferase reporter viruses for 48 h. Cells were lysed and assessed for luciferase production (Promega) with a 1450 MicroBeta TriLux microplate luminescence counter (PerkinElmer).

2.5.5 Fluorescence Microscopy

For fixed cell imaging, HeLa cells or macrophages were plated in MatTek dishes overnight. Synchronized infections were performed by incubation at 4° C for 10 min, followed by aspiration of medium, addition of cold fluorescently labeled HIV-1 (5 ng p24), and further incubation at 4° C for 15 min to allow virus attachment. Cells were then incubated at 37° C for 20 min, followed by washing with warm medium and incubation in fresh medium. At 1 h post-infection, cells were washed with phosphate buffered saline, pH 7.4 (PBS) and fixed with 2% paraformaldehyde (PFA). After permeabilization with 0.1% TritonX-100 for 15 min, the fixed sample was blocked with serum matching the secondary antibody for 45 min. Primary antibodies were added to the fixed cells in PBB buffer (2% bovine serum albumin in PBS) for 1 h and washed with PBB. Secondary

antibodies were added to the cells in PBB buffer for 1 h. After washing with PBB and PBS, the cells were stained with Hoechst (1:2000) and mounted with a coverslip using gelvetol.

A Nikon Ti inverted confocal microscope was used to acquire 3D stacks images of fixed samples with a 100X 1.49 NA oil-immersion objective. LU-NV laser launch (Nikon) was used to emit lasers at 405 nm, 488 nm, 561 nm, and 640 nm. Fields of view were randomly chosen by quick scanning in the Hoechst channel. ND Acquisition in Elements (Nikon) was applied to collect 3D multi-channel imaging (1024 x 1024 pixels) with 2X line averaging. Images of 488 nm and 561 nm channels were acquired by GaAsP detectors (Nikon). 3D stacks were acquired with 0.5 μm step intervals to cover the entire cell volume (6-10 μm) with a motorized piezo Z stage (Nikon).

For live-cell HILO imaging, a Nikon Ti TIRF microscope with a 100X 1.49 NA oil-immersion objective and a Photometrics Prime 95B sCMOS camera was used. In multi-color live-cell imaging experiments, a FLI high speed filter wheel was used. Synchronized infections in HeLa cells were performed as described above. After shifting to 37° C for 20 min, cells were washed with pre-warmed fresh FluoroBrite medium (Thermo Fisher Scientific). After 1 h post-infection, the MatTek dish was loaded on the stage insert and maintained at 37° C (Tokai Hit stage chamber). Each image was acquired at least 1 frame per second (FPS) to track viruses for 10 min. For visualizing microtubules, 1 M SiR-tubulin (Cytoskeleton) was added to the medium 30 min prior to imaging. For visualizing viral membranes, the MG-B-Tau FAP dye [233] was added to the virus at 500 nM for 10 min prior to addition to cells. RAM capture in Nikon Elements was used to achieve faster multi-color live-cell imaging (2 frame per sec).

2.5.6 Imaging Quantification and Data Analysis

All imaging quantification was performed with General Analysis 3 in Nikon Elements (5.20.00 or above). Briefly, a cell nucleus binary mask was created by Hoechst signal to calculate the number of cells in each field of view. CPSF6 localization and quantification was determined by creating binary masks of CPSF6 within the cells. Cytoplasmic CPSF6 was determined by subtracting the CPSF6 binaries from ones colocalized with Hoechst (nucleus) signal. Mean intensity and volume were recorded for each binary. Virus localization was determined by the Spot Detection function to create binary masks for spots positive for mRuby3/tagRFP, FAP-GPI, or p24 signals. Trafficking data of HIV-1 was determined by using the Track Function with the spot binaries in random and constant motion mode. Any tracks with less than 20 frames were excluded in the data analysis.

2.5.7 Protein Expression and Purification

The full length CPSF6 protein was expressed in a suspension-adapted HEK293 cell line (Expi 293F, Thermo Fisher Scientific) by transfection of expression plasmid using ExpiFectamine 293 (Thermo Fisher Scientific) according to the manufacturer's instructions. Following transfection, the cells were grown at 37°C by shaking at 125 rpm in 8% CO2, 80% humidity for 2 days. The cells were harvested after 48 h of transfection by centrifugation at 100g for 10 min. The cell pellet was washed with cold PBS and flash-frozen and stored at -80° C.

The thawed cell pellet was resuspended in buffer A (50 mM HEPES-KOH (pH 8), 500 mM NaCl, and 5% glycerol, 2 mM DTT) supplemented with detergents (1% Tween 20 and 0.3% NP-40), deoxyribonuclease I (50 g/ml; Sigma Aldrich) in the presence of a cocktail of protease

inhibitors (Roche). After 2 h of rotation at 4° C, the lysate was homogenized by 15 strokes in an ice-cold, tight-fitting Dounce homogenizer. The homogenate was then centrifuged at 21,000*g* at 4°C for 30 min. After centrifugation, the supernatant was collected and mixed with 1 ml of amylose agarose resin (New England Biolabs) pre-equilibrated with buffer A per 50 ml of cell homogenate. The mixture was incubated with rotation at 4° C for 2 h and then transferred to a column. The resin was washed with 50x resin volume of buffer A. To elute the recombinant protein, the resin was incubated, in batch, with buffer A containing 100 mM maltose for 15 min at 4° C, and the flow through was collected as eluate. The eluate was applied to a Hi-Load Superdex 200 16/60 column (GE Healthcare) in a buffer A, and fractions containing target protein were collected and concentrated to 6-8 mg/ml using Amicon concentrators (Millipore, Billerica, MA, USA), flash-frozen with liquid nitrogen, and stored at -80° C.

2.5.8 SDS-PAGE and Western Blot Analysis

For *in vitro* CPSF6 experiments, an equal volume of cell lysate and each fraction from the column were mixed with 4x NuPAGE LDS sample buffer (Thermo Fisher Scientific) supplemented with 10 mM DTT and loaded onto a 10% Bis-Tris NuPAGE gel (Thermo Fisher Scientific), alongside a protein molecular weight marker (BLUEstain protein ladder, Gold Biotechnology). Gels were run at 100 V for 15 min and then 150 V for 40 min in NuPAGE MES SDS running buffer and the proteins were subsequently transferred onto PVDF or nitrocellulose membranes using iBlot transfer stacks (Thermo Fisher Scientific). The membranes were blocked at ambient temperature for 1 h in BSA blocking buffers, followed by overnight at 4° C with rabbit anti-Maltose Binding Protein antibody (ab9084, Abcam) or rabbit anti-CPSF6 antibody (EPR12898, Abcam), then a further hour with monoclonal anti-rabbit immunoglobulins−alkaline

phosphatase antibody at ambient temperature. Between each antibody incubation, the membranes were washed three times with Tris-Buffered Saline (TBS) buffer containing 0.1% Tween 20 and finally the membranes were developed with BCIP/NBT color development substrate (Promega) to enable visualization of protein bands (Promega, USA). Each experiment was performed at least three times.

For measurement of CPSF6 expression in cells, an equal number of transduced and puromycin-selected HeLa cells or PBMCs were lysed with RIPA buffer (Bio-Rad), mixed with sample buffer (Bio-Rad), and heated to 100° C for 5 min. Denatured cell lysate was run on pre-casted 4- 15% Criterion Tris-HCl gels (Bio-Rad) at 150 V for 1.5 h. Proteins were transferred to nitrocellulose membranes using a semi-dry transfer apparatus (Thermo Fisher Scientific) at 160 mA for 1 h. The membranes were blocked with 5% milk in PBS containing 0.1% Tween-20 at room temperature for 20 min. Primary antibodies anti-CPSF6 (NBP1-85676) and anti-tubulin (T5168, Sigma Aldrich) were used with secondary anti-mouse IgG or anti-rabbit IgG conjugated with horseradish peroxidase antibodies (A9917 and AP132P, Sigma Aldrich). SuperSignal West Pico Chemiluminescent substrate (Thermo Fisher Scientific) was used to visualize protein bands with Amersham Hyperfilm (GE).

2.5.9 Capsid Binding Assay

Tubular assemblies of WT HIV-1 CA protein were prepared at 80 μM (2 mg/ml) in 1 M NaCl and 50 mM Tris-HCl (pH 8.0) buffer at 37° C for 1 h. N74D CA was dialyzed against 1 M NaCl and 50 mM Tris-HCl (pH 8.0) buffer at 4° C overnight at the concentration of 20 mg/ml. Before binding, the assembled mixture was diluted to 80 μM (2 mg/ml). For the binding assays, the binding buffer was the same as the stock buffer for purified CPSF6-358 or MBP-CPSF6

proteins described above. Different concentrations of CPSF6-358 or MBP-CPSF6 were added to preassembled CA tubes at CA concentration of 64 μM. The reaction mixtures were incubated on a rocking platform at room temperature for 1 h with gentle mixing at 10 min intervals. At the end of incubation, 5 μl samples were withdrawn from the reaction mixtures and immediately used for EM analysis. The remaining samples were pelleted at 21,000 g with a SORVAL Legend micro 21R centrifuge (Thermo Fisher Scientific) for 30 min and supernatants (s) and pellets (p, resuspended in the same volume) were mixed with 4x LDS loading buffer for gel analysis. Supernatant and pellet samples, without boiling, were loaded on 10% SDS-PAGE and stained with Coomassie Blue. Each experiment was performed at least three times.

To determine the binding ratio of CPSF6-358 or MBP-CPSF6:CA, SDS-PAGE gels were scanned using an Epson 4990 scanner. The integrated intensities of CA and CPSF6-358 or MBP-CPSF6 protein bands were measured using Image J 1.40 program (NIH). The molar ratios were calculated according to the formula (MBP-CPSF6 intensity/MBP-CPSF6 molecular weight)/(CA intensity/CA molecular weight) and calibrated using the input ratios as standards.

2.5.10 TEM Analysis

The morphologies of different variants of CA assemblies and CA–MBP-CPSF6 or CPSF6-358 complexes were characterized by TEM. Samples were stained with fresh 2% uranyl formate, deposited onto 400-mesh carbon-coated copper grids, and dried for 30 min. TEM images were acquired on a Tecnai T12 transmission electron microscope at 120 kV.

2.5.11 Statistics

Each virus infection experiment and associated imaging analysis was performed in at least two separate replicates. Compiled data was obtained from minimally two independent experiments or three donors. Statistical significance was determined by two-sided unpaired Student's *t* test using Prism (GraphPad). *P* values of <0.05 were considered statistically significant. *P* values > 0.05, ns; 0.01 - 0.05, *; 0.01 - 0.001, **; 0.001 - 0.0001, ***; < 0.0001, ****.

2.6 Acknowledgements

We would like to thank Mark Ross, Greg Gibson, Stephanie Ander, Sharie Ganchua and Chris Kline for technical assistance; and Rahm Gummuluru, Vineet KewalRamani, and Ned Landau for reagents. This work was supported by National Institutes of Health (NIH) P50 grant AI150481 (A.N.E., P.Z., S.C.W., and Z.A.), NIH R01 grant AI052014 (A.N.E.), NIH R01 grant GM114075 (C.T. and M.P.B.), NIH T32 training grant AI065380 (E.A.B.), and the UK Wellcome Trust Investigator Award 206422/Z/17/Z (P.Z.).

3.0 Chapter 3: Depletion of CPSF6 Alters HIV-1 Trafficking and Infection

3.1 Project Summary

This chapter is comprised of results and data adapted from the following manuscript:

Zhong Z, Ning J, Boggs EA, Jang S, Wallace C, Telmer C, Bruchez M., Ahn J, Engelman AN, Zhang P, Watkins SC, Ambrose Z. Cytoplasmic CPSF6 regulates HIV-1 capsid trafficking and infection in a cyclophilin A dependent manner, submitted.

For this chapter, I performed all experiments.

3.2 Introduction

The HIV-1 capsid comprises multiple copies of the capsid (CA) protein assembled into hexamers and pentamers [234], which further assemble into a conical protein shell that encapsulates the viral RNA genome. Following HIV-1 entry into cells, the viral capsid interacts with numerous host cell factors that facilitate uncoating and downstream viral events, including reverse transcription, nuclear entry, and integration site targeting. The surface of the capsid acts as a docking platform for many host cell factors, which either promote infection or enable virus restriction by innate immune responses [116,235,236]. While the structure of the capsid has been well characterized [71,73], much less is known about the detailed structure and function of capsid-binding host factors and their interactions with HIV-1 capsid. In addition, some host factors, including TRIM5α, TRIMCyp, and MxB, must oligomerize to functionally interact with the assembled viral

capsid [237–239]. As such, capsid pattern recognition by host factor oligomers is emerging as a key feature and determinant of viral restriction by these factors. For most capsid-binding host proteins, including CPSF6, how virus-host protein-protein interactions contribute to viral replication or restriction remains unclear.

CPSF6 has been suggested to regulate HIV-1 nuclear entry and integration site targeting through interaction with HIV-1 capsid [153,240]. CPSF6 is a pre-mRNA processing protein as part of the CFIm complex [241,242]. CPSF6-358, which lacks the RS domain, has greater cytoplasmic localization and potent inhibition of HIV-1 infection [141,223]. The antiviral activity of CPSF6-358 depends on its direct binding to HIV-1 capsid at a stage after reverse transcription and before nuclear entry [223], but the mechanism of this inhibition is unclear. The crystal structures of a cross-linked CA hexamer in complex with a CPSF6-358 peptide (residues 314 to 322) reveal a hydrophobic binding pocket encompassing the intermolecular interface between the NTD and the CTD, in which the peptide is anchored via a phenylalanine-glycine (FG) motif [144,243]. This binding pocket is shared among CPSF6, NUP153, and the small-molecule compounds PF-74 and BI-2 [144,243]. Single point mutations in the pocket are sufficient to diminish binding of CPSF6-358 and to rescue infectivity [141,144,213,223]. Importantly, several HIV-1 capsid mutations (A105T, N74D, N57A, A77V, R132K/L136M, M66F, Q67A, K70A, and T107A) have been highly informative for understanding the role of CPSF6 as an HIV-1 cofactor [144,146]. Of particular interest, the HIV-1 CA mutation N74D abolishes CPSF6-358 binding and its antiviral activity [141,144]. While N74D is able to escape the restriction of CPSF6-358, it is restricted in primary macrophages. The restriction has been mapped to the initiation of reverse transcription [142]. Rasaiyaah et al. provided additional information on N74D restriction in macrophages likely due to the fact that HIV-1 N74D is unable

to recruit CPSF6 to evade innate immune sensing [236]. However, the mechanistic basis of N74D restriction in macrophages is not known.

To gain insight into how CPSF6 is involved in HIV-1 early infection and evasion of innate immunity, we evaluated the effect of CPSF6 depletion on HIV-1 infection in multiple cell types. CPSF6 depletion in HeLa cells does not show a significant difference in infectivity and trafficking for both WT and N74D HIV-1. However, the depletion of CPSF6 altered HIV-1 trafficking in macrophages. This corresponds to an alleviated interferon alpha (INFα) production. Together, our data provide new evidence of the role of CPSF6 in HIV-1 trafficking and innate response.

3.3 Results

3.3.1 HIV-1 Trafficking in HeLa Cells Is not Affected by CPSF6 Depletion

To validate that the effect CPSF6 depletion on WT viral complex trafficking, HeLa cells were transduced with lentiviruses expressing an shRNA targeting CPSF6 or a scrambled control shRNA. Knockdown (KD) of CPSF6 was verified by immunofluorescence staining (Figure 18A). Infectivity of WT HIV-1 decreased after CPSF6 depletion (Figure 18B), which may be attributable to previously described reduced cell proliferation or viability [153]. CPSF6 depletion led to no significant effect on WT or N74D HIV-1 particle trafficking speed (Figure 18C).

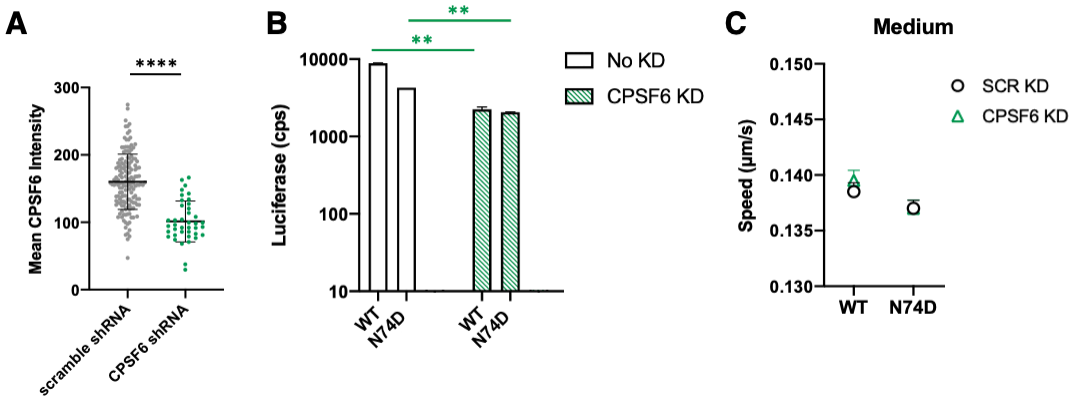

Figure 18 CPSF6 KD in HeLa cells. (A) The mean intensity of CPSF6 immunofluorescence by confocal imaging is shown from individual HeLa cells transduced with lentiviruses expressing scrambled (SCR) or CPSF6 shRNA. The error bars indicate STDEV (n ≥ 157 cells). (B) The infection of WT or N74D HIV-1 in the same cells shown in (C) are graphed. Error bars indicate STDEV of duplicates. (C) The average particle speeds of WT, N74D, or G89V HIV-1 mRuby3-IN complexes in HeLa cells expressing SCR or CPSF6. A representative of 2 independent experiments. Error bars indicate SEM.

3.3.2 CPSF6 Depletion Induces Interferon (IFN) α Production in Primary PBMCs

Infectivity of WT HIV-1 and N74D mutant were performed in phytohemagglutinin (PHA)-stimulated PBMC from 3 donors. Cells were infected in the presence or absence of CPSF6 depletion. Depletion of CPSF6 was verified by western blot quantification (Figures 19A, B). Infection of N74D HIV-1 was inhibited in primary PBMC (Figure 19C), as previously reported [236]. The depletion of CPSF6 also reduces the infectivity of WT HIV-1 (Figure 19C). But we did not see a further reduction of N74D infectivity in CPSF6 depleted PBMCs. Our results agree with the previous report showing CPSF6 is important for optimal HIV-1 infection in primary PMBCs.

It has been suggested that a loss of HIV-1 capsid interaction with host factors, such as CPSF6, can lead to induction of type I interferon in primary T cells and macrophages [236]. Thus,

IFNα production was quantified after HIV-1 infection from the supernatants of PBMC depleted of CPSF6. WT and N74D HIV-1 induced similar levels of IFNα after infection of PMBC cells (Figure 19D). The depletion of CPSF6 significantly increased IFNα production after infection by both WT and N74D viruses, consistent with previous results [236]. Overall, IFNα production in primary PBMCs is dependent on CPSF6. CPSF6 depletion induces IFNα production for both WT and N74D HIV-1.

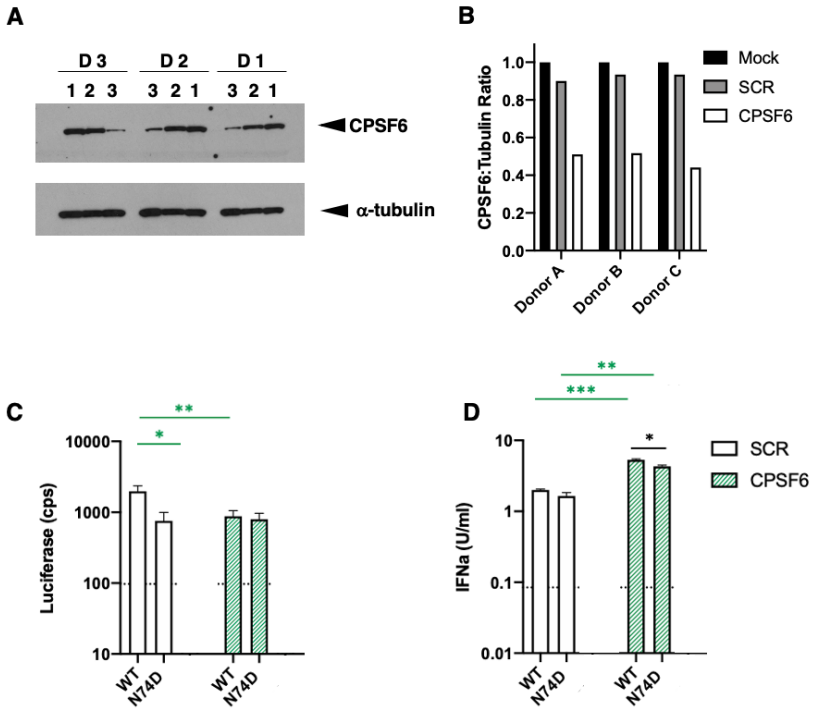

Figure 19 CPSF6 depletion in PBMCs. (A) CPSF6 depletion by shRNA was visualized in stimulated PBMCs by western blot. A scrambled shRNA was used as a knockdown control and α-tubulin was used as a loading control for the gel. Lane 1, no shRNA; Lane 2, scrambled shRNA; Lane 3, CPSF6 shRNA. (B) CPSF6 depletion was quantified by the ratio of CPSF6 to α-tubulin measured by western blot for activated PBMCs from each donor. (C) Infections with WT and N74D HIV-1 were measured in primary PBMC cells after the shRNA depletion of CPSF6. Data from one representative donor was shown. (D) IFNα production from infected PBMC shown in (C) was quantified using HEK 293T ISRE-luc indicator cells.

3.3.3 Depletion of CPSF6 in Macrophages Results in Decreased HIV-1 infectivity and Altered Trafficking

As we and others previously showed that N74D HIV-1 has an early infectivity defect in monocyte-derived macrophages (MDM), we investigated whether intracellular trafficking of HIV-1 is dependent on CPSF6. MDMs were stained for endogenous CPSF6 expression. As in HeLa cells, CPSF6 expression was nuclear in MDMs (Figure 20A). However, infection with WT HIV-1 failed to induce higher order CPSF6 complex formation in the cytoplasm (data not shown), consistent with previous results and indicative of less cytoplasmic CPSF6 expression in MDMs compared to HeLa cells.

CPSF6 was depleted with shRNA in MDMs, which was confirmed and quantified by immunostaining (Figures 20A, B). Trafficking of mRuby3-IN complexes was evaluated in MDM from 3 donors with and without CPSF6 depletion. CPSF6 depletion led to a significant increase in speed and track length of WT HIV-1 complexes (Figure 20C). However, loss of CPSF6 led to a modest decrease in WT HIV-1 single-cycle infectivity with only Donor 2 being significant (Figure 20D). Despite effects on infectivity, CPSF6 KD resulted in significantly increased IFNα production in all 3 donors (Figure 20E). Replication of WT HIV-1 is inhibited in macrophages with CPSF6 depletion (Figure 31B). These results suggest that loss of CPSF6 in macrophages affects WT HIV-1 CA trafficking and increased production of type I IFN, leading to decreased infection.

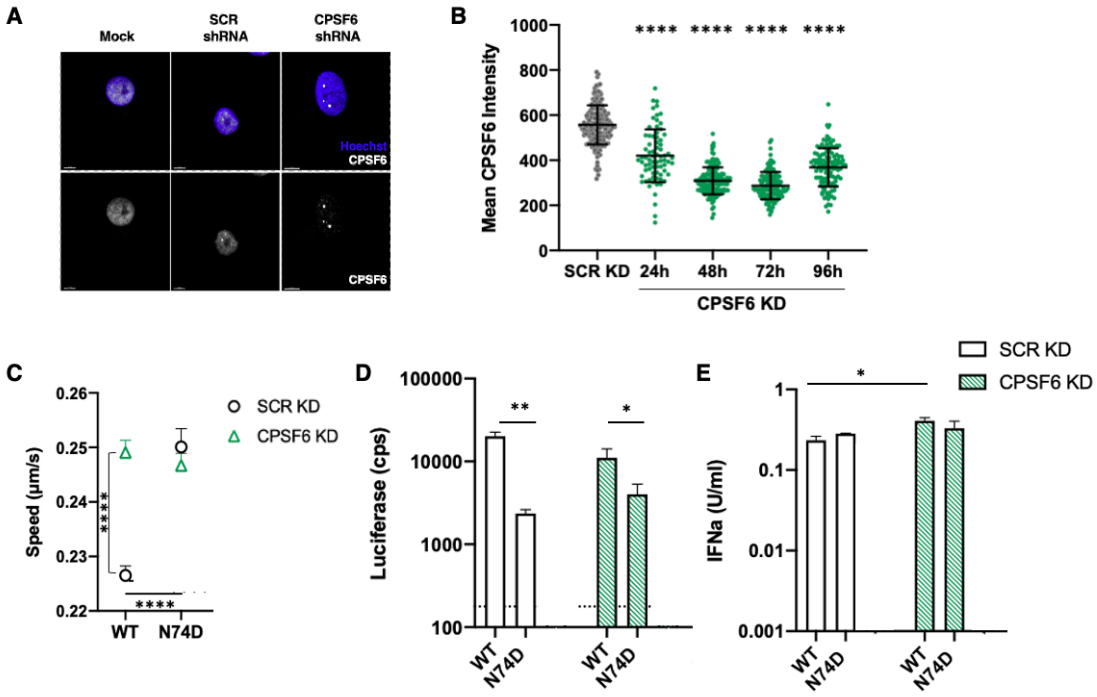

Figure 20 CPSF6 depletion in macrophages. (A) Representative confocal micrographs of MDM, transduced with scrambled shRNA (SCR) or CPSF6 shRNA, stained with Hoechst (blue) are shown. (B) The mean intensity of CPSF6 antibody staining is shown from individual MDM transduced with lentiviruses expressing SCR or CPSF6 shRNA. MDM cells were fixed at different time point post transduction and imaged by confocal microscopy. The error bars indicate STDEV of n ≥ 77 cells. (C) The average particle speeds of WT or N74D HIV-1 mRuby3-IN complexes in MDM from 1 of 3 individual donors with SCR KD or CPSF6 KD are shown. Error bars indicate SEM. (D) The infection of WT or N74D HIV-1 in the same cells shown in (B) are graphed. Error bars indicate STDEV of duplicates and the dotted line represents the average luciferase expression of uninfected cells. (E) IFNα was measured in the supernatants of cells shown. Error bars indicate STDEV of duplicates. The limit of detection is 0.001 U/ml. Results are shown as means +/- STDEV.

3.4 Discussion

Although studies have shown depletion of CPSF6 has minimal effect on HIV-1 infectivity in cell models [145,153], the interaction between HIV-1 CA and CPSF6 is important for HIV-1 infection *in vivo* [146]. In fact, the use of CPSF6 as a facilitatory factor is unique for primate lentiviruses [244]. In this study, we showed that the effect of CPSF6 depletion varies in different cell types. In HeLa cells, no significant defect in trafficking and infectivity was observed upon CPSF6 depletion. In contrast, infection of HIV-1 after CPSF6 knock down leads to a significant increase of INFα production in PBMCs and macrophages. This corresponds to reduced infectivity and replication in CPSF6-depleted primary cells. Together, these data are consistent with the result from Rasaiyaah et al. [236], suggesting that CPSF6 helps HIV-1 directly or indirectly to evade innate immune detection in primary cell types.

HIV-1 trafficking has been shown to be an important step in HIV-1 infection [108,194–196]. Recently, Bejarano et al. showed that depletion of CPSF6 had no effect on HIV-1 trafficking to the nucleus in macrophages [227]. Bejarano et al. utilized a longer and slower duration of imaging to capture the start and end of particle trafficking to examine whether HIV-1 arrives at the nucleus. However, this method lacks the ability to analyze HIV-1 trafficking patterns and movement data at high temporal resolution. Here, we showed that either depletion of CPSF6 or infection with N74D HIV-1 led to an altered HIV-1 trafficking pattern. HILO imaging is much faster (≥ 1 frame per second for 10 mins) and focuses on speed and track length. Therefore, we can differentiate increased speed and length of viral particles when CPSF6 was depleted or capsid had the N74D mutation. This altered trafficking pattern was correlated to the reduced infection and replication, and induction of IFNα production. Together, our data suggest CPSF6 is important for proper HIV-1 trafficking. Lack of CPSF6 interaction, either by depletion of CPSF6 or HIV-1 CA mutation

N74D, leads to an altered trafficking potentially by exposing HIV-1 to innate sensing factors and therefore restricts the infection in macrophages.

Interestingly, these differences were not observed in HeLa cells, as depletion of CPSF6 had no significant effect on trafficking and infection for either WT or N74D HIV-1. It is possible that HeLa cells lack the host factors that recognize HIV-1 to mount a type I interferon response. Moreover, the increased level of another host factor, cyclophilin A (CypA), in HeLa cells may also lead to this cell type difference [245]. It will be of interest to examine the role of CypA and CPSF6 in HIV-1 early infection.

3.5 Materials and Methods

3.5.1 Plasmids

The replication-defective HIV-1 proviral plasmid pNLdE-luc (WT and mutants) has been described [141,142]. Viruses were pseudotyped with pL-VSV-G [229]. N74D was also introduced by PCR based mutagenesis in a replication-competent proviral plasmid pNL4-BAL (gift from Ned Landau).

Lentiviral vectors were used to introduce tagged host proteins or shRNA to cells. Fluorescently tagged CPSF6 and related mutants were introduced into the pSICO vector using BamHI and NotI sites. The lentiviral vector pHIVSIREN expressing CPSF6 shRNA [236] was a gift from Greg Towers. pLKO.1-puro-shNT (gift from Jacob Corn, Addgene #109012) was used as a scrambled shRNA control lentiviral packaging plasmid psPAX2 (gift from Dr. Didier Trono, Addgene #109012) and pCMV-VSV-G were used to produce viruses.

3.5.2 Cells

HeLa and HEK 293T cell lines were cultured in Dulbecco's modified Eagle medium (DMEM; Thermo Fisher Scientific) supplemented with 10% fetal bovine serum (FBS; Atlanta Biologicals), 100 U/ml penicillin, 100 g/ml streptomycin, and 2 mM L-glutamine (PSG; Thermo Fisher Scientific) at 37° C, 5% CO_2. HEK 293T cells stably expressing the firefly luciferase gene downstream of the interferon-sensitive response element (HEK293-ISRE-luc) [246] were a gift from Rahm Gummuluru and were cultured in complete DMEM supplemented with 2 g/ml puromycin (Invitrogen). GHOST-R3/X4/R5 lentiviral reporter cells [232] were cultured in DMEM supplemented 10% FBS, PSG, 100 g/ml geneticin G418 (Thermo Fisher Scientific), 0.5 g/ml puromycin (Invitrogen), and 100 g/ml hygromycin B (Invitrogen). Human PBMCs were isolated from leukapheresis obtained from the Central Blood Bank (Pittsburgh, PA) using Ficoll-Paque Plus (GE Healthcare) density gradient centrifugation, following the manufacturer's instructions. PBMCs were cultured in RPMI 1640 medium (Thermo Fisher Scientific) supplemented with 10% FBS, PSG, and 20 U/ml recombinant interleukin-2 (IL-2; Thermo Fisher Scientific) at 37° C, 5% CO_2. To expand T lymphocytes, PBMCs were stimulated with 50 U/ml IL-2 and 5 μg/ml phytohemagglutinin (PHA; Sigma-Aldrich) for 72 h prior to infection or transduction. CD14+ monocytes were isolated from PBMCs using human anti-CD14 magnetic beads with LS Columns (Miltenyi Biotec). CD14+ monocytes were differentiated into MDM in RPMI 1640 medium supplemented with 10% FBS, PSG, and 50 ng/ml recombinant granulocyte–macrophage colony-stimulating factor (R&D Systems) for 7 days at 37° C, 5% CO_2 prior to experimentation.

3.5.3 Viruses

Replication-defective HIV-1_{NL4-3}-luciferase virus pseudotyped with VSV-G was produced by transfection of HEK 293T cells with pNLdE-luc, pL-VSV-G, and pVpr-pcs-mRuby3-IN/pVpr-tagRFP-IN at a weight ratio of 5:5:1. Replication-competent HIV-1 was produced by transfection of HEK 293T cells with the full-length proviral construct. Lentiviruses encoding fluorescent host proteins were produced by transfecting HEK 293T cells with lentiviral, packaging, and pCMV-VSV-G plasmids at a weight ratio of 4:3:1. Transfections were performed using Lipofectamine 2000 (Invitrogen). Viruses were filtered through a 0.45 M filters, concentrated with Lenti-X (Takara Bio) following the manufacturer's protocol, and stored at -80° C. Viruses were quantified by p24 ELISA (XpressBio) and titered on GHOST-R3/X4/R5 cells. mRuby3-IN labeled viruses were assessed for labeling efficiency by TIRF imaging.

3.5.4 HIV-1 Infection Assays

HeLa cells, stimulated PBMC, and differentiated macrophages were seeded in 24-well plates overnight and then transduced with shRNA encoding viruses. 48 h post transduction, cells were infected with equal p24 amounts of luciferase reporter viruses for 48 h. Cells were lysed and assessed for luciferase production (Promega) with a 1450 MicroBeta TriLux microplate luminescence counter (PerkinElmer).

3.5.5 Fluorescence Microscopy

For fixed cell imaging, HeLa cells or macrophages were plated in MatTek dishes overnight. Synchronized infections were performed by incubation at 4° C for 10 min, followed by aspiration of medium, addition of cold fluorescently labeled HIV-1 (5 ng p24), and further incubation at 4° C for 15 min to allow virus attachment. Cells were then incubated at 37° C for 20 min, followed by washing with warm medium and incubation in fresh medium. At 1 h post-infection, cells were washed with phosphate buffered saline, pH 7.4 (PBS) and fixed with 2% paraformaldehyde (PFA). After permeabilization with 0.1% TritonX-100 for 15 min, the fixed sample was blocked with serum matching the secondary antibody for 45 min. Primary antibodies were added to the fixed cells in PBB buffer (2% bovine serum albumin in PBS) for 1 h and washed with PBB. Secondary antibodies were added to the cells in PBB buffer for 1 h. After washing with PBB and PBS, the cells were stained with Hoechst (1:2000) and mounted with a coverslip using gelvetol.

A Nikon Ti inverted confocal microscope was used to acquire 3D stacks images of fixed samples with a 100X 1.49 NA oil-immersion objective. LU-NV laser launch (Nikon) was used to emit lasers at 405 nm, 488 nm, 561 nm, and 640 nm. Fields of view were randomly chosen by quick scanning in the Hoechst channel. ND Acquisition in Elements (Nikon) was applied to collect 3D multi-channel imaging (1024 x 1024 pixels) with 2X line averaging. Images of 488 nm and 561 nm channels were acquired by GaAsP detectors (Nikon). 3D stacks were acquired with 0.5 μm step intervals to cover the entire cell volume (6-10 μm) with a motorized piezo Z stage (Nikon).

For live-cell HILO imaging, a Nikon Ti TIRF microscope with a 100X 1.49 NA oil-immersion objective and a Photometrics Prime 95B sCMOS camera was used. In multi-color live-cell imaging experiments, a FLI high speed filter wheel was used. Synchronized infections in HeLa cells were performed as described above. After shifting to 37° C for 20 min, cells were washed

with pre-warmed fresh FluoroBrite medium (Thermo Fisher Scientific). After 1 h post-infection, the MatTek dish was loaded on the stage insert and maintained at 37° C (Tokai Hit stage chamber). Each image was acquired at least 1 frame per second (FPS) to track viruses for 10 min. For visualizing microtubules, 1 μM SiR-tubulin (Cytoskeleton) was added to the medium 30 min prior to imaging. For visualizing viral membranes, the MG-B-Tau FAP dye [233] was added to the virus at 500 nM for 10 min prior to addition to cells. RAM capture in Nikon Elements was used to achieve faster multi-color live-cell imaging (2FPS).

3.5.6 Imaging Quantification and Data Analysis

All imaging quantification was performed with General Analysis 3 in Nikon Elements (5.20.00 or above). Briefly, a cell nuclei binary mask was created by Hoechst signal to calculate the number of cells in each field of view. CPSF6 localization and quantification was determined by creating binary masks of CPSF6 within the cells. Cytoplasmic CPSF6 was determined by subtracting the CPSF6 binaries from ones colocalized with Hoechst (nucleus) signal. Mean intensity and volume were recorded for each binary. Virus localization was determined by the Spot Detection function to create binary masks for spots positive for mRuby3/tagRFP, FAP-GPI, or p24 signals. Trafficking data of HIV-1 was determined by using the Track Function with the spot binaries in random and constant motion mode. Any tracks with less than 20 frames were excluded in the data analysis.

3.5.7 SDS-PAGE and Western Blot Analysis

For measurement of CPSF6 expression in cells, an equal number of transduced and puromycin-selected PBMCs were lysed with RIPA buffer (Bio-Rad), mixed with sample buffer (Bio-Rad), and heated to 100° C for 5 min. Denatured cell lysate was run on pre-casted 4-15% Criterion Tris-HCl gels (Bio-Rad) at 150 V for 1.5 h. Proteins were transferred to nitrocellulose membranes using a semi-dry transfer apparatus (Thermo Fisher Scientific) at 160 mA for 1 h. The membranes were blocked with 5% milk in PBS containing 0.1% Tween-20 at room temperature for 20 min. Primary antibodies anti-CPSF6 (NBP1-85676) and anti-tubulin (T5168, Sigma Aldrich) were used with secondary anti-mouse IgG or anti-rabbit IgG conjugated with horseradish peroxidase antibodies (A9917 and AP132P, Sigma Aldrich). SuperSignal West Pico Chemiluminescent substrate (Thermo Fisher Scientific) was used to visualize protein bands with Amersham Hyperfilm (GE).

3.5.8 Statistics

Each virus infection experiment and associated imaging analysis was performed in at least two separate replicates. Compiled data was obtained from minimally two independent experiments or three donors. Statistical significance was determined by two-sided unpaired Student's *t* test using Prism (GraphPad). *P* values of <0.05 were considered statistically significant. *P* values > 0.05, ns; 0.01 - 0.05, *; 0.01 - 0.001, **; 0.001 - 0.0001, ***; < 0.0001, ****.

3.6 Acknowledgements

We would like to thank Chris Kline for technical assistance; and Rahm Gummuluru, Vineet KewalRamani, and Ned Landau for reagents. This work was supported by National Institutes of Health (NIH) P50 grant AI150481 (A.N.E., P.Z., S.C.W., and Z.A.), NIH R01 grant AI052014 (A.N.E.), NIH R01 grant GM114075 (C.T. and M.P.B.), NIH T32 training grant AI065380 (E.A.B.), and the UK Wellcome Trust Investigator Award 206422/Z/17/Z (P.Z.).

4.0 Chapter 4: CypA Modulates CPSF6-Dependent HIV-1 Trafficking in HeLa Cells but not in Macrophages

4.1 Project Summary

This chapter is comprised of results and data adapted from the following manuscripts:

Ning J*, **Zhong Z***, Fischer DK, Harris G, Watkins SC, Ambrose Z, Zhang P. Truncated CPSF6 Forms Higher-Order Complexes That Bind and Disrupt HIV-1 Capsid. J Virol. 2018 Jun 13;92(13):e00368-18. doi: 10.1128/JVI.00368-18. PMID: 29643241; PMCID: PMC6002704.

Zhong Z, Ning J, Boggs EA, Jang S, Wallace C, Telmer C, Bruchez M., Ahn J, Engelman AN, Zhang P, Watkins SC, Ambrose Z. Cytoplasmic CPSF6 regulates HIV-1 capsid trafficking and infection in a cyclophilin A dependent manner, submitted.

In this chapter, I performed experiments to show that CPSF6 forms higher order complexes upon infection with HIV-1, CypA binding to capsid can protect HIV-1 from premature access of CPSF6. I also conducted imaging and infection experiments to show CypA modulates CPSF6-dependent HIV-1 trafficking in HeLa cells but not in macrophages, and depletion of CPSF6 can restore HIV-1 trafficking and infectivity for G89V HIV-1 in HeLa cells and PMBC cells but not in macrophages. Lastly, my imaging results suggest the difference between HeLa cells and PMBC cells compared to macrophages may be due to the distinguished CypA localization in each cell type. Jiying Ning performed the *in vitro* CA-NC tube binding assay and quantification. Emerson Boggs conducted confocal fixed-cell imaging of HeLa cells and macrophages to examine the expression of CypA, CPSF6, and tubulin.

4.2 Introduction

HIV-1 capsid is a unique structure that assembles after viral proteolytic cleavage of the Gag and Gag-Pol polyproteins during or after virus budding and release from cells. Multiple HIV-1 CA proteins form a conical-shaped core consisting of approximately 200 hexamers and 12 pentamers, which encapsulates two copies of the RNA genome [72,73]. HIV-1 capsid uncoating is dependent on microtubule trafficking [194,196,247,248], and may occur in a multi-step process [107]. HIV-1 infection requires active transport of the viral RTC/PIC through the cellular NPC [249], and the majority of CA is likely uncoated at the NPC and/or within the nucleus [105,106,109,250,251]. Single mutations in CA can greatly impact the stability of HIV-1 capsid, altering its uncoating and affecting virus infectivity [252,253].

HIV-1 capsid has been shown to bind several host proteins during infection [224]. Two examples are CypA [182,254], which is relatively abundant in cells [255], and CPSF6 [141]. Disruption of HIV-1 capsid binding to CypA can occur via amino acid substitution, such as G89V and P90A [256,257], in the loop between helices 4 and 5 in CA or by treatment with small molecule inhibitors, such as cyclosporine A (CsA) [182]. Inability to bind to CypA in target cells can affect the infectivity of the invading HIV-1 particle [258]. CypA dependence is cell type specific and has been shown to affect multiple steps in the virus life cycle, including capsid uncoating, reverse transcription, nuclear import, or integration [140,259–261].

In this study, we investigated whether CPSF6 competes for HIV-1 CA binding with CypA in the host cell cytoplasm. In addition, we explored whether CypA binding affects capsid trafficking and subsequent virus infectivity in different cell types. Using live-cell microscopy, we demonstrated that inhibiting HIV-1 capsid interaction with CypA led to the increased association

of viral particles or *in vitro* CA assemblies with CPSF6 and changes in WT HIV-1 complex trafficking that corresponded to reduced infectivity.

4.3 Results

4.3.1 HIV-1 Infection Induces Higher-Order Complexes of CPSF6-358 in Cells

Our previous in vitro data suggest that multiple copies of CPSF6-358 bind HIV-1 capsid and that binding induces capsid disassembly. To visualize the interaction of CPSF6-358 with HIV-1 in vivo, we engineered HeLa cells to stably express fluorescently tagged CPSF6-358 and then infected the cells with HIV-1. For CPSF6-358, eGFP or iRFP670 was fused to the C terminus and stably expressed in HeLa cells. Similar to what has previously been shown, expression of CPSF6-358 potently restricted infection by WT HIV-1, but not N74D HIV-1 [141].

In uninfected HeLa cells expressing CPSF6-358–eGFP, CPSF6-358–eGFP expression was relatively uniform throughout the cell cytoplasm and nucleus (Figure 21A). In contrast, upon WT HIV-1 infection of HeLa cells expressing CPSF6-358–eGFP, distinct green puncta were observed in the cytoplasm (Figure 21A). However, the formation of CPSF6-358–eGFP puncta was not observed after infection with N74D HIV-1 (Figure 21A). To determine if HIV-1 capsid binding is necessary for the formation of the puncta, infections were performed with WT HIV-1 in the presence of PF-74 or with another HIV-1 CA mutant that does not bind to CPSF6, A77V [146]. Like N74D HIV-1, the formation of CPSF6-358–eGFP puncta was not observed despite the presence of mRuby-IN-containing complexes within the cells (Figure 21B). Similar results were observed in cells expressing CPSF6-358–iRFP670 or HIV-1 labeled with Vpr-tagRFP-IN (data not shown).

These results suggest that an increase in the local concentration of CPSF6-358 upon HIV-1 capsid binding likely leads to the formation of higher-order complexes of CPSF6-358.

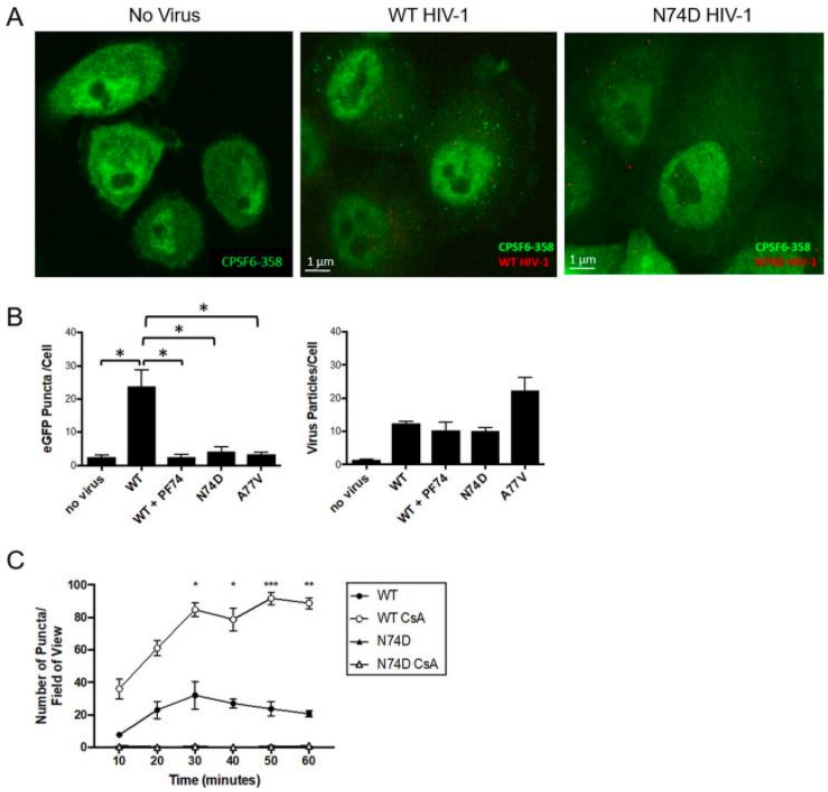

Figure 21 WT HIV-1 infection induces the formation of CPSF6-358 higher-order complexes in HeLa cells. (A) Confocal images of HeLa cells stably expressing CPSF6-358–eGFP before or 30 min after infection with WT HIV-1 or N74D HIV-1. (B) CPSF6-358–eGFP puncta and mRuby-IN particles were quantified per cell (n ≥ 25 z-stacks) at 30 min post-infection with WT HIV-1 in the presence or absence of 10 µM PF-74, N74D HIV-1, or A77V HIV-1. The asterisks denote comparisons with P values of <0.05. (C) HeLa cells stably expressing CPSF6-358–eGFP were treated (open symbols) or not (solid symbols) with 2 µM CsA and synchronously infected with WT HIV-1 or N74D HIV-1. The number of CPSF6-358–eGFP puncta per field of view was determined. The error bars represent the standard error of the mean (SEM). *, P < 0.05; **, P < 0.005; ***, P < 0.001.

4.3.2 CsA Treatment Leads to Faster Formation of CPSF6-358 Higher-Order Complexes

CPSF6-358–eGFP puncta did not always form simultaneously after synchronized infection with WT HIV-1, leading us to hypothesize that another host factor could prevent immediate access of CPSF6-358 to the intracellular capsid. As CypA is known to bind to HIV-1 capsid [182], disruption of CypA-capsid interaction was performed by treatment of cells with CsA, a small molecule binds CypA and prevents CypA to bind to HIV-1 CA. We observed that treatment of cells with CsA resulted in greater numbers of CPSF6-358–eGFP puncta than in untreated cells (Figure 21C). Quantification of mRuby3-IN particles and CPSF6-358–eGFP puncta showed no difference in the number of IN-containing complexes in cells under each treatment condition (data not shown). However, the number of CPSF6-358–eGFP higher-order complexes was significantly higher 30 min post-infection in the presence of CsA (Figure 21C). Live-cell imaging similarly showed that CPSF6-358–eGFP puncta formed more rapidly and increased in number in CsA-treated cells after infection with WT HIV-1 (data not shown), but not after N74D HIV-1 infection. These results suggest that CypA may shield capsid from access and binding by CPSF6-358.

4.3.3 HIV-1 Induces Cytoplasmic Higher-Order CPSF6 Complex Formation in a CypA-Dependent Manner

To determine if full-length higher order CPSF6 complexes form in the cytoplasm, immunostaining of CPSF6 was performed before and after HIV-1 infection. Higher-order CPSF6 complexes were visualized in the perinuclear region after WT HIV-1 infection but not after N74D HIV-1 infection (Figures 22A, B), and were associated with IN-containing complexes (Figure 7A) and CA (p24) staining. CPSF6 puncta were also observed in the nuclei of cells at later time points

after WT HIV-1 infection (Figure 24). Consistent with our *in vitro* results (Figure 15), these data suggest that CPSF6 binds to WT capsid in the cytoplasm of infected cells.

Our work demonstrated that higher-order CPSF6-358 complexes were larger and formed more rapidly with CsA treatment. It suggests that preventing CypA binding to CA would enhance CPSF6-358 interaction with HIV-1 CA. Therefore, we examined whether the same would be true for full-length CPSF6. Indeed, when cells were treated with CsA and infected with WT HIV-1, greater numbers of CPSF6 higher order complexes were observed (Figures 22A, B). The volume of the complexes that formed in the presence of WT virus increased with increasing concentrations of CsA (Figure 22C), suggesting that inhibiting more CypA binding allowed more CPSF6 to bind to HIV-1 capsid. In contrast, CPSF6 complex formation was indistinguishable from background after infection with N74D HIV-1 (Figure 22A, B). To confirm that loss of CypA binding to capsid was responsible for the increase in CPSF6 higher order complexes, cells were infected with HIV-1 CA mutant G89V that is defective for CypA binding. Because G89V HIV-1 is restricted by CPSF6-358 and thus can still bind CPSF6, we expected that this virus would induce CPSF6-GFP puncta that would not increase in number in the presence of CsA, which is what was observed (Figure 22B). However, CypA-DsRed does not rescue the infectivity of HIV-1 in presence of CPSF6-358 (Figure 22C), suggesting the protective effect against CPSF6 is limited prior to nuclear import.

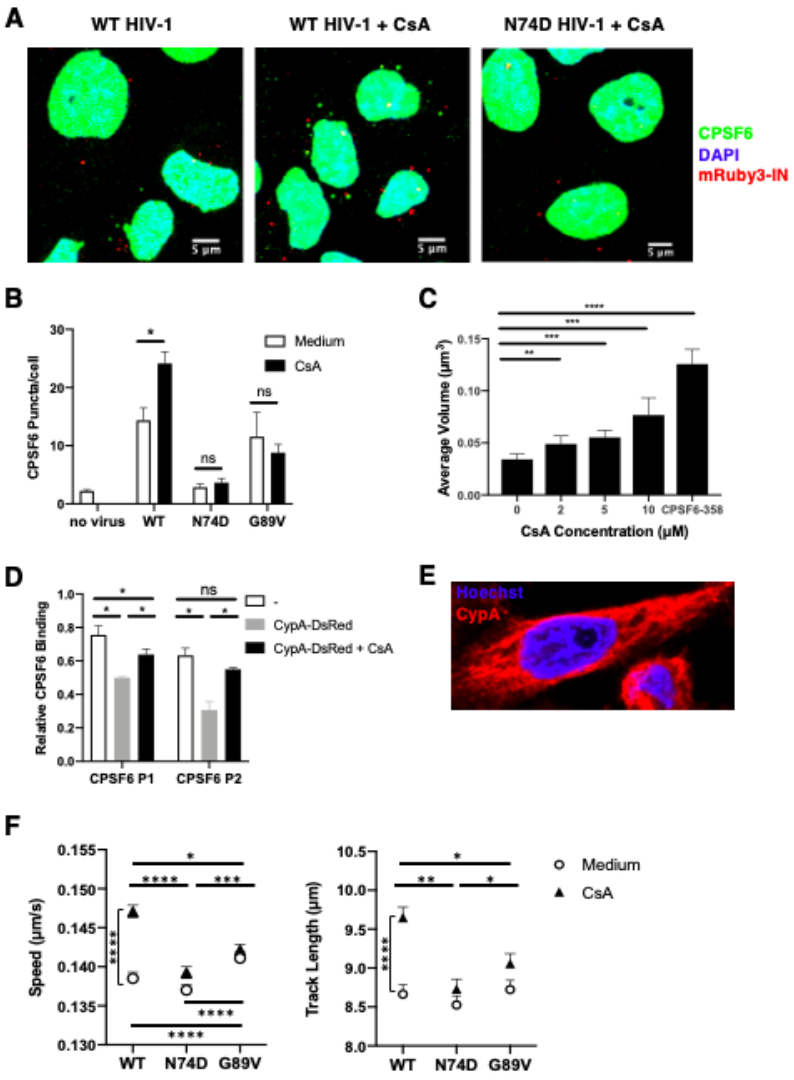

Figure 22 CsA treatment alters HIV-1 interaction with CPSF6 and trafficking. (A) Representative confocal micrographs are shown of HeLa cells stained with CPSF6 antibodies (green) and Hoechst (blue) after infection with WT HIV-1 and WT or N74D HIV-1 in the presence of 10 µM CsA. Viruses contain mRuby3-IN (red). (B) Cytoplasmic CPSF6 staining was quantified in cells (n ≥ 1235) treated with or without 10 µM CsA and infected for 1 h with WT, N74D, or G89V HIV-1. (C) The average volume of cytoplasmic CPSF6 puncta (n ≥ 1235) was quantified in HeLa cells treated with or without CsA. Cells expressing CPSF6-358-GFP were used as a positive control. (D) CA-NC assemblies were incubated for 1 h in the buffer, with CypA-DsRed, or CypA-DsRed and CsA, then incubated with MBP-CPSF6 P1 or P2 for 1 h. The relative binding of CPSF6 to CA-NC assemblies was quantified in each sample from stained SDS-PAGE gels. Error bars indicate STDEV from 3 independent experiments. (E) A representative confocal micrograph of a HeLa cell stained with Hoechst (blue) and CypA

antibodies (red). (F) The average particle speeds and track lengths of WT, N74D, or G89V HIV-1 mRuby3-IN complexes in HeLa cells treated with or without 10 µM CsA are shown for 1 of 3 independent experiments (see also Figure 29). Error bars indicate SEM.

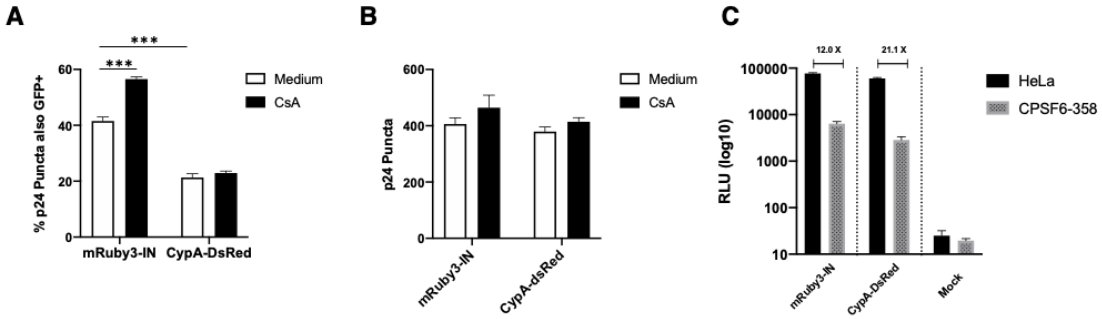

Figure 23 . CypA-DsRed prevents the formation of HIV-1-induced CPSF6-358-GFP higher order complexes. HeLa cells were infected with WT HIV-1 containing mRuby-IN or CypA-DsRed in the presence or absence of 10 µM CsA for 1 h. Cells were fixed and stained with p24 antibodies. (A) The percentage of red viral complexes that were also positive for GFP was plotted. (B) The total number of p24+ particles in cells was plotted. Error bars represent STDEV. (C) Infectivity of HIV-1 made with mRuby3-IN vs. CypA-DsRed in HeLa and HeLa expressing CPSF6-358 cells.

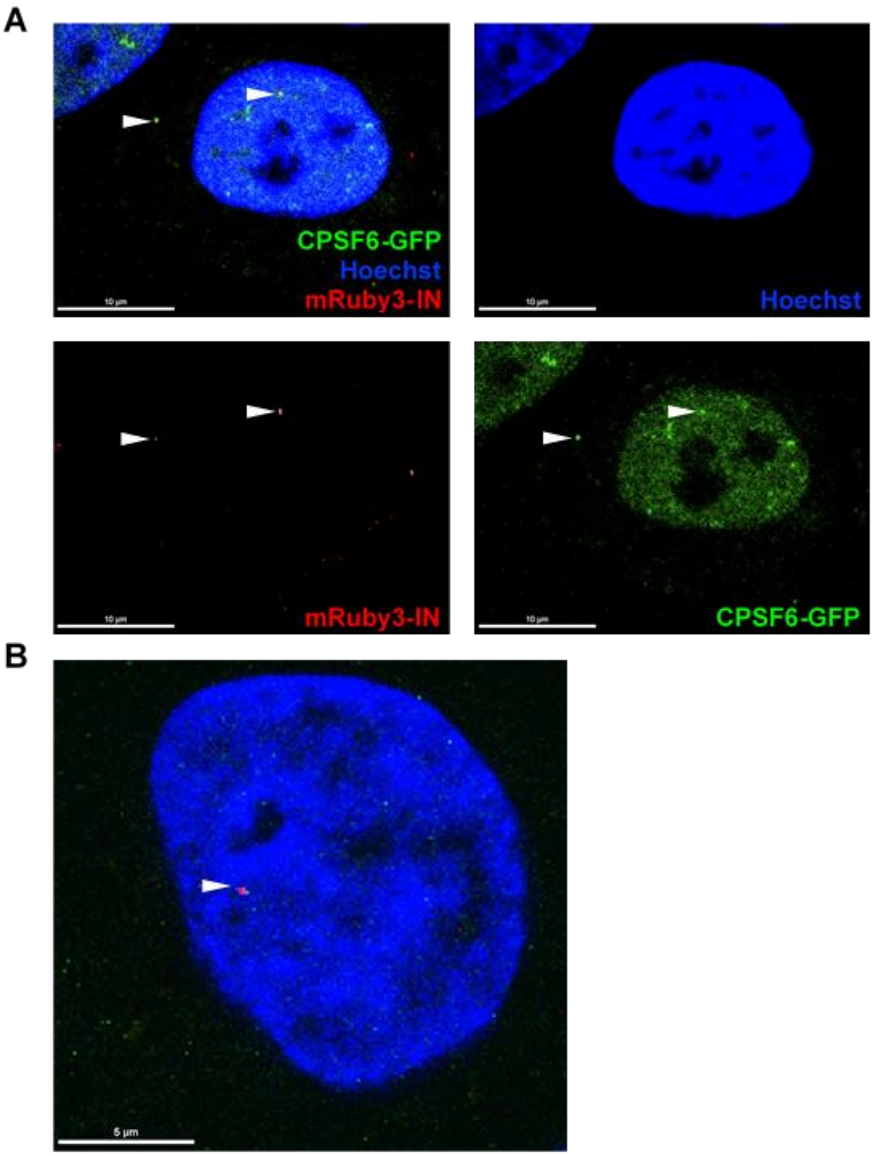

Figure 24 . WT HIV-1 induces the formation of CPSF6-GFP puncta in nuclei. HeLa cells expressing CPSF6-GFP were infected with WT HIV-1 containing mRuby3-IN and fixed after 2 h. (A) A representative cell is shown in which a mRuby3-IN complex is colocalized with CPSF6-GFP in the cytoplasm and another in the nucleus. (B) Another representative cell in which mRuby3-IN is colocalized with CPSF6-GFP in the nucleus. White bars, 5 µm or 10 µm.

As the removal of CypA from HIV-1 capsid enhanced CPSF6 higher-order complex formation, we hypothesized that CPSF6 complex formation may be prevented if CypA binding to

capsid was enhanced. Thus, virus was produced in the presence of CypA-DsRed, an oligomeric form of fluorescently labeled CypA with higher avidity to HIV-1 capsid than unlabeled CypA [204]. Cells were infected with WT HIV-1 labeled with CypA-DsRed or with mRuby3-IN in the presence or absence of CsA and stained for CA (p24; Figure 23B). Similar levels of p24 staining were observed under all conditions. Virus containing mRuby3-IN led to the formation of many CPSF6-358-GFP puncta associated with p24 that increased with CsA treatment (Figure 23A). However, cells infected with CypA-DsRed-labeled HIV-1 had significantly fewer GFP puncta and CsA treatment did not increase their formation, suggesting that enhanced CypA binding to capsid prevents HIV-1 interaction with CPSF6-358 and, likely, also CPSF6.

To directly test the ability of CypA to shield CPSF6 binding to HIV-1 capsid, MBP-CPSF6 protein (P1 and P2) binding to nanotubes composed of recombinant WT CA-SP1-nucleocapsid (CA-NC) protein was quantified in the presence or absence of CypA-DsRed, and in the presence or absence of CsA. (Figure 25A). Binding of CypA-DsRed to CA-NC tubes was not affected by subsequent MBP-CPSF6 binding but was inhibited by CsA treatment (Figure 25B). MBP-CPSF6 binding to HIV-1 CA-NC tubes decreased when CypA-DsRed was already bound, effects that were rescued partially (P1) or completely (P2) by the presence of CsA (Figure 22D). Collectively, these data demonstrate that CypA binding to capsid prevents CPSF6 from binding.

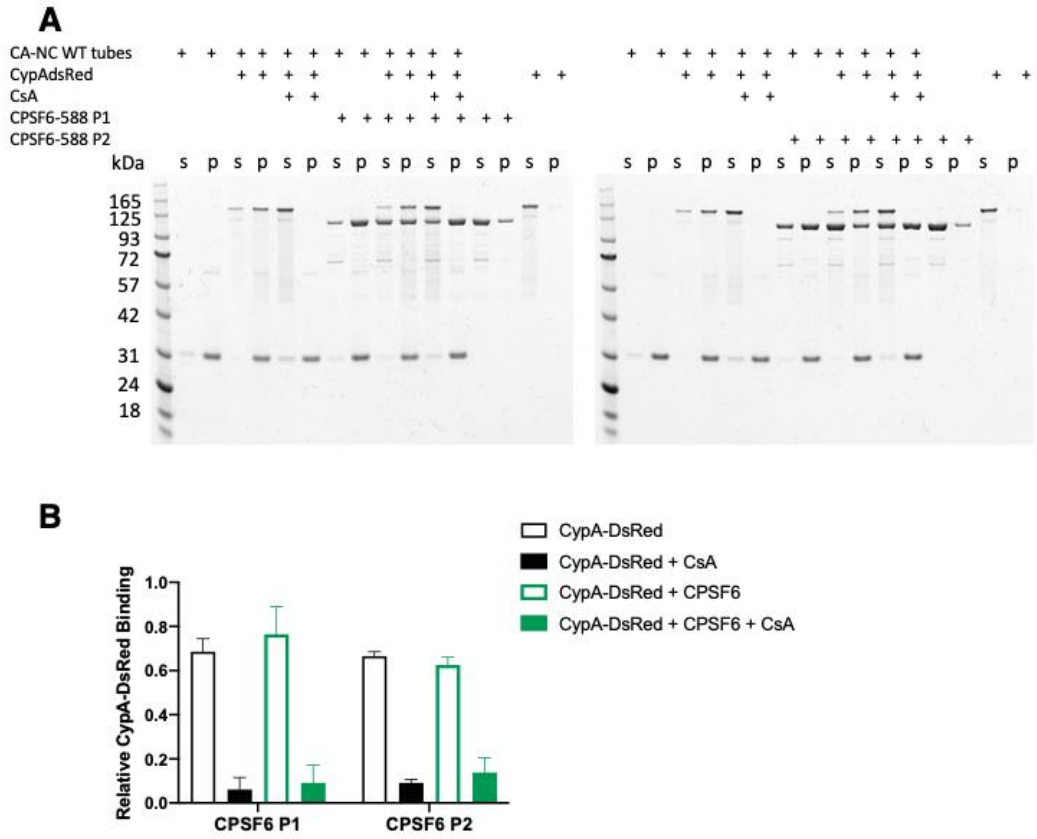

Figure 25 CypA prevents HIV-1 capsid binding to CPSF6. (A) SDS-PAGE gel of WT CA-NC assemblies were incubated with CypA-DsRed with or without CsA for 1hr at room temperature, following incubation with MBP-CPSF6 P1 (left) or P2 (right) and then centrifuged. The gel was Coomassie blue stained, with supernatant (s) and pellet (p) samples indicated. (B) The binding ratio of CypA-DsRed with WT CA-NC assemblies. The error bars indicate the standard deviation of the values of three independent experiments.

4.3.4 Loss of CypA Binding Leads to Altered Cytoplasmic Trafficking of WT HIV-1 Complexes in a CPSF6-Dependent Manner

Although CypA is packaged into virions, HIV-1 capsid interactions with target cell CypA dictate infectivity [258]. In contrast to CPSF6 expression, endogenous CypA localized to the cytoplasm of HeLa cells with somewhat of a filamentous appearance (Figures 23E). Interestingly,

not only was CypA excluded from the nucleus, its expression was absent from portions of the perinuclear region (Figure 26A) that corresponded to the microtubule-organizing center (MTOC) (Figure 27). Expression of CypA in the more biologically relevant T cell line, SupT1, showed similar CypA expression of profile (Figure 26B).

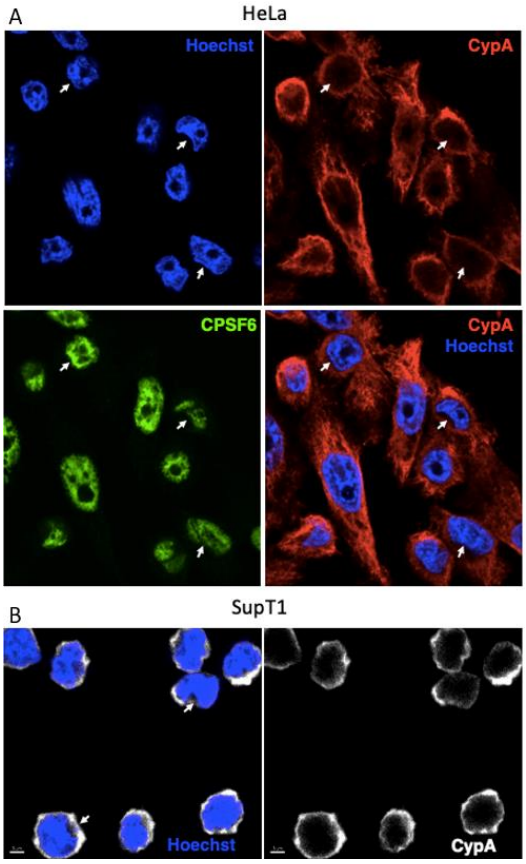

Figure 26 CypA is excluded from the nucleus of (A) HeLa and (B) SupT1 cells. Confocal micrographs are shown of cells stained with Hoechst, CypA antibodies, CPSF6 antibodies. Arrows show the perinuclear exclusion of CypA.

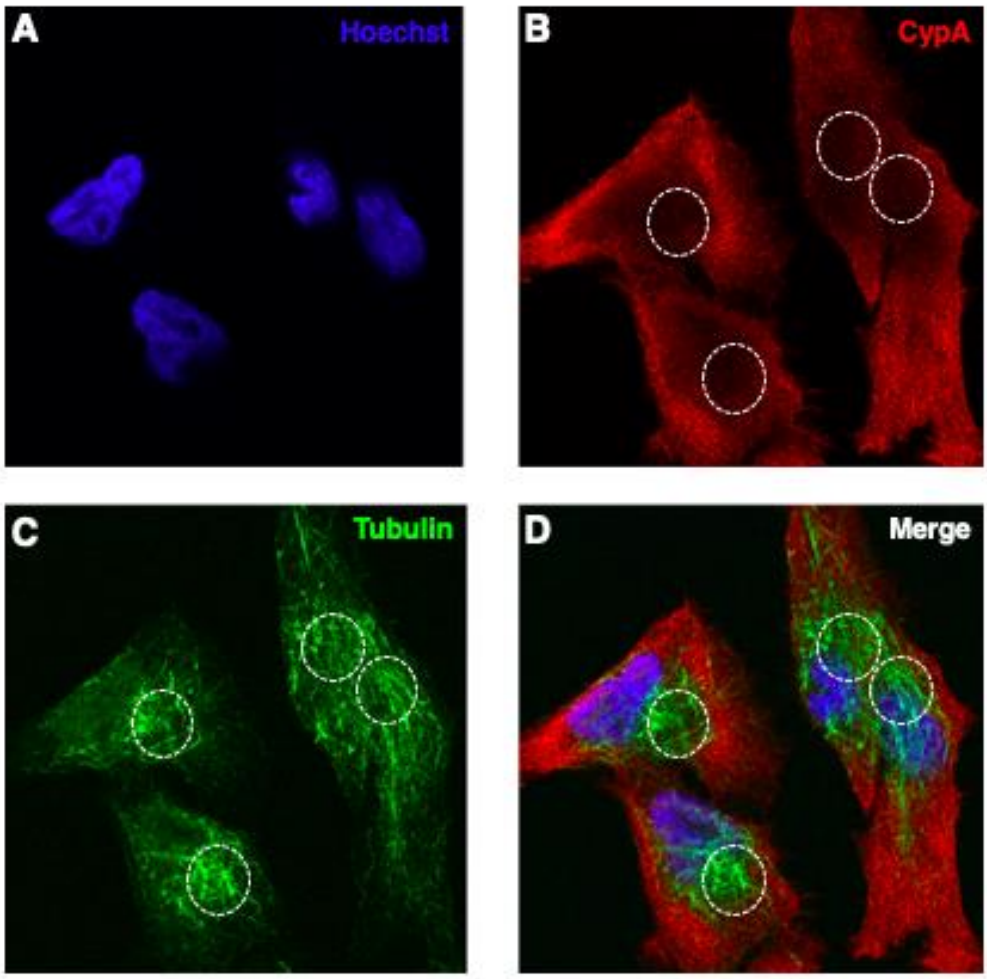

Figure 27 CypA is excluded from the microtubule-organizing center of HeLa cells. Confocal micrographs are shown of HeLa cells stained with (A) Hoechst, (B) CypA antibodies, (C) tubulin antibodies, and (D) all stains.

To determine whether loss of CypA binding to HIV-1 capsid could affect virus trafficking, live-cell microscopy was performed on WT, N74D, and G89V HIV-1 in the presence and absence of CsA in HeLa cells (Figures 22F, 28A) or HeLa cells expressing CPSF6-GFP (Figure 28B, C). In the absence of CsA, the average speed and track length of viral complexes were similar for WT HIV-1 and N74D HIV-1, while G89V HIV-1 complexes trafficked significantly faster and had similar track lengths. As observed for WT HIV-1 trafficking in cells expressing mutant CPSF6

(Figure 9), a higher rate of speed of G89V viral complexes was associated with lower infectivity (Figure 29C). However, CsA treatment led to significantly increased speed and track length of WT HIV-1 particles. CsA did not affect N74D or G89V viral particles. These results suggest that loss of CypA binding to WT capsid influences trafficking of HIV-1 complexes in the cytoplasm in a CPSF6-dependent manner, as N74D viral particles were not affected by CsA treatment. G89V complexes that bind to CPSF6 but not CypA had altered trafficking and lower infectivity irrespective of CsA treatment. The expression and trafficking data together suggest that CypA prevents virus cores from binding prematurely to CPSF6 during trafficking to the nucleus.

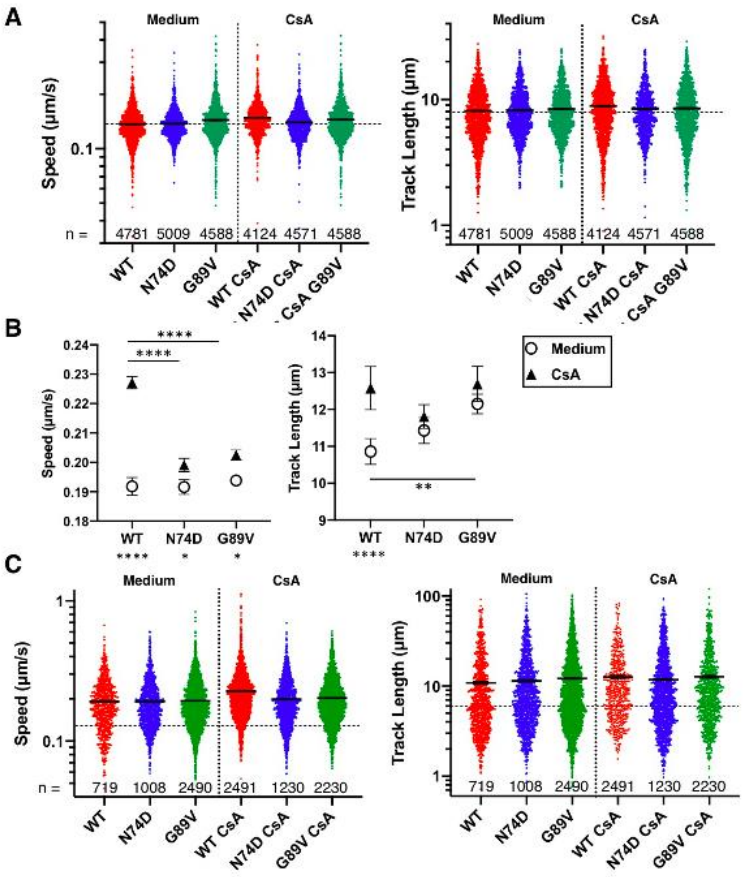

Figure 28 CsA treatment of HeLa cells alters HIV-1 trafficking. Results from HILO live-cell imaging are shown. (A) As summarized in Figure 23F, the speed and track length of individual WT, N74D, or G89V HIV-1 mRuby3-IN complexes in HeLa cells treated with or without 10 µm CsA are shown. Dotted lines denote the mean of WT complexes. Error bars indicate SEM. The number (n) of mRuby3-IN complexes analyzed for each condition is listed at the bottom of the graph. (B) The average particle speeds and track lengths of WT, N74D, or G89V HIV-1 mRuby3-IN complexes in HeLa cells expressing CPSF6-GFP treated with or without 10 µm CsA are shown. Error bars indicate SEM. (C) The speed and track length of individual WT, N74D, or G89V HIV-1 mRuby3-IN complexes from (B) are shown. Dotted lines denote the mean of WT complexes. Error bars indicate SEM. The number (n) of mRuby3-IN complexes analyzed for each condition is listed at the bottom of the graph.

4.3.5 Depletion of CPSF6 Rescues HIV-1 Complex Trafficking Defect Caused by Loss of CypA Binding

To validate that the effect of CsA treatment on WT viral complex trafficking is mediated by CPSF6, CPSF6 was depleted from cells using shRNA knockdown. HeLa cells were transduced with lentiviruses expressing an shRNA targeting CPSF6 or a scrambled control shRNA. KD of CPSF6 was verified by immunofluorescence staining (Figure 29A). In the absence of CsA, CPSF6 KD had no effect on WT virus particle tracking (Figure 29B). Infectivity of WT HIV-1 in untreated cells decreased after CPSF6 depletion (Figure 29C), which may be attributable to previously described reduced cell proliferation of CPSF6 knockout cells [153]. As shown above (Figure 22F), CsA led to a significant increase in WT HIV-1 complex speed and track length in HeLa cells (Figure 29B). However, CPSF6 KD led to decreased WT HIV-1 particle speed to that of unmodified, untreated HeLa cells.

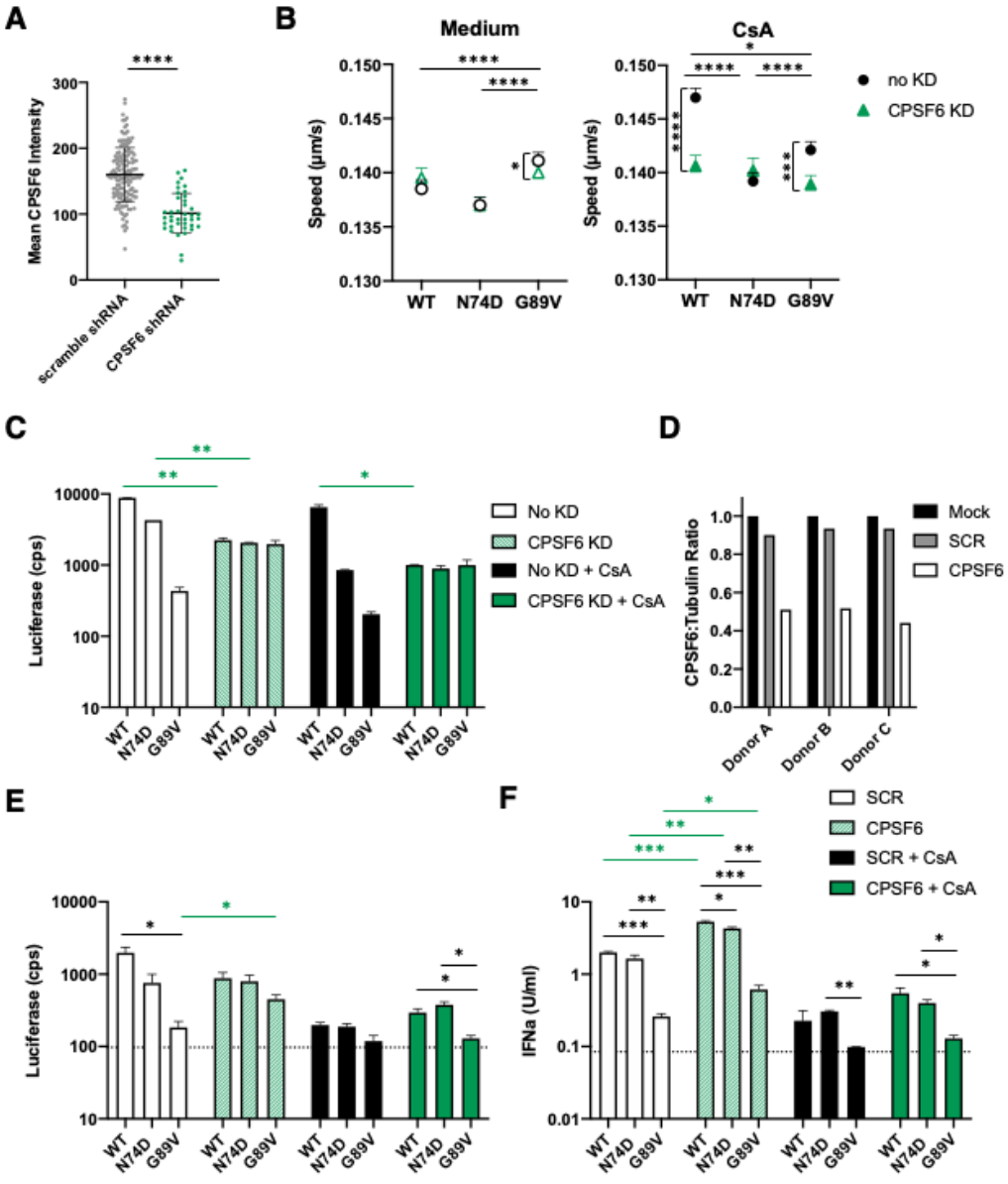

Figure 29 CPSF6 knockdown in HeLa cells and primary PBMC alters HIV-1 trafficking and decreases infection in the absence of CypA binding. (A) The maximum intensity of CPSF6 antibody staining is shown from individual HeLa cells transduced with lentiviruses expressing scrambled (SCR) or CPSF6 shRNA. The error bars indicate STDEV (n ≥ 157 cells). (B) The average particle speeds of WT, N74D, or G89V HIV-1 mRuby3-IN complexes in HeLa cells expressing SCR or CPSF6 shRNA and treated with or without 10 μm CsA are shown. Representative of 2 independent experiments (see also Figure 28). Error bars indicate SEM. (C) The infection of WT, N74D, or G89V HIV-1 in the same cells shown in (B) is graphed. Error bars indicate STDEV of duplicates. (D) CPSF6 depletion was quantified by the ratio of CPSF6 to α-tubulin measured by

western blot for activated PBMCs from each donor. (E) Representative infections with WT, N74D, and G89V HIV-1 were measured in primary PBMC cells from a donor after shRNA depletion of CPSF6, treatment with CsA, or both. (See also Figure 32.) (F) IFNα production from infected PBMC shown in (E) was quantified using HEK 293T ISRE-luc indicator cells. (See also Figure 32.)

The CA mutants showed different cytoplasmic trafficking patterns compared to WT HIV-1, while N74D complex trafficking was unaffected by CPSF6 KD and CsA treatment (Figure 29B). Interestingly, the depletion of CPSF6 led to a significant decrease in G89V HIV-1 complex trafficking with or without CsA treatment (Figure 29B), which corresponded to a rescue of the infectivity defect of this mutant (Figure 29C). Our data indicate that CypA alters HIV-1 trafficking in a CPSF6-dependent manner, further suggesting that CypA binding protects HIV-1 capsid from binding too prematurely to or too much of CPSF6.

4.3.6 Depletion of CPSF6 Rescues G89V HIV-1 Infectivity and Induces IFNα Production in Primary PBMC

Infectivity of WT HIV-1 and CA mutants were performed in phytohemagglutinin (PHA)-stimulated primary human peripheral blood mononuclear cells (PBMC) from 3 donors. Cells were infected in the presence or absence of CPSF6 depletion and CsA treatment. The depletion of CPSF6 was verified by western blot quantification (Figure 29D). Similar to the HeLa cell data, infection of N74D and G89V HIV-1 was inhibited in primary PBMC (Figure 29E), as previously reported [236]. The depletion of CPSF6 partially rescued G89V HIV-1 infectivity (Figure 29E), similar to what was observed in HeLa cells (Figure 29C).

It has been suggested that a loss of HIV-1 capsid interaction with host factors, such as CPSF6 and CypA, can lead to the induction of type I interferon in primary immune cells. Thus, IFNα production was quantified after HIV-1 infection from the supernatants of PBMC depleted of CPSF6 and/or treated with CsA. WT and N74D HIV-1 induced similar levels of IFNα after infection of CD4+ T cells, whereas G89V HIV-1 did not (Figure 29F). The depletion of CPSF6 significantly increased IFNα production after infection by all three viruses, consistent with previous results [236]. Treatment with CsA further inhibited IFNα production after infection with the viruses. Overall, IFNα production in primary CD4+ T cells correlated with the infectivity data, such that higher infection levels led to greater IFNα production.

4.3.7 Depletion of CPSF6 in Macrophages Results in Decreased HIV-1 Infectivity Independent of CypA Binding

As we and others previously showed that N74D HIV-1 has an early infectivity defect in MDM, we investigated whether intracellular trafficking of HIV-1 is dependent on CPSF6 and CypA. MDM were stained for endogenous CypA and CPSF6 expression. As in HeLa cells, CPSF6 expression was nuclear in MDM (Figure 20A). However, infection with WT HIV-1 failed to induce higher order CPSF6 complex formation in the cytoplasm (data not shown), consistent with previous results [104,227] and indicative of less cytoplasmic CPSF6 expression in MDM compared to HeLa cells. In contrast, CypA expression differed greatly between cell types. MDM had pronounced nuclear CypA expression in addition to patches of the plasma membrane and cytoplasmic expression (Figure 20A and 30A).

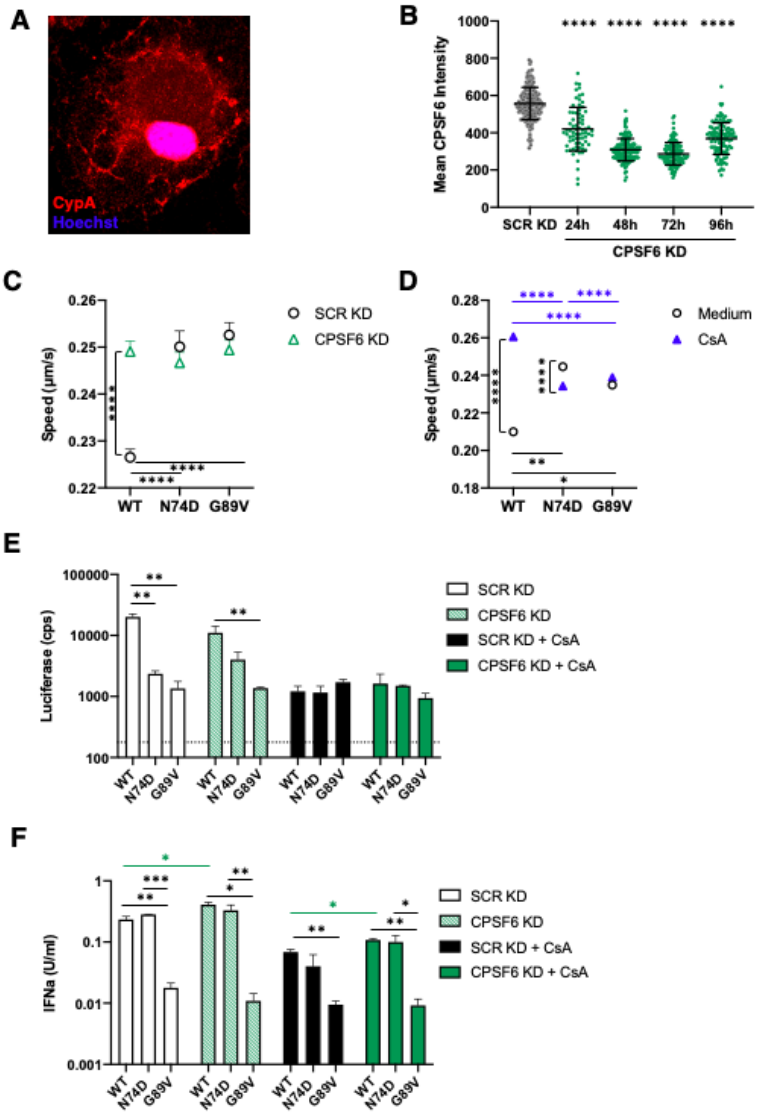

Figure 30 CPSF6 KD decreases HIV-1 infection in MDM and enhances IFNα. (A) A representative confocal micrograph of an MDM stained with Hoechst (blue) and CypA (red) is shown. (B) The mean intensity of CPSF6 antibody staining is shown from individual MDM transduced with lentiviruses expressing SCR or CPSF6 shRNA. The error bars indicate STDEV of n ≥ 77 cells. (C) The average particle speeds of WT, N74D, or G89V HIV-1 mRuby3-IN complexes in MDM from 1 of 3 individual donors with SCR KD or CPSF6 KD are shown. Error bars indicate SEM. (D) The average particle speeds of WT, N74D, or G89V HIV-1 mRuby3-IN complexes in MDM from a representative donor treated with or without CsA are shown. Error bars indicate SEM. (E) The infection of WT, N74D, or G89V HIV-1 in the same cells shown in (B) are graphed. Error bars indicate STDEV of duplicates and the dotted line represents the average luciferase expression of uninfected cells. (F)

IFNα was measured in the supernatants of cells shown in E. Error bars indicate STDEV of duplicates. The limit of detection is 0.001 U/ml.

CPSF6 was depleted with shRNA in MDM, which was confirmed by immunostaining (Figure 30B). Trafficking of mRuby3-IN complexes was evaluated in MDM from 3 donors with and without CPSF6 depletion. CPSF6 depletion led to a significant increase in speed and track length of WT HIV-1 complexes (Figure 30C). Loss of CPSF6 led to a modest decrease in WT HIV-1 single-cycle infectivity with only Donor 2 being significant (Figures 30E, 31A). However, CPSF6 depletion led to a significant decrease in spreading infection with WT HIV-1 but not with N74D HIV-1 in MDM (Figure 31B). Despite effects on infectivity, CPSF6 KD resulted in significantly increased IFNα production in all 3 donors (Figures 30F, 31C). In normal MDM, both N74D and G89V HIV-1 had significantly decreased infectivity which corresponded to faster mRuby3-IN trafficking. CPSF6 depletion had no effect on the trafficking of mutant CA complexes or subsequent infection. Interestingly, despite having low infectivity in MDM, N74D HIV-1 led to high IFNα production in MDM with or without CPSF6 KD, similar to WT HIV-1 infection (Figure 30F, 31C). Increased type I interferon production by N74D HIV-1 during reverse transcription in macrophages has been described previously [236]. G89V HIV-1 resulted in low infection and IFNα production. These results suggest that loss of CPSF6 in macrophages affects WT HIV-1 CA trafficking and increased production of type I IFNα, leading to decreased infectivity.

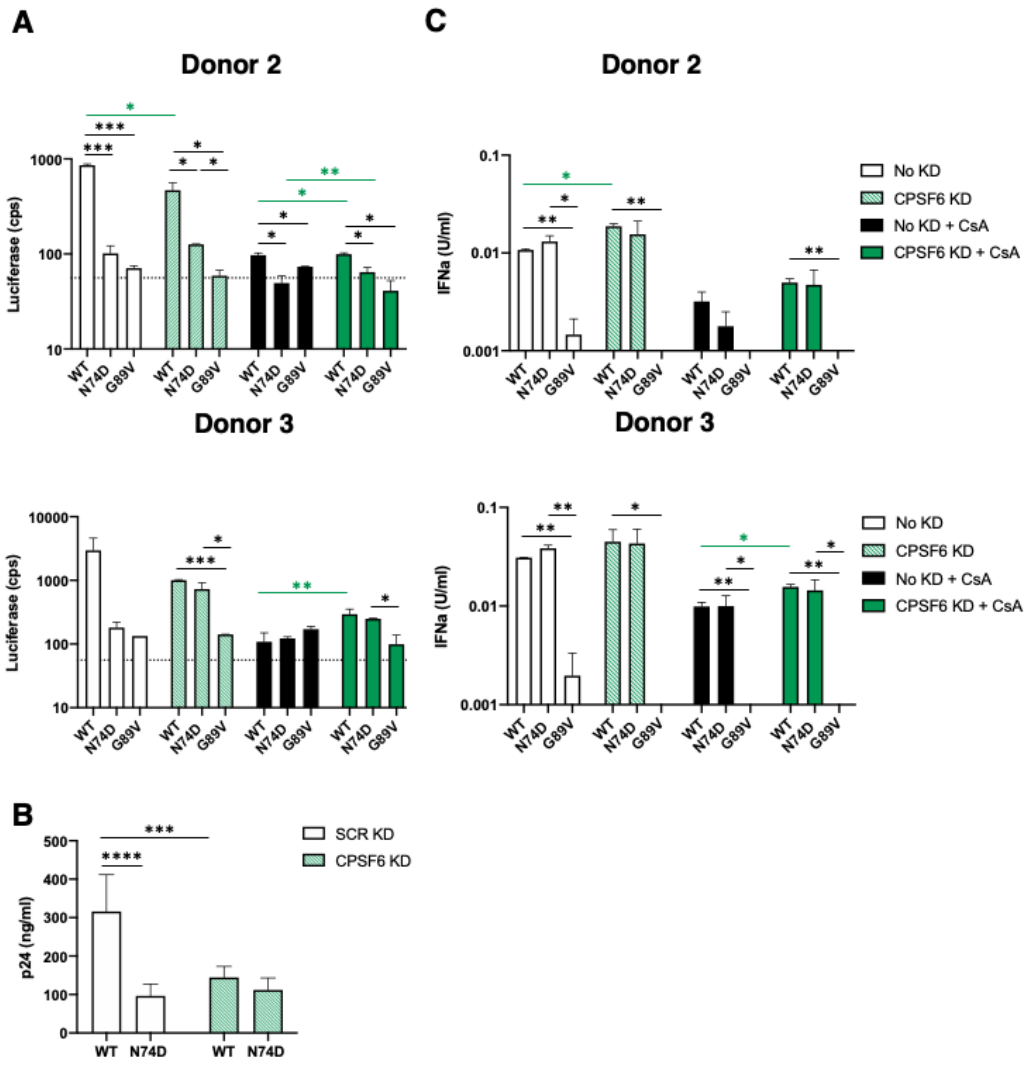

Figure 31 CPSF6 knockdown or loss of CypA binding decreases HIV-1 infectivity in MDM. (A) Infection of WT, N74D, or G89V HIV-1 in cells from Donor 2 and 3 are graphed. Error bars indicate STDEV of duplicates and the dotted line represents the average luciferase expression of uninfected cells. (B) WT and N74D HIV-$1_{NL4\text{-}BAL}$ virus production of duplicate MDM infections was measured by p24 ELISA on d 8 post-infection. Results are shown as means +/- STDEV. (C) IFNα was measured in the supernatants of the cells from (A). Error bars indicate STDEV of duplicates. The limit of detection is 0.001 U/ml.

CsA treatment of MDM significantly increased WT HIV-1 complex trafficking speed (Fig 30D) with a corresponding decrease in infection in all donors (Figures 30E, 31A). The low

infectivity of WT virus corresponded to a decrease in IFNα (Figures 30F, 31C). CPSF6 KD with CsA treatment (i.e. loss of CPSF6 and CypA binding) led to a significant increase in infectivity of WT virus in all donors with an increase of IFNα production compared to CsA treatment alone. N74D HIV-1 infection was significantly reduced during CsA treatment, with or without CPSF6 KD, but still resulted in higher IFNα. Although the loss of CypA binding significantly reduces virus infectivity, these results suggest that alteration of HIV-1 trafficking, infectivity, and type I IFNα response by depletion of CPSF6 is independent of CypA binding in macrophages.

4.4 Discussion

HIV-1 capsid has been shown to interact directly or indirectly with many host cell factors [224]. Included in this list is CPSF6, which is involved in mRNA splicing and polyadenylation in the nucleus [241]. In this study, we detected the cytoplasmic, punctate expression of endogenous CPSF6 and fluorescently tagged CPSF6 in the perinuclear region of cells. Full-length MBP-CPSF6 protein forms oligomers *in vitro* that are capable of binding to HIV-1 CA assemblies, similar to what we previously reported for CPSF6-358, which lacks the RS domain but retains the central proline-rich domain that mediates CA binding [115]. In cells, CPSF6 puncta likely also represent higher-order complexes that bind to HIV-1 capsid in the cytoplasm after viral entry [109]. This is consistent with a recent study in which CPSF6 was associated with HIV-1 complexes in the cytoplasm prior to nuclear import [109]. Removal or truncation of the CPSF6 RS domain leads to mislocalization of CPSF6 to the periphery of the cell due to loss of TNPO3 binding, and reduced HIV-1 nuclear import and infectivity [141,145,213]. Here we demonstrate with live-cell imaging that HIV-1 complexes traffic with CPSF6 in a capsid-dependent manner. In addition, virus complexes increase in speed

by introducing the CA N74D mutation that abolishes CPSF6 binding. Interestingly, increased microtubule trafficking of HIV-1 is associated with reduced infectivity. This altered trafficking could be the result of HIV-1 switching to a different set of motor and motor adapter protein(s) by interacting with CPSF6. Previously, we showed significant colocalization of CPSF6-358 to mRuby3-IN complexes in the cytoplasm, likely due to high concentrations at the cell periphery that is not seen with full-length CPSF6. It is possible that overall faster and longer trafficking is due to CPSF6-mediated modulation of capsid integrity, which may alter the accessibility of capsid to other host proteins, such as certain microtubule motor proteins or motor adaptors that can alter cargo trafficking speed, track length, and bidirectional transport [194–196].

Previously it was shown that HIV-1 capsid traffics on microtubules on its way to the nucleus [195,196,247]. HIV-1 capsid uncoating is delayed by destabilization of microtubules or knockdown of microtubule motor proteins kinesin and dynein or NPC protein Nup358, suggesting that microtubule trafficking and NPC binding is linked to capsid uncoating [108,196]. Recent work from different groups suggests that the main uncoating event occurs at or inside the nucleus [109,110]. Our previous work demonstrated that CPSF6-358 is associated with HIV-1 complexes in a CA-dependent manner and leads to more rapid uncoating kinetics and reduced virus infectivity [115]. Therefore, CPSF6 may play a role in both HIV-1 capsid uncoating, which may initiate in the cytoplasm and nuclear import.

CypA binding to HIV-1 capsid was described nearly three decades ago [182]. Yet until recently, its role in HIV-1 infection was ill-defined. Here we show that loss of CypA binding to HIV-1 capsid in infected cells due to CsA treatment or G89V CA mutation leads to increased capsid binding to CPSF6, which is consistent with our previous results with fluorescently labeled CPSF6-358 [115]. Conversely, the production of HIV-1 in the presence of CypA-DsRed, which has

increased binding to capsid compared to untagged CypA, reduces CPSF6 binding to capsid. This is also seen *in vitro* in a competitive binding assay with CA-NC assemblies in the presence of CypA-DsRed and MBP-CPSF6 proteins. Trafficking of HIV-1 complexes in cells increases in the presence of CsA or with the G89V CA mutation, which is again correlated with decreased infectivity. These results suggest that CypA binding to capsid prevents CPSF6 binding. As CypA expression in HeLa cells is exclude from cell nucleus and potentially MTOC, where CPSF6 expression is observed, we hypothesize that CypA interacts with HIV-1 capsid in the cell periphery first and prevents CPSF6 binding to HIV-1 capsid before the MTOC region, ensuring that uncoating does not occur prematurely (Figure 32).

The depletion of CPSF6 in cells does not affect HIV-1 infection in HeLa cells or PBMC, nor does it alter HIV-1 trafficking to the nucleus in HeLa cells [141]. As N74D HIV-1 is associated with microtubules and traffics in a linear fashion like WT HIV-1, it suggests that HIV-1 microtubule trafficking and nuclear import can be independent of CPSF6. Surprisingly, loss of CPSF6 expression does affect WT and G89V HIV-1 trafficking during CsA treatment but not N74D HIV-1 trafficking. Alterations in HeLa trafficking under these conditions correspond with HeLa infectivity data. These results again highlight the interplay of CPSF6 and CypA in capsid interaction. As it has not been possible to knockout CPSF6 or completely deplete CPSF6 in HeLa and PBMC cells, these data further suggest that loss of CypA binding allows more CPSF6 binding to occur outside of the nucleus, which affects trafficking and infectivity.

Although high-speed imaging of HIV-1 particles in CD4+ T cells was not possible, infection results after CPSF6 depletion and/or CsA treatment in primary PBMC largely mimic those seen in HeLa cells. However, CsA treatment significantly reduces the infectivity of WT HIV-1 as well as the CA mutants. These results correlate with IFNα production. A recent report shows

that loss of CypA binding, either by depletion, CsA treatment, or CA mutations, leads to significant restriction by human TRIM5α in CD4+ T cells [184]. Thus, CypA binding to HIV-1 capsid may be protective against multiple capsid-binding cellular factors.

Capsid has been shown to play an important part in the infection of non-dividing cells such as macrophages [262]. CPSF6-independent HIV-1 (e.g., N74D CA mutant) and mutants that do not bind to CypA (e.g., P90A CA mutant) are restricted in MDM prior to or at the initiation of reverse transcription [142,184]. Here we show that trafficking of N74D and G89V HIV-1 complexes in the cytoplasm is aberrant in MDM. The depletion of CPSF6 or treatment with CsA in MDM also leads to improper trafficking of WT HIV-1 complexes, which corresponds with reduced infectivity. Interestingly, WT HIV-1 infection of MDM with CPSF6 knockdown or N74D HIV-1 infection of MDM leads to increased IFNα production, consistent with a previous study showing that CPSF6 plays a role in immune sensing in MDM [236]. As in CD4+ T cells, loss of CypA binding to HIV-1 capsid leads to human TRIM5α restriction prior to the completion of reverse transcription [184].

Differences in capsid uncoating and PIC composition have also been observed in MDM compared to other cell types. For example, cytoplasmic HIV-1 DNA staining was nearly 100% colocalized with CA staining in TZM-bl cells whereas there was less than 50% colocalization in MDMs [104]. Whereas most CA staining is lost from PICs in the nucleus of HeLa cells, most nuclear PICs in MDMs were CA positive [104,228] and colocalized with CPSF6 puncta [227]. Here we show that localization of CypA in MDM is both cytoplasmic and nuclear, whereas it is only expressed in the periphery of the cell in HeLa cells (Figure 32). Also, little to no cytoplasmic CPSF6 puncta are detected in MDM. As we show that CPSF6 binding to capsid is prevented by CypA binding and promotes capsid dissociation, CypA expression in the perinuclear region and nucleus of MDM could explain why more CA remains associated with the viral genome in these nuclei as compared

to HeLa cells. Our results contribute to the growing literature of the ability of HIV-1 capsid to bind multiple host cell factors in a highly orchestrated manner to promote viral infectivity, which differs depending on the specific cellular environment.

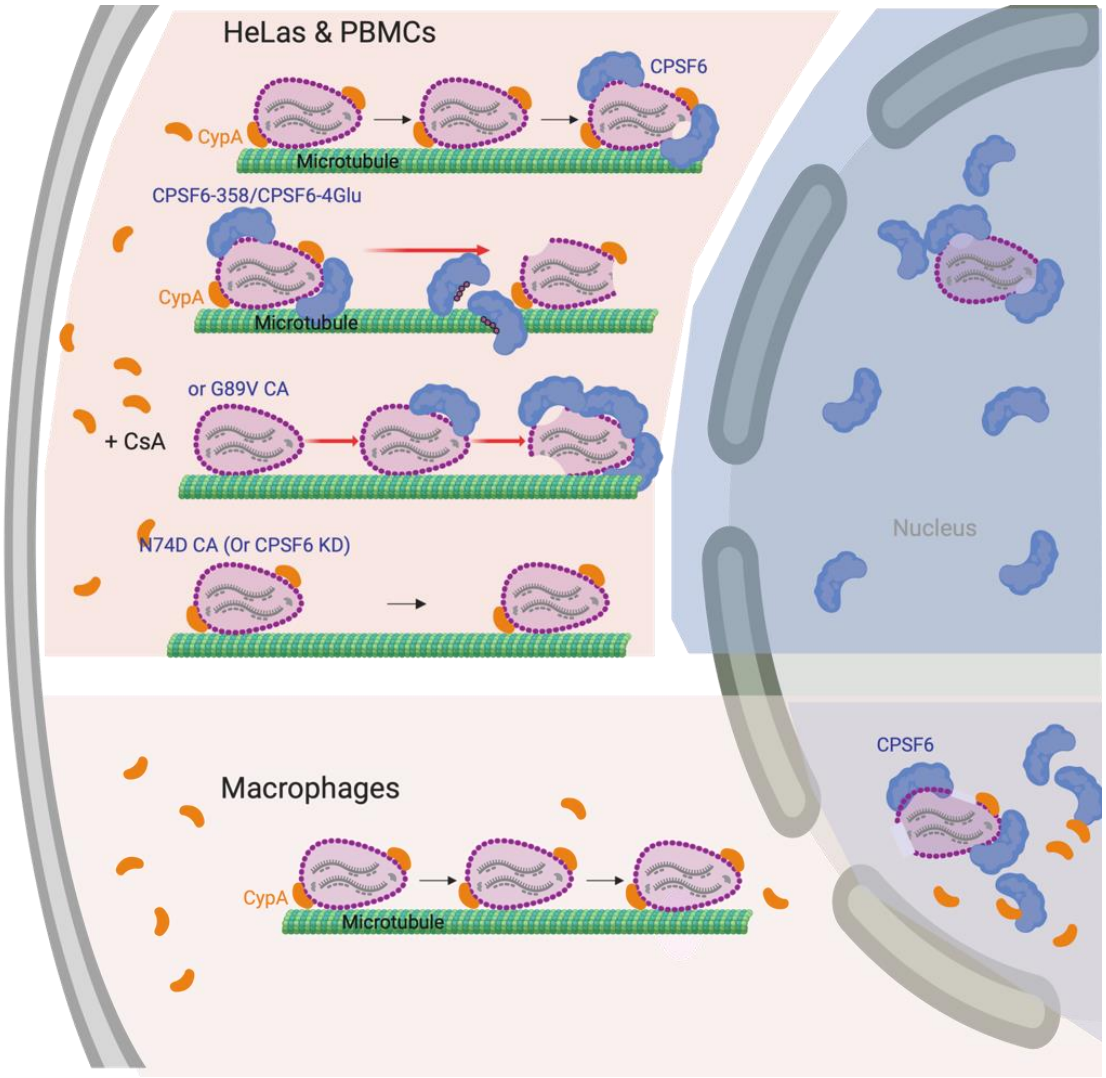

Figure 32 Model of CypA and CPSF6 interaction with HIV-1 capsid in HeLa/CD4+ T cells and macrophages.

4.5 Materials and Methods

4.5.1 Plasmids

The replication-defective HIV-1 proviral plasmid pNLdE-luc (WT and mutants) has been described [141,142]. Viruses were pseudotyped with pL-VSV-G [229]. N74D was also introduced by PCR based mutagenesis in a replication-competent proviral plasmid pNL4-BAL (gift from Ned Landau). pVpr-mRuby3-IN was previously described [115] and a similar version, pVpr-tagRFP-IN was also used.

Lentiviral vectors were used to introduce tagged host proteins or shRNA to cells. Fluorescently tagged CPSF6 and related mutants were introduced into the pSICO vector using BamHI and NotI sites. A plasmid encoding CypA-DsRed [105] was a gift from Greg Melikyan. The lentiviral vector pHIVSIREN expressing CPSF6 shRNA [236] was a gift from Greg Towers. pLKO.1-puro-shNT (gift from Jacob Corn, Addgene #109012) was used as a scrambled shRNA control. The lentiviral packaging plasmid psPAX2 (gift from Dr. Didier Trono, Addgene #109012) and pCMV-VSV-G were used to produce viruses.

The *CPSF6* gene and the MBP tag were amplified by PCR and subcloned into the pcDNA3.1(+) mammalian expression vector (Thermo Fisher Scientific) using the NEBuilder HiFi Assembly kit (New England Biolabs) after linearization with the restriction enzymes Eco RV and Xba I. The resulting insert, designated as MBP-His_6-CPSF6-588, has a leading Kozak sequence, an N-terminal MBP tag, followed by a hexahistidine tag (His_6).

HIV-1 CA and CA-NC were previously described [226,230]. In brief, they were cloned from the cDNA of $Pr55^{Gag}$, which was obtained from the NIH AIDS Research and Reference Reagent Program, Division of AIDS, NIAID, NIH. Briefly, CA and CA-NC regions were amplified and

subcloned into pET21 (EMD Chemicals Inc.) using NdeI and XhoI sites. Proteins were expressed and purified as previously described for Gag ($\Delta MA_{15–100}\Delta p6$) [73,231]. CypA-DsRed-Exp2 (gift from Greg Melikyan) was cloned into the pET28 vector, resulting in a N-terminal His_6-tagged protein.

4.5.2 Cells

HeLa and HEK 293T cell lines were cultured in Dulbecco's modified Eagle medium (DMEM; Thermo Fisher Scientific) supplemented with 10% fetal bovine serum (FBS; Atlanta Biologicals), 100 U/ml penicillin, 100 μg/ml streptomycin, and 2 mM L-glutamine (PSG; Thermo Fisher Scientific) at 37° C, 5% CO_2. HEK 293T cells stably expressing the firefly luciferase gene downstream of the interferon-sensitive response element (HEK293-ISRE-luc) were a gift from Rahm Gummuluru and were cultured in complete DMEM supplemented with 2 μg/ml puromycin (Invitrogen). SupT1 cells were cultured in in RPMI 1640 medium (Thermo Fisher Scientific) supplemented with 10% FBS, PSG at 37° C, 5% CO_2. Stable cell lines were made by transduction with lentiviruses expressing fluorescently tagged host proteins followed by fluorescence activated cell sorting. GHOST-R3/X4/R5 lentiviral reporter cells [232] were cultured in DMEM supplemented 10% FBS, PSG, 100 μg/ml geneticin G418 (Thermo Fisher Scientific), 0.5 μg/ml puromycin (Invitrogen), and 100 μg/ml hygromycin B (Invitrogen).

Human PBMCs were isolated from leukapheresis obtained from the Central Blood Bank (Pittsburgh, PA) using Ficoll-Paque Plus (GE Healthcare) density gradient centrifugation, following the manufacturer's instructions. PBMCs were cultured in RPMI 1640 medium (Thermo Fisher Scientific) supplemented with 10% FBS, PSG, and 20 U/ml recombinant interleukin-2 (IL-2; Thermo Fisher Scientific) at 37° C, 5% CO_2. To expand T lymphocytes, PBMCs were stimulated with 50 U/ml IL-2 and 5 μg/ml phytohemagglutinin (PHA; Sigma-Aldrich) for 72 h

prior to infection or transduction. CD14+ monocytes were isolated from PBMCs using human anti-CD14 magnetic beads with LS Columns (Miltenyi Biotec). CD14+ monocytes were differentiated into MDM in RPMI 1640 medium supplemented with 10% FBS, PSG, and 50 ng/ml recombinant granulocyte–macrophage colony-stimulating factor (R&D Systems) for 7 days at 37° C, 5% CO_2 prior to experimentation.

4.5.3 Viruses

Replication-defective HIV-1_{NL4-3}-luciferase virus pseudotyped with VSV-G was produced by transfection of HEK 293T cells or HEK 293T cells stably expressing FAP-GPI with pNLdE-luc, pL-VSV-G, and pVpr-pcs-mRuby3-IN/pVpr-tagRFP-IN/CypA-DsRed at a weight ratio of 5:5:1. Replication-competent HIV-1 was produced by transfection of HEK 293T cells with the full-length proviral construct. Lentiviruses encoding fluorescent host proteins were produced by transfecting HEK 293T cells with lentiviral, packaging, and pCMV-VSV-G plasmids at a weight ratio of 4:3:1. Transfections were performed using Lipofectamine 2000 (Invitrogen). Viruses were filtered through a 0.45 μM filters, concentrated with Lenti-X (Takara Bio) following the manufacturer's protocol, and stored at -80° C. Viruses were quantified by p24 ELISA (XpressBio) and titered on GHOST-R3/X4/R5 cells. mRuby3-IN and CypA-DsRed labeled viruses were assessed for labeling efficiency by TIRF imaging.

4.5.4 HIV-1 Infection Assays

HeLa cells and differentiated macrophages were seeded in 24-well plates overnight and then transduced with shRNA encoding viruses. 48 h post transduction, cells were infected with

equal p24 amounts of luciferase reporter viruses for 48 h. Cells were lysed and assessed for luciferase production (Promega) with a 1450 MicroBeta TriLux microplate luminescence counter (PerkinElmer). CPSF6 KD efficiency was assessed by CPSF6 antibody staining (NBP1-85676). PHA-stimulated PBMCs were transduced with viruses encoding shRNA and selected with 2 μg/mL puromycin for 72 h. KD efficiency was measured by western blot. PBMCs were re-stimulated with PHA and challenged with luciferase reporter viruses for 72 h prior to luciferase measurement. For assays including treatment with CsA, cells were treated with CsA (10 μM) at the time of plating and remained in drug-containing medium throughout the assay.

Replication of HIV-1 in macrophages was performed in duplicate by infecting transduced macrophages with WT or N74D HIV-$1_{NL4\text{-}BAL}$ at a multiplicity of infection of 0.1. Supernatant was collected and new medium was added every two days. Viral replication was quantified by p24 production in the supernatant by ELISA (XpressBio) at day 8.

4.5.5 Fluorescence Microscopy

For fixed cell imaging, HeLa cells or macrophages were plated in MatTek dishes overnight. Synchronized infections were performed by incubation at 4° C for 10 min, followed by aspiration of medium, addition of cold fluorescently labeled HIV-1 (5 ng p24), and further incubation at 4° C for 15 min to allow virus attachment. Cells were then incubated at 37° C for 20 min, followed by washing with warm medium and incubation in fresh medium. At 1 h post-infection, cells were washed with phosphate buffered saline, pH 7.4 (PBS) and fixed with 2% paraformaldehyde (PFA). After permeabilization with 0.1% TritonX-100 for 15 min, the fixed sample was blocked with serum matching the secondary antibody for 45 min. Primary antibodies were added to the fixed cells in PBB buffer (2% bovine serum albumin in PBS) for 1 h and washed with PBB. Secondary

antibodies were added to the cells in PBB buffer for 1 h. After washing with PBB and PBS, the cells were stained with Hoechst (1:2000) and mounted with a coverslip using gelvetol. For SupT1 cells, cells were washed with phosphate buffered saline, pH 7.4 (PBS) and fixed with 2% paraformaldehyde (PFA) in suspension before left on MatTek dishes pre-coated with Cell-Tak (Corning) for 30 min to adhere. After incubation, the same staining protocol was applied as mentioned above.

A Nikon Ti inverted confocal microscope was used to acquire 3D stacks images of fixed samples with a 100X 1.49 NA oil-immersion objective. LU-NV laser launch (Nikon) was used to emit lasers at 405 nm, 488 nm, 561 nm, and 640 nm. Fields of view were randomly chosen by quick scanning in the Hoechst channel. ND Acquisition in Elements (Nikon) was applied to collect 3D multi-channel imaging (1024 x 1024 pixels) with 2X line averaging. Images of 488 nm and 561 nm channels were acquired by GaAsP detectors (Nikon). 3D stacks were acquired with 0.5 μm step intervals to cover the entire cell volume (6-10 μm) with a motorized piezo Z stage (Nikon).

For live-cell HILO imaging, a Nikon Ti TIRF microscope with a 100X 1.49 NA oil-immersion objective and a Photometrics Prime 95B sCMOS camera was used. In multi-color live-cell imaging experiments, a FLI high speed filter wheel was used. Synchronized infections in HeLa cells or macrophages were performed as described above. After shifting to 37° C for 20 min, cells were washed with pre-warmed fresh medium: FluoroBrite medium (Thermo Fisher Scientific) for HeLa cells or RPMI 1640 medium for macrophages. After 1 h post-infection, the MatTek dish was loaded on the stage insert and maintained at 37° C (Tokai Hit stage chamber). Each image was acquired at least 1 frame per second (FPS) to track viruses for 10 min. For visualizing microtubules, 1 μM SiR-tubulin (Cytoskeleton) was added to the medium 30 min prior to imaging. For visualizing viral membranes, the MG-B-Tau FAP dye [222,233] was added to the virus at 500 nM

for 10 min prior to addition to cells. RAM capture in Nikon Elements was used to achieve faster multi-color live-cell imaging (≥ 2FPS).

4.5.6 Imaging Quantification and Data Analysis

All imaging quantification was performed with General Analysis 3 in Nikon Elements (5.20.00 or above). Briefly, a cell nuclei binary mask was created by Hoechst signal to calculate the number of cells in each field of view. CPSF6 localization and quantification was determined by creating binary masks of CPSF6 within the cells. Cytoplasmic CPSF6 was determined by subtracting the CPSF6 binaries from ones colocalized with Hoechst (nucleus) signal. Mean intensity and volume were recorded for each binary. Virus localization was determined by the Spot Detection function to create binary masks for spots positive for mRuby3/tagRFP, FAP-GPI, CypA-DsRed, or p24 signals. Trafficking data of HIV-1 was determined by using the Track Function with the spot binaries in random and constant motion mode. Any tracks with less than 20 frames were excluded in the data analysis.

4.5.7 Protein Expression and Purification

The full length CPSF6 protein was expressed in a suspension-adapted HEK293 cell line (Expi 293F, Thermo Fisher Scientific) by transfection of expression plasmid using ExpiFectamine 293 (Thermo Fisher Scientific) according to the manufacturer's instructions. Following transfection, the cells were grown at 37°C by shaking at 125 rpm in 8% CO2, 80% humidity for 2 days. The cells were harvested after 48 h of transfection by centrifugation at 100g for 10 min. The cell pellet was washed with cold PBS and flash-frozen and stored at -80° C.

The thawed cell pellet was resuspended in buffer A (50 mM HEPES-KOH (pH 8), 500 mM NaCl, and 5% glycerol, 2 mM DTT) supplemented with detergents (1% Tween 20 and 0.3% NP-40), deoxyribonuclease I (50 μg/ml; Sigma Aldrich) in the presence of a cocktail of protease inhibitors (Roche). After 2 h of rotation at 4° C, the lysate was homogenized by 15 strokes in an ice-cold, tight-fitting Dounce homogenizer. The homogenate was then centrifuged at 21,000*g* at 4°C for 30 min. After centrifugation, the supernatant was collected and mixed with 1 ml of amylose agarose resin (New England Biolabs) pre-equilibrated with buffer A per 50 ml of cell homogenate. The mixture was incubated with rotation at 4° C for 2 h and then transferred to a column. The resin was washed with 50x resin volume of buffer A. To elute the recombinant protein, the resin was incubated, in batch, with buffer A containing 100 mM maltose for 15 min at 4° C, and the flow through was collected as eluate. The eluate was applied to a Hi-Load Superdex 200 16/60 column (GE Healthcare) in a buffer A, and fractions containing target protein were collected and concentrated to 6-8 mg/ml using Amicon concentrators (Millipore, Billerica, MA, USA), flash-frozen with liquid nitrogen, and stored at -80° C.

His_6-tagged CypA-DsRED-Exp2 was expressed in *E. coli* Rosetta 2 (DE3) cells (EMD Millipore) with autoinduction medium at 18° C for 16 h. Protein was purified using 5 mL Ni-NTA column (GE Healthcare) and a HiLoad Superdex200 16/60 size exclusion column (GE Healthcare) equilibrated with a buffer containing 25 mM sodium phosphate, pH 7.5, 150 mM NaCl, 1 mM dithiothreitol (DTT), 10% glycerol, and 0.02% sodium azide.

4.5.8 SDS-PAGE and Western Blot Analysis

For *in vitro* CPSF6 experiments, an equal volume of cell lysate and each fraction from the column were mixed with 4x NuPAGE LDS sample buffer (Thermo Fisher Scientific)

supplemented with 10 mM DTT and loaded onto a 10% Bis-Tris NuPAGE gel (Thermo Fisher Scientific), alongside a protein molecular weight marker (BLUEstain protein ladder, Gold Biotechnology). Gels were run at 100 V for 15 min and then 150 V for 40 min in NuPAGE MES SDS running buffer and the proteins were subsequently transferred onto PVDF or nitrocellulose membranes using iBlot transfer stacks (Thermo Fisher Scientific). The membranes were blocked at ambient temperature for 1 h in BSA blocking buffers, followed by overnight at 4° C with rabbit anti-Maltose Binding Protein antibody (ab9084, Abcam) or rabbit anti-CPSF6 antibody (EPR12898, Abcam), then a further hour with monoclonal anti-rabbit immunoglobulins−alkaline phosphatase antibody at ambient temperature. Between each antibody incubation, the membranes were washed three times with TBS buffer containing 0.1% Tween 20 and finally the membranes were developed with BCIP/NBT color development substrate (Promega) to enable visualization of protein bands (Promega, USA). Each experiment was performed at least three times.

For measurement of CPSF6 expression in cells, an equal number of transduced and puromycin-selected HeLa cells or PBMCs were lysed with RIPA buffer (Bio-Rad), mixed with sample buffer (Bio-Rad), and to 100° C for 5 min. Denatured cell lysate was run on pre-casted 4-15% Criterion Tris-HCl gels (Bio-Rad) at 150 V for 1.5 h. Proteins were transferred to nitrocellulose membranes using a semi-dry transfer apparatus (Thermo Fisher Scientific) at 160 mA for 1 h. The membranes were blocked with 5% milk in PBS containing 0.1% Tween-20 at room temperature for 20 min. Primary antibodies anti-CPSF6 (NBP1-85676) and anti-α-tubulin (T5168, Sigma Aldrich) were used with secondary anti-mouse IgG or anti-rabbit IgG conjugated with horseradish peroxidase antibodies (A9917 and AP132P, Sigma Aldrich). SuperSignal West Pico Chemiluminescent substrate (Thermo Fisher Scientific) was used to visualize protein bands with Amersham Hyperfilm (GE).

4.5.9 Capsid Binding Assay

Tubular assemblies of WT HIV-1 CA protein were prepared at 80 µM (2 mg/ml) in 1 M NaCl and 50 mM Tris-HCl (pH 8.0) buffer at 37° C for 1 h. N74D CA was dialyzed against 1 M NaCl and 50 mM Tris-HCl (pH 8.0) buffer at 4° C overnight at the concentration of 20 mg/ml. Before binding, the assembled mixture was diluted to 80 µM (2 mg/ml). For the binding assays, the binding buffer was the same as the stock buffer for MBP-CPSF6 proteins described above. Different concentrations of MBP-CPSF6 were added to preassembled CA tubes at CA concentration of 64 µM. The reaction mixtures were incubated on a rocking platform at room temperature for 1 h with gentle mixing at 10 min intervals. At the end of incubation, 5 µl samples were withdrawn from the reaction mixtures and immediately used for EM analysis. The remaining samples were pelleted at 21,000 g with a SORVAL Legend micro 21R centrifuge (Thermo Fisher Scientific) for 30 min and supernatants (s) and pellets (p, resuspended in the same volume) were mixed with 4x LDS loading buffer for gel analysis. Supernatant and pellet samples, without boiling, were loaded on 10% SDS-PAGE and stained with Coomassie Blue. Each experiment was performed at least three times.

To determine the binding ratio of MBP-CPSF6:CA, SDS-PAGE gels were scanned using an Epson 4990 scanner. The integrated intensities of CA and MBP-CPSF6 protein bands were measured using Image J 1.40 program (NIH). The molar ratios were calculated according to the formula (MBP-CPSF6 intensity/MBP-CPSF6 molecular weight)/(CA intensity/CA molecular weight) and calibrated using the input ratios as standards.

For binding of CypA and MBP-CPSF6 with HIV-1 capsid, 5 µM of CypA-DsRed was added to 10 µM pre-assembled WT CA-NC tubes, and at the same time 15 µM of competitive

inhibitor CsA was added as a negative control. The reaction mixtures were incubated on a rocking platform at room temperature for 1 h with gentle mixing at 10 min intervals. 5 μM of MBP-CPSF6 P1 or P2 was added to the reaction and incubated on a rocking platform at room temperature for 1 h with gentle mixing at 10 min intervals. At the end of the incubation, the samples were pelleted as described above. Each experiment was performed at least three times. Nikon Elements 5.0 was used to quantify the binding ratio of CypA and MBP-CPSF6 with pre-assembled CA-NC tubes.

4.5.10 TEM Analysis

The morphologies of different variants of CA assemblies and CA–MBP-CPSF6 complexes were characterized by TEM. Samples were stained with fresh 2% uranyl formate, deposited onto 400-mesh carbon-coated copper grids, and dried for 30 min. TEM images were acquired on a Tecnai T12 transmission electron microscope at 120 kV.

4.5.11 Type I IFN Assay

To measure type I IFN from infected cells, HEK93-ISRE-luc cells were incubated with Cellstriper buffer (Thermo Fisher Scientific) for 30 min at room temperature to detach the cells and plated in 96-well plates. Media from infected cultures were added to cells in duplicate. Cells were lysed 21 h later and assessed for luciferase production. Dilutions of IFNα (Sigma-Aldrich) was included as a standard (0.001 – 2 U/ml).

4.5.12 Statistics

Each virus infection experiment and associated imaging analysis was performed in at least two separate replicates. Compiled data was obtained from minimally two independent experiments or three donors. Statistical significance was determined by two-sided unpaired Student's *t* test using Prism (GraphPad). *P* values of <0.05 were considered statistically significant. *P* values > 0.05, ns; 0.01 - 0.05, *; 0.01 - 0.001, **; 0.001 - 0.0001, ***; < 0.0001, ****.

4.6 Acknowledgements

The authors thank Stephanie Ander, Douglas Fischer, Sharie Ganchua, and Chris Kline, for technical assistance; and Rahm Gummuluru, Vineet KewalRamani, Ned Landau, Greg Melikian, and Greg Towers for reagents. This work was supported by National Institutes of Health (NIH) P50 grant AI150481 (A.N.E., P.Z., S.C.W., and Z.A.), NIH R01 grant AI052014 (A.N.E.), NIH R01 grant GM114075 (C.T. and M.P.B.), NIH T32 training grant AI065380 (E.A.B.), and the UK Wellcome Trust Investigator Award 206422/Z/17/Z (P.Z.).

5.0 Discussion and Future Directions

5.1 Discussion

In this thesis, we have used a combination of methods, including virological, biochemical, biophysical and optical techniques to study the relationship of two host factors, CPSF6 and CypA, with HIV-1 infection. Specifically, we have demonstrated that CPSF6 oligomerizes and exists in the cytoplasm. We are the first to show that cytoplasmic CPSF6 can traffic on microtubules. We also visualized the karyopherin for CPSF6 nuclear import, TNPO3, which can move with CPSF6 outside of the nucleus. Our imaging data shows that HIV-1 can interact with cytoplasmic CPSF6 in a CA-dependent manner. While it was known that HIV-1 uses microtubules for movement towards the nucleus, it was unknown whether HIV-1 and CPSF6 (and potentially TNPO3) shared similar trafficking.

CPSF6-358 and CPSF6 were purified and the biophysical data suggest both CPSF6-358 and CPSF6 have the intrinsic tendency to form oligomers. Our *in vitro* binding data show that both purified CPSF6-358 and CPSF6 can bind and disrupt HIV-1 CA assemblies. Together with our in HIV-1 capsid permeabilization experiment in cells expressing CPSF6-358, CPSF6 binding to capsid appears to result in destabilization of the capsid. Yet, the exact mechanism of this destabilizing effect remains unknown.

Live-cell particle tracking experiments to compare HIV-1 trafficking with CPSF6 to CPSF6 mutants (CPSF6-4Glu and CPSF6-358) demonstrated that an increase in speed and track lengths occurred when WT HIV-1 encountered mutant CPSF6. The extent of the increases in speed and track length correlates with (i) the amount of CPSF6 in the cytoplasm and (ii) extent of reduced

infectivity. Interestingly, when CPSF6 is depleted in macrophages, we also noticed an increase in track speed and length. HIV-1 CA mutants (N74D and G89V), which are restricted in macrophages, also showed increasing speed and track length. Collectively, our data suggest there is potentially an optimal trafficking pattern for HIV-1 infection. Alteration in the HIV-1 trafficking pattern generally results in reduced infection. This can be the result of the altered interaction with crucial host factors, such as CPSF6 depletion in macrophages or expression of mutant CPSF6 in HeLa cells. The altered trafficking patterns generally correspond to reduced infectivity. It is of interest to explore the mechanism between HIV-1 cytoplasmic trafficking pattern and the subsequent infection cycle, such as uncoating, nuclear import, and integration.

We reported a novel characteristic of CypA that can prevent HIV-1 capsid binding to CPSF6. In both HeLa cells or HeLa cells expressing CPSF6-358, the treatment of CsA significantly enhanced the formation of higher-order complexes of CPSF6 or CPSF6-358. Using virus produced in the presence of CypA-DsRed, which binds HIV-1 CA better due to its higher avidity by DsRed tetramerization, we showed significantly reduced formation of CPSF6 and CPSF6-358 complexes. Besides, our *in vitro* CA-NC assembly prevented the binding of CPSF6 in presence of CypA-DsRed. Together, these results suggest a protective role of CypA for HIV-1 in the cytoplasm from CPSF6 interaction. In addition, we also showed that the G89V CA mutation or WT HIV-1 in the presence of CsA treatment leads to altered trafficking patterns in both HeLa cells and macrophages. Surprisingly, the depletion of CPSF6 can restore the trafficking pattern and rescue the infectivity defect of G89V HIV-1 and WT HIV-1 treated with CsA in HeLa cells. These data suggest that CypA can modulate HIV-1 trafficking by shielding CPSF6. Without CypA, HIV-1 encounters CPSF6 prematurely and results in altered trafficking and potentially faster uncoating. We did see a rescue of G89V infectivity in PMBC cells after CPSF6 depletion,

suggesting a similar model for PBMCs. However, we did not see similar results in macrophages. These data suggest that the specific interplay between CPSF6 and CypA and HIV-1 capsid is cell type specific.

Stimulation of IFNα production plays an important role in both HIV-1 infection and host immune response. Consistent with previous study [236], we showed that the depletion of CPSF6 leads to an increase of IFNα production with WT HIV-1 infection. Besides, HIV-1 with CA N74D, which does not bind CPSF6, also induces robust IFNα production. However, Rasaiyaah et al. showed infection in primary cells with a CypA binding deficient mutant, P90A, elicited a robust IFNα production [236]. In contrast, we used the G89V mutant, which is also unable to efficiently bind to CypA. Our data show that G89V mutant is not effective to stimulate efficient IFNα production. This discrepancy could not be explained yet. It is possible besides the loss of CypA binding, there may be some other differences between G89V and P90A HIV-1.

5.2 Future Directions

5.2.1 Identify Motor Adaptor Proteins for CPSF6 and TNPO3

In this thesis work, we showed that both CPSF6 and TNPO3 are able to traffic on microtubules in the cytoplasm. To date, there is no known motor protein and motor adapter protein identified to traffic CPSF6 and TNPO3. We can efficiently block CPSF6 trafficking by treating cells with nocodazole. This data suggests the involvement of microtubule and motor proteins for CPSF6 trafficking. It is of interest to find which host motor adapter(s) is/are involved in the trafficking of CPSF6 and TNPO3. Particularly, we may focus on the motor adapter proteins known

to move HIV-1, such as FEZ1, BICD2, and KIF5B [108,194,195]. However, it is also likely CPSF6 and TNPO3 may use a different set of motor adapter protein(s).

5.2.2 Effect of HIV-1 CA Inhibitors on HIV-1 Trafficking

Recently, a new antiretroviral drug, GS-6207, that targets HIV-1 CA has shown good promises in clinical trials [263,264]. Data from these publications indicate that GS-6207 binds HIV-1 CA where CPSF6 engages. Binding of this drug leads to inhibited nuclear import, reduced integration, and increased formation of the aberrant virus at picomolar concentration. It will be interesting to explore the role of the CA drug in HIV-1 trafficking as it may block HIV-1 interaction with CPSF6 and potentially motor adapters as well.

5.2.3 The Role of TRIM5α and TRIM34 in HIV-1 Trafficking

Recently, two groups discovered that CypA shields HIV-1 from detection from TRIM5α in macrophages and T cells [184,185]. In addition, the Emerman group found that TRIM34 restricts HIV-1 with N74D CA in a TRIM5α dependent manner [265]. Both proteins have been shown to bind to HIV-1 CA and destabilize capsid. However, little is known about their roles in HIV-1 trafficking. It will be interesting to explore how TRIM5α and TRIM34 affect HIV-1 trafficking.

5.2.4 The Implications of CypA in HIV-1 Infection

With our imaging data, we showed a clear difference in CypA localization in HeLa cells and macrophages. Considering HIV-1 dependency on CPSF6 and its trafficking pattern in

macrophages, it is possible that the strong nuclear localization of CypA in macrophages may play a role in HIV-1 nuclear import. Other studies have demonstrated rapid nuclear import of HIV-1 in macrophages [109,110]. It is possible that the difference in nuclear import kinetics of HIV-1 is due to localization of CypA.

Normally, the nuclear localization of a host protein requires binding to a karyopherin for nuclear import. However, the molecular weight of CypA is only 18 kDa, which is much smaller compared to the nuclear pore diffusion limit (~ 60 kDa) [266]. CypA likely enters the nucleus via passive rather than active import. The difference in CypA localization between HeLa cells and T cells (excluded from the MTOC and nucleus) and macrophages (in both the cytoplasm and nucleus) could be the result of two possibilities: i. CypA is bound to a nuclear protein in macrophages, which is not present, or such interaction is blocked in HeLa cells and T cells or ii. CypA nuclear export is restricted in macrophages. Either possibility will be of interest to explore. A better understanding of CypA localization in different cell types could provide new insights into its role in HIV-1 infection.

Bibliography

1. Avery, O. T., MacLeod, C. M. & McCarty, M. STUDIES ON THE CHEMICAL NATURE OF THE SUBSTANCE INDUCING TRANSFORMATION OF PNEUMOCOCCAL TYPES. *J. Exp. Med.* **79**, 137–158 (1944).
2. Baltimore, D. Viral RNA-dependent DNA polymerase: RNA-dependent DNA polymerase in virions of RNA tumour viruses. *Nature* **226**, 1209–1211 (1970).
3. Temin, H. M. & Mizutani, S. Viral RNA-dependent DNA polymerase: RNA-dependent DNA polymerase in virions of Rous sarcoma virus. *Nature* (1970) doi:10.1038/2261211a0.
4. Morgan, D. A., Ruscetti, F. W. & Gallo, R. Selective in vitro growth of T lymphocytes from normal human bone marrows. *Science (80-.).* **193**, 1007–1008 (1976).
5. Ruscetti, F. W., Morgan, D. A. & Gallo, R. C. Functional and morphologic characterization of human T cells continuously grown in vitro. *J. Immunol.* **119**, 131–8 (1977).
6. Mizutani, S. & Temin, H. M. An RNA-Dependent DNA Polymerase in Virions of Rous Sarcoma Virus. *Cold Spring Harb. Symp. Quant. Biol.* **35**, 847–849 (1970).
7. Poiesz, B. J., Ruscetti, F. W., Gazdar, A. F., Bunn, P. A., Minna, J. D. & Gallo, R. C. Detection and isolation of type C retrovirus particles from fresh and cultured lymphocytes of a patient with cutaneous T-cell lymphoma. *Proc. Natl. Acad. Sci. U. S. A.* **77**, 7415–7419 (1980).
8. Yoshida, M., Miyoshi, I. & Hinuma, Y. Isolation and characterization of retrovirus from cell lines of human adult T-cell leukemia and its implication in the disease. *Proc. Natl. Acad. Sci. U. S. A.* **79**, 2031–2035 (1982).
9. Kalyanaraman, V. S., Sarngadharan, M. G., Robert-Guroff, M., Miyoshi, I., Blayney, D.,

Golde, D. & Gallo, R. C. A new subtype of human T-cell leukemia virus (HTLV-II) associated with a T-cell variant of hairy cell leukemia. *Science (80-.).* **218**, 571–573 (1982).

10. Kannian, P. & Green, P. L. Human T Lymphotropic Virus Type 1 (HTLV-1): Molecular Biology and Oncogenesis. *Viruses* **2**, 2037–2077 (2010).
11. Mirvish, E. D., Pomerantz, R. G. & Geskin, L. J. Infectious agents in cutaneous T-cell lymphoma. *Journal of the American Academy of Dermatology* vol. **64** 423–431 (2011).
12. Ciminale, V., Rende, F., Bertazzoni, U. & Romanelli, M. G. HTLV-1 and HTLV-2: highly similar viruses with distinct oncogenic properties. *Front. Microbiol.* **5**, 398 (2014).
13. Pneumocystis pneumonia--Los Angeles. *MMWR. Morb. Mortal. Wkly. Rep.* (1981).
14. Centers for Disease Control (CDC). Kaposi's sarcoma and Pneumocystis pneumonia among homosexual men--New York City and California. *MMWR. Morb. Mortal. Wkly. Rep.* **30**, 305–8 (1981).
15. Epidemiologic Aspects of the Current Outbreak of Kaposi's Sarcoma and Opportunistic Infections. *N. Engl. J. Med.* **306**, 248–252 (1982).
16. Centers for Disease Control (CDC). Persistent, generalized lymphadenopathy among homosexual males. *MMWR. Morb. Mortal. Wkly. Rep.* **31**, 249–51 (1982).
17. Barré-Sinoussi, F., Chermann, J. C., Rey, F., Nugeyre, M. T., Chamaret, S., Gruest, J., Dauguet, C., Axler-Blin, C., Vézinet-Brun, F., Rouzioux, C., Rozenbaum, W. & Montagnier, L. Isolation of a T-lymphotropic retrovirus from a patient at risk for acquired immune deficiency syndrome (AIDS). *Science (80-.).* **220**, 868–871 (1983).
18. Gallo, R. C., Salahuddin, S. Z., Popovic, M., Shearer, G. M., Kaplan, M., Haynes, B. F., Palker, T. J., Redfield, R., Oleske, J., Safai, B., White, G., Foster, P. & Markham, P. D. Frequent detection and isolation of cytopathic retroviruses (HTLV-III) from patients with

AIDS and at risk for AIDS. *Science (80-.).* **224**, 500–503 (1984).

19. Coffin, J., Haase, A., Levy, J. A., Montagnier, L., Oroszlan, S., Teich, N., Temin, H., Toyoshima, K., Varmus, H. & Vogt, P. What to call the AIDS virus? *Nature* **321**, 10–10 (1986).

20. Marx, J. L. A virus by any other name... *Science (80-.).* **227**, 1449–1451 (1985).

21. Peeters, M., Honoré, C., Huett, T., Bedjabaga, L., Ossari, S., Bussi, P., Cooper, R. W. & Delaporte, E. Isolation and partial characterization of an HIV-related virus occurring naturally in chimpanzees in Gabon. *Aids* **3**, 625–630 (1989).

22. Huet, T., Cheynier, R., Meyerhans, A., Roelants, G. & Wain-Hobson, S. Genetic organization of a chimpanzee lentivirus related to HIV-1. *Nature* **345**, 356–359 (1990).

23. Zhu, T., Korber, B. T., Nahmias, A. J., Hooper, E., Sharp, P. M. & Ho, D. D. An African HIV-1 sequence from 1959 and implications for the of the epidemic. *Nature* **391**, 594–597 (1998).

24. Gao, F., Balles, E., Robertson, D. L., Chen, Y., Rodenburg, C. M., Michael, S. F., Cummins, L. B., Arthur, L. O., Peeters, M., Shaw, G. M., Sharp, P. M. & Hahn, B. H. Origin of HIV-1 in the chimpanzee Pan troglodytes troglodytes. *Nature* **397**, 436–441 (1999).

25. Korber, B., Muldoon, M., Theiler, J., Gao, F., Gupta, R., Lapedes, A., Hahn, B. H., Wolinsky, S. & Bhattacharya, T. Timing the ancestor of the HIV-1 pandemic strains. *Science (80-.).* **288**, 1789–1796 (2000).

26. Keele, B. F., Van Heuverswyn, F., Li, Y., Bailes, E., Takehisa, J., Santiago, M. L., Bibollet-Ruche, F., Chen, Y., Wain, L. V., Liegeois, F., Loul, S., Ngole, E. M., Bienvenue, Y., Delaporte, E., Brookfield, J. F. Y., Sharp, P. M., Shaw, G. M., Peeters, M. & Hahn, B. H. Chimpanzee reservoirs of pandemic and nonpandemic HIV-1. *Science (80-.).* **313**, 523–

526 (2006).

27. Popper, S. J., Sarr, A. D., Travers, K. U., Guèye-Ndiaye, A., Mboup, S., Essex, M. E. & Kanki, P. J. Lower human immunodeficiency virus (HIV) type 2 viral load reflects the difference in pathogenicity of HIV-1 and HIV-2. *J. Infect. Dis.* **180**, 1116–1121 (1999).

28. Campbell-Yesufu, O. T. & Gandhi, R. T. Update on human immunodeficiency virus (HIV)-2 infection. *Clin. Infect. Dis.* **52**, 780–787 (2011).

29. Global HIV & AIDS statistics - 2020 fact sheet. *UNAIDS* (2020).

30. Schacker, T., Collier, A. C., Hughes, J., Shea, T. & Corey, L. Annals of Internal Medicine: Clinical and Epidemiologic Features of Primary HIV Infection. *Ann. Intern. Med.* **125**, 257–264 (1996).

31. Lackner, A. A., Lederman, M. M. & Rodriguez, B. HIV pathogenesis: the host. *Cold Spring Harb. Perspect. Med.* **2**, a007005 (2012).

32. Ribeiro, R. M., Qin, L., Chavez, L. L., Li, D., Self, S. G. & Perelson, A. S. Estimation of the Initial Viral Growth Rate and Basic Reproductive Number during Acute HIV-1 Infection. *J. Virol.* **84**, 6096–6102 (2010).

33. Shaw, G. M. & Hunter, E. HIV transmission. *Cold Spring Harb. Perspect. Med.* **2**, (2012).

34. Cohen, M. S., Shaw, G. M., McMichael, A. J. & Haynes, B. F. Acute HIV-1 Infection. *N. Engl. J. Med.* (2011) doi:10.1056/nejmra1011874.

35. Shearer, G. M. & Clerici, M. Early T-helper cell defects in HIV infection. *AIDS* **5**, 245–254 (1991).

36. Doitsh, G., Cavrois, M., Lassen, K. G., Zepeda, O., Yang, Z., Santiago, M. L., Hebbeler, A. M. & Greene, W. C. Abortive HIV Infection Mediates CD4 T Cell Depletion and Inflammation in Human Lymphoid Tissue. *Cell* **143**, 789–801 (2010).

37. Epstein, F. H., Pantaleo, G., Graziosi, C. & Fauci, A. S. The Immunopathogenesis of Human Immunodeficiency Virus Infection. *New England Journal of Medicine* vol. **328** 327–335 (1993).

38. Fischl, M. A., Richman, D. D., Grieco, M. H., Gottlieb, M. S., Volberding, P. A., Laskin, O. L., Leedom, J. M., Groopman, J. E., Mildvan, D., Schooley, R. T., Jackson, G. G., Durack, D. T. & King, D. The Efficacy of Azidothymidine (AZT) in the Treatment of Patients with AIDS and AIDS-Related Complex. *N. Engl. J. Med.* **317**, 185–191 (1987).

39. Popovic, M., Sarngadharan, M. G., Read, E. & Gallo, R. C. Detection, isolation, and continuous production of cytopathic retroviruses (HTLV-III) from patients with AIDS and pre-AIDS. *Science (80-.).* **224**, 497–500 (1984).

40. Levy, J. A., Hoffman, A. D., Kramer, S. M., Landis, J. A., Shimabukuro, J. M. & Oshiro, L. S. Isolation of lymphocytopathic retroviruses from San Francisco patients with AIDS. *Science (80-.).* **225**, 840–842 (1984).

41. Poorolajal, J., Hooshmand, E., Mahjub, H., Esmailnasab, N. & Jenabi, E. Survival rate of AIDS disease and mortality in HIV-infected patients: a meta-analysis. *Public Health* (2016) doi:10.1016/j.puhe.2016.05.004.

42. Sluis-Cremer, N., Temiz, N. & Bahar, I. Conformational Changes in HIV-1 Reverse Transcriptase Induced by Nonnucleoside Reverse Transcriptase Inhibitor Binding. *Curr. HIV Res.* **2**, 323–332 (2005).

43. Kohlstaedt, L. A., Wang, J., Friedman, J. M., Rice, P. A. & Steitz, T. A. Crystal structure at 3.5 Å resolution of HIV-1 reverse transcriptase complexed with an inhibitor. *Science (80-.).* **256**, 1783–1790 (1992).

44. Spence, R. A., Kati, W. M., Anderson, K. S. & Johnson, K. A. Mechanism of inhibition of

HIV-1 reverse transcriptase by nonnucleoside inhibitors. *Science (80-.).* **267**, 988–993 (1995).

45. De Clercq, E. Anti-HIV drugs: 25 compounds approved within 25 years after the discovery of HIV. *International Journal of Antimicrobial Agents* vol. **33** 307–320 (2009).

46. Sluis-Cremer, N. The emerging profile of cross-resistance among the nonnucleoside HIV-1 reverse transcriptase inhibitors. *Viruses* vol. **6** 2960–2973 (2014).

47. Kohl, N. E., Emini, E. A., Schleif, W. A., Davis, L. J., Heimbach, J. C., Dixon, R. A. F., Scolnick, E. M. & Sigal, I. S. Active human immunodeficiency virus protease is required for viral infectivity. *Proc. Natl. Acad. Sci. U. S. A.* (1988) doi:10.1073/pnas.85.13.4686.

48. DHHS Panel. Guidelines for the Use of Antiretroviral Agents in Adults and Adolescents with HIV. *Department of Health and Human Services* 298 https://aidsinfo.nih.gov/contentfiles/lvguidelines/adultandadolescentgl.pdf (2019).

49. Wang, Y., Lv, Z. & Chu, Y. HIV protease inhibitors: a review of molecular selectivity and toxicity. *HIV/AIDS - Res. Palliat. Care* 95 (2015).

50. Espeseth, A. S., Felock, P., Wolfe, A., Witmer, M., Grobler, J., Anthony, N., Egbertson, M., Melamed, J. Y., Young, S., Hamill, T., Cole, J. L. & Hazuda, D. J. HIV-1 integrase inhibitors that compete with the target DNA substrate define a unique strand transfer conformation for integrase. *Proc. Natl. Acad. Sci. U. S. A.* **97**, 11244–11249 (2000).

51. Hazuda, D. J., Felock, P., Witmer, M., Wolfe, A., Stillmock, K., Grobler, J. A., Espeseth, A., Gabryelski, L., Schleif, W., Blau, C. & Miller, M. D. Inhibitors of strand transfer that prevent integration and inhibit HIV-1 replication in cells. *Science (80-.).* **287**, 646–650 (2000).

52. Hare, S., Smith, S. J., Métifiot, M., Jaxa-Chamiec, A., Pommier, Y., Hughes, S. H. &

Cherepanov, P. Structural and functional analyses of the second-generation integrase strand transfer inhibitor dolutegravir (S/GSK1349572). *Mol. Pharmacol.* (2011) doi:10.1124/mol.111.073189.

53. Coffin, J. M. HIV population dynamics in vivo: Implications for genetic variation, pathogenesis, and therapy. *Science (80-.).* (1995) doi:10.1126/science.7824947.

54. Nieuwkerk, P. T., Sprangers, M. A. G., Burger, D. M., Hoetelmans, R. M. W., Hugen, P. W. H., Danner, S. A., Van Der Ende, M. E., Schneider, M. M. E., Schrey, G., Meenhorst, P. L., Sprenger, H. G., Kauffmann, R. H., Jambroes, M., Chesney, M. A., De Wolf, F. & Lange, J. M. A. Limited patient adherence to highly active antiretroviral therapy for HIV-1 infection in an observational cohort study. *Arch. Intern. Med.* (2001) doi:10.1001/archinte.161.16.1962.

55. Biebricher, C. K. & Eigen, M. What is a quasispecies? *Current Topics in Microbiology and Immunology* vol. **299** 1–31 (2006).

56. Clavel, F. & Hance, A. J. HIV Drug Resistance. *N. Engl. J. Med.* (2004) doi:10.1056/nejmra025195.

57. Shafer, R. W. & Vuitton, D. A. Highly active antiretroviral therapy (HAART) for the treatment of infection with human immunodeficiency virus type 1. *Biomed. Pharmacother.* (1999) doi:10.1016/S0753-3322(99)80063-8.

58. Saag, M. S., Benson, C. A., Gandhi, R. T., Hoy, J. F., Landovitz, R. J., Mugavero, M. J., Sax, P. E., Smith, D. M., Thompson, M. A., Buchbinder, S. P., Del Rio, C., Eron, J. J., Fätkenheuer, G., Günthard, H. F., Molina, J. M., Jacobsen, D. M. & Volberding, P. A. Antiretroviral drugs for treatment and prevention of HIV infection in adults: 2018 recommendations of the international antiviral society-USA panel. in *JAMA - Journal of the*

American Medical Association (2018). doi:10.1001/jama.2018.8431.

59. Panganiban, A. T. & Fiore, D. Ordered interstrand and intrastrand DNA transfer during reverse transcription. *Science (80-.).* (1988) doi:10.1126/science.2457948.

60. Hu, W. S. & Temin, H. M. Retroviral recombination and reverse transcription. *Science (80-.).* (1990) doi:10.1126/science.1700865.

61. Isel, C., Lanchy, J. M., Le Grice, S. F. J., Ehresmann, C., Ehresmann, B. & Marquet, R. Specific initiation and switch to elongation of human immunodeficiency virus type 1 reverse transcription require the post-transcriptional modifications of primer tRNA3Lys. *EMBO J.* (1996) doi:10.1002/j.1460-2075.1996.tb00426.x.

62. Charneau, P., Alizon, M. & Clavel, F. A second origin of DNA plus-strand synthesis is required for optimal human immunodeficiency virus replication. *J. Virol.* (1992) doi:10.1128/jvi.66.5.2814-2820.1992.

63. Hungnesi, O., Tjøtta, E. & Grinde, B. Mutations in the central polypurine tract of HIV-1 result in delayed replication. *Virology* (1992) doi:10.1016/0042-6822(92)91230-R.

64. Swanstrom, R., Varmus, H. E. & Bishop, J. M. The terminal redundancy of the retrovirus genome facilitates chain elongation by reverse transcriptase. *J. Biol. Chem.* **256**, 1115–21 (1981).

65. Whitcomb, J. M., Kumar, R. & Hughes, S. H. Sequence of the circle junction of human immunodeficiency virus type 1: implications for reverse transcription and integration. *J. Virol.* (1990) doi:10.1128/jvi.64.10.4903-4906.1990.

66. Kwong, P. D., Wyatt, R., Robinson, J., Sweet, R. W., Sodroski, J. & Hendrickson, W. A. Structure of an HIV gp 120 envelope glycoprotein in complex with the CD4 receptor and a neutralizing human antibody. *Nature* vol. **393** 648–659 (1998).

67. Finzi, A., Xiang, S. H., Pacheco, B., Wang, L., Haight, J., Kassa, A., Danek, B., Pancera, M., Kwong, P. D. & Sodroski, J. Topological Layers in the HIV-1 gp120 Inner Domain Regulate gp41 Interaction and CD4-Triggered Conformational Transitions. *Mol. Cell* **37**, 656–667 (2010).

68. Jacks, T., Power, M. D., Masiarz, F. R., Luciw, P. A., Barr, P. J. & Varmus, H. E. Characterization of ribosomal frameshifting in HIV-1 gag-pol expression. *Nature* (1988) doi:10.1038/331280a0.

69. Narayan, O. & Clements, J. E. Biology and pathogenesis of lentiviruses. *Journal of General Virology* vol. **70** 1617–1639 (1989).

70. Katz, R. A. & Skalka, A. M. The retroviral enzymes. *Annu. Rev. Biochem.* **63**, 133–173 (1994).

71. Byeon, I. J. L., Meng, X., Jung, J., Zhao, G., Yang, R., Ahn, J., Shi, J., Concel, J., Aiken, C., Zhang, P. & Gronenborn, A. M. Structural Convergence between Cryo-EM and NMR Reveals Intersubunit Interactions Critical for HIV-1 Capsid Function. *Cell* **139**, 780–790 (2009).

72. Ganser, B. K., Li, S., Klishko, V. Y., Finch, J. T. & Sundquist, W. I. Assembly and analysis of conical models for the HIV-1 core. *Science (80-.).* **283**, 80–83 (1999).

73. Zhao, G., Perilla, J. R., Yufenyuy, E. L., Meng, X., Chen, B., Ning, J., Ahn, J., Gronenborn, A. M., Schulten, K., Aiken, C. & Zhang, P. Mature HIV-1 capsid structure by cryo-electron microscopy and all-atom molecular dynamics. *Nature* **497**, 643–646 (2013).

74. Watts, J. M., Dang, K. K., Gorelick, R. J., Leonard, C. W., Bess, J. W., Swanstrom, R., Burch, C. L. & Weeks, K. M. Architecture and secondary structure of an entire HIV-1 RNA genome. *Nature* **460**, 711–716 (2009).

75. Chang, D. D. & Sharp, P. A. Regulation by HIV Rev depends upon recognition of splice sites. *Cell* (1989) doi:10.1016/0092-8674(89)90602-8.

76. Frankel, A. D. & Young, J. A. T. HIV-1: Fifteen proteins and an RNA. *Annu. Rev. Biochem.* **67**, 1–25 (1998).

77. Arya, S. K. & Gallo, R. C. Three novel genes of human T-lymphotropic virus type III: Immune reactivity of their products with sera from acquired immune deficiency syndrome patients. *Proc. Natl. Acad. Sci. U. S. A.* (1986) doi:10.1073/pnas.83.7.2209.

78. Luciw, P. A., Cheng-Mayer, C. & Levy, J. A. Mutational analysis of the human immunodeficiency virus: The orf-B region down-regulates virus replication. *Proc. Natl. Acad. Sci. U. S. A.* (1987) doi:10.1073/pnas.84.5.1434.

79. Kestier, H. W., Ringler, D. J., Mori, K., Panicali, D. L., Sehgal, P. K., Daniel, M. D. & Desrosiers, R. C. Importance of the nef gene for maintenance of high virus loads and for development of AIDS. *Cell* (1991) doi:10.1016/0092-8674(91)90097-I.

80. Cullen, B. R. Trans-activation of human immunodeficiency virus occurs via a bimodal mechanism. *Cell* **46**, 973–982 (1986).

81. Emerman, M., Vazeux, R. & Peden, K. The rev gene product of the human immunodeficiency virus affects envelope-specific RNA localization. *Cell* **57**, 1155–1165 (1989).

82. Ooms, M., Abbink, T. E. M., Pham, C. & Berkhout, B. Circularization of the HIV-1 RNA genome. *Nucleic Acids Res.* (2007) doi:10.1093/nar/gkm564.

83. Sierra, S., Kupfer, B. & Kaiser, R. Basics of the virology of HIV-1 and its replication. *Journal of Clinical Virology* vol. **34** 233–244 (2005).

84. Lu, K., Heng, X. & Summers, M. F. Structural determinants and mechanism of HIV-1

genome packaging. *Journal of Molecular Biology* vol. **410** 609–633 (2011).

85. Briggs, J. A. G., Wilk, T., Welker, R., Kräusslich, H. G. & Fuller, S. D. Structural organization of authentic, mature HIV-1 virions and cores. *EMBO J.* **22**, 1707–1715 (2003).

86. Fontana, J., Jurado, K. A., Cheng, N., Ly, N. L., Fuchs, J. R., Gorelick, R. J., Engelman, A. N. & Steven, A. C. Distribution and Redistribution of HIV-1 Nucleocapsid Protein in Immature, Mature, and Integrase-Inhibited Virions: a Role for Integrase in Maturation. *J. Virol.* **89**, 9765–9780 (2015).

87. Kessl, J. J., Kutluay, S. B., Townsend, D., Rebensburg, S., Slaughter, A., Larue, R. C., Shkriabai, N., Bakouche, N., Fuchs, J. R., Bieniasz, P. D. & Kvaratskhelia, M. HIV-1 Integrase Binds the Viral RNA Genome and Is Essential during Virion Morphogenesis. *Cell* **166**, 1257-1268.e12 (2016).

88. Di Marzo Veronese, F., Copeland, T. D., Devico, A. L., Rahman, R., Oroszlan, S., Gallo, R. C. & Sarngadharan, M. G. Characterization of highly immunogenic p66/p51 as the reverse transcriptase of HTLV-III/LAV. *Science (80-.).* **231**, 1289–1291 (1986).

89. Davies, J. F., Hostomska, Z., Hostomsky, Z., Jordan, S. R. & Matthews, D. A. Crystal structure of the ribonuclease H domain of HIV-1 reverse transcriptase. *Science (80-.).* (1991) doi:10.1126/science.1707186.

90. Hu, W.-S. & Hughes, S. H. HIV-1 Reverse Transcription. *Cold Spring Harb. Perspect. Med.* **2**, a006882–a006882 (2012).

91. Collin, M. & Gordon, S. The kinetics of human immunodeficiency virus reverse transcription are slower in primary human macrophages than in a lymphoid cell line. *Virology* **200**, 114–120 (1994).

92. Penno, C., Kumari, R., Baranov, P. V., Van Sinderen, D. & Atkins, J. F. Stimulation of

reverse transcriptase generated cDNAs with specific indels by template RNA structure: Retrotransposon, dNTP balance, RT-reagent usage. *Nucleic Acids Res.* **45**, 10143–10155 (2017).

93. Trono, D. Partial reverse transcripts in virions from human immunodeficiency and murine leukemia viruses. *J. Virol.* **66**, 4893–4900 (1992).

94. Ambrose, Z. & Aiken, C. HIV-1 uncoating: Connection to nuclear entry and regulation by host proteins. *Virology* vols **454**–**455** 371–379 (2014).

95. Fassati, A. & Goff, S. P. Characterization of Intracellular Reverse Transcription Complexes of Human Immunodeficiency Virus Type 1. *J. Virol.* **75**, 3626–3635 (2001).

96. Miller, M. D., Farnet, C. M. & Bushman, F. D. Human immunodeficiency virus type 1 preintegration complexes: studies of organization and composition. *J. Virol.* **71**, 5382–5390 (1997).

97. Lewis, P., Hensel, M. & Emerman, M. Human immunodeficiency virus infection of cells arrested in the cell cycle. *EMBO J.* **11**, 3053–3058 (1992).

98. Pornillos, O., Ganser-Pornillos, B. K. & Yeager, M. Atomic-level modelling of the HIV capsid. *Nature* **469**, 424–427 (2011).

99. Dick, R. A., Zadrozny, K. K., Xu, C., Schur, F. K. M., Lyddon, T. D., Ricana, C. L., Wagner, J. M., Perilla, J. R., Ganser-Pornillos, B. K., Johnson, M. C., Pornillos, O. & Vogt, V. M. Inositol phosphates are assembly co-factors for HIV-1. *Nature* **560**, 509–512 (2018).

100. Mallery, D. L., Márquez, C. L., McEwan, W. A., Dickson, C. F., Jacques, D. A., Anandapadamanaban, M., Bichel, K., Towers, G. J., Saiardi, A., Böcking, T. & James, L. C. IP6 is an HIV pocket factor that prevents capsid collapse and promotes DNA synthesis. *Elife* **7**, (2018).

101. Engelman, A. & Cherepanov, P. The structural biology of HIV-1: Mechanistic and therapeutic insights. *Nature Reviews Microbiology* (2012) doi:10.1038/nrmicro2747.

102. Campbell, E. M. & Hope, T. J. HIV-1 capsid: The multifaceted key player in HIV-1 infection. *Nature Reviews Microbiology* vol. **13** 471–483 (2015).

103. Matreyek, K. A., Yücel, S. S., Li, X. & Engelman, A. Nucleoporin NUP153 Phenylalanine-Glycine Motifs Engage a Common Binding Pocket within the HIV-1 Capsid Protein to Mediate Lentiviral Infectivity. *PLoS Pathog.* **9**, e1003693 (2013).

104. Peng, K., Muranyi, W., Glass, B., Laketa, V., Yant, S. R., Tsai, L., Cihlar, T., Müller, B. & Kräusslich, H. G. Quantitative microscopy of functional HIV post-entry complexes reveals association of replication with the viral capsid. *Elife* **3**, e04114 (2014).

105. Francis, A. C. & Melikyan, G. B. Single HIV-1 Imaging Reveals Progression of Infection through CA-Dependent Steps of Docking at the Nuclear Pore, Uncoating, and Nuclear Transport. *Cell Host Microbe* **23**, 536-548.e6 (2018).

106. Zurnic Bönisch, I., Dirix, L., Lemmens, V., Borrenberghs, D., De Wit, F., Vernaillen, F., Rocha, S., Christ, F., Hendrix, J., Hofkens, J. & Debyser, Z. Capsid-Labelled HIV To Investigate the Role of Capsid during Nuclear Import and Integration. *J. Virol.* **94**, (2020).

107. Xu, H., Franks, T., Gibson, G., Huber, K., Rahm, N., De Castillia, C. S., Luban, J., Aiken, C., Watkins, S., Sluis-Cremer, N. & Ambrose, Z. Evidence for biphasic uncoating during HIV-1 infection from a novel imaging assay. *Retrovirology* **10**, (2013).

108. Dharan, A., Talley, S., Tripathi, A., Mamede, J. I., Majetschak, M., Hope, T. J. & Campbell, E. M. KIF5B and Nup358 Cooperatively Mediate the Nuclear Import of HIV-1 during Infection. *PLOS Pathog.* **12**, e1005700 (2016).

109. Burdick, R. C., Li, C., Munshi, M. H., Rawson, J. M. O., Nagashima, K., Hu, W. S. &

Pathak, V. K. HIV-1 uncoats in the nucleus near sites of integration. *Proc. Natl. Acad. Sci. U. S. A.* **117**, 5486–5493 (2020).

110. Dharan, A., Bachmann, N., Talley, S., Zwikelmaier, V. & Campbell, E. M. Nuclear pore blockade reveals that HIV-1 completes reverse transcription and uncoating in the nucleus. *Nat. Microbiol.* **5**, 1088–1095 (2020).

111. Forshey, B. M., von Schwedler, U., Sundquist, W. I. & Aiken, C. Formation of a Human Immunodeficiency Virus Type 1 Core of Optimal Stability Is Crucial for Viral Replication. *J. Virol.* **76**, 5667–5677 (2002).

112. Hulme, A. E., Perez, O. & Hope, T. J. Complementary assays reveal a relationship between HIV-1 uncoating and reverse transcription. *Proc. Natl. Acad. Sci. U. S. A.* **108**, 9975–9980 (2011).

113. Cosnefroy, O., Murray, P. J. & Bishop, K. N. HIV-1 capsid uncoating initiates after the first strand transfer of reverse transcription. *Retrovirology* **13**, 58 (2016).

114. Rankovic, S., Varadarajan, J., Ramalho, R., Aiken, C. & Rousso, I. Reverse Transcription Mechanically Initiates HIV-1 Capsid Disassembly. *J. Virol.* **91**, (2017).

115. Ning, J., Zhong, Z., Fischer, D. K., Harris, G., Watkins, S. C., Ambrose, Z. & Zhang, P. Truncated CPSF6 Forms Higher-Order Complexes That Bind and Disrupt HIV-1 Capsid. *J. Virol.* **92**, (2018).

116. Liu, C., Perilla, J. R., Ning, J., Lu, M., Hou, G., Ramalho, R., Himes, B. A., Zhao, G., Bedwell, G. J., Byeon, I.-J., Ahn, J., Gronenborn, A. M., Prevelige, P. E., Rousso, I., Aiken, C., Polenova, T., Schulten, K. & Zhang, P. Cyclophilin A stabilizes the HIV-1 capsid through a novel non-canonical binding site. *Nat. Commun.* **7**, 10714 (2016).

117. Stremlau, M., Owens, C. M., Perron, M. J., Kiessling, M., Autissier, P. & Sodroski, J. The

cytoplasmic body component TRIM5α restricts HIV-1 infection in Old World monkeys. *Nature* **427**, 848–853 (2004).

118. Pertel, T., Hausmann, S., Morger, D., Züger, S., Guerra, J., Lascano, J., Reinhard, C., Santoni, F. A., Uchil, P. D., Chatel, L., Bisiaux, A., Albert, M. L., Strambio-De-Castillia, C., Mothes, W., Pizzato, M., Grütter, M. G. & Luban, J. TRIM5 is an innate immune sensor for the retrovirus capsid lattice. *Nature* **472**, 361–365 (2011).

119. Yamashita, M. & Emerman, M. Capsid Is a Dominant Determinant of Retrovirus Infectivity in Nondividing Cells. *J. Virol.* **78**, 5670–5678 (2004).

120. Brass, A. L., Dykxhoorn, D. M., Benita, Y., Yan, N., Engelman, A., Xavier, R. J., Lieberman, J. & Elledge, S. J. Identification of host proteins required for HIV infection through a functional genomic screen. *Science (80-.).* **319**, 921–926 (2008).

121. König, R., Zhou, Y., Elleder, D., Diamond, T. L., Bonamy, G. M. C., Irelan, J. T., Chiang, C. yuan, Tu, B. P., De Jesus, P. D., Lilley, C. E., Seidel, S., Opaluch, A. M., Caldwell, J. S., Weitzman, M. D., Kuhen, K. L., Bandyopadhyay, S., Ideker, T., Orth, A. P., Miraglia, L. J., *et al.* Global Analysis of Host-Pathogen Interactions that Regulate Early-Stage HIV-1 Replication. *Cell* **135**, 49–60 (2008).

122. Zhou, H., Xu, M., Huang, Q., Gates, A. T., Zhang, X. D., Castle, J. C., Stec, E., Ferrer, M., Strulovici, B., Hazuda, D. J. & Espeseth, A. S. Genome-Scale RNAi Screen for Host Factors Required for HIV Replication. *Cell Host Microbe* **4**, 495–504 (2008).

123. Yamashita, M. & Emerman, M. Retroviral infection of non-dividing cells: Old and new perspectives. *Virology* vol. **344** 88–93 (2006).

124. Zennou, V., Petit, C., Guetard, D., Nerhbass, U., Montagnier, L. & Charneau, P. HIV-1 genome nuclear import is mediated by a central DNA flap. *Cell* **101**, 173–185 (2000).

125. Dvorin, J. D., Bell, P., Maul, G. G., Yamashita, M., Emerman, M. & Malim, M. H. Reassessment of the Roles of Integrase and the Central DNA Flap in Human Immunodeficiency Virus Type 1 Nuclear Import. *J. Virol.* **76**, 12087–12096 (2002).

126. Bukrinsky, M. I., Haggerty, S., Dempsey, M. P., Sharova, N., Adzhubei, A., Spitz, L., Lewis, P., Goldfarb, D., Emerman, M. & Stevenson, M. A nuclear localization signal within HIV-1 matrix protein that governs infection of non-dividing cells. *Nature* **365**, 666–669 (1993).

127. Haffar, O. K., Popov, S., Dubrovsky, L., Agostini, I., Tang, H., Pushkarsky, T., Nadler, S. G. & Bukrinsky, M. Two nuclear localization signals in the HIV-1 matrix protein regulate nuclear import of the HIV-1 pre-integration complex. *J. Mol. Biol.* **299**, 359–368 (2000).

128. Armon-Omer, A., Graessmann, A. & Loyter, A. A Synthetic Peptide Bearing the HIV-1 Integrase 161-173 Amino Acid Residues Mediates Active Nuclear Import and Binding to Importin α: Characterization of a Functional Nuclear Localization Signal. *J. Mol. Biol.* **336**, 1117–1128 (2004).

129. Bouyac-Bertoia, M., Dvorin, J. D., Fouchier, R. A. M., Jenkins, Y., Meyer, B. E., Wu, L. I., Emerman, M. & Malim, M. H. HIV-1 Infection Requires a Functional Integrase NLS. *Mol. Cell* **7**, 1025–1035 (2001).

130. Gallay, P., Hope, T., Chin, D. & Trono, D. HIV-1 infection of nondividing cells through the recognition of integrase by the importin/karyopherin pathway. *Proc. Natl. Acad. Sci. U. S. A.* **94**, 9825–9830 (1997).

131. Rivière, L., Darlix, J.-L. & Cimarelli, A. Analysis of the Viral Elements Required in the Nuclear Import of HIV-1 DNA. *J. Virol.* **84**, 729–739 (2010).

132. Fouchier, R. A. M., Meyer, B. E., Simon, J. H. M., Fischer, U. & Malim, M. H. HIV-1

infection of non-dividing cells: Evidence that the amino-terminal basic region of the viral matrix protein is important for Gag processing but not for post-entry nuclear import. *EMBO J.* **16**, 4531–4539 (1997).

133. Freed, E. O., Englund, G., Maldarelli, F. & Martin, M. A. Phosphorylation of residue 131 of HIV-1 matrix is not required for macrophage infection. *Cell* **88**, 171–173 (1997).

134. Reil, H., Bukovsky, A. A., Gelderblom, H. R. & Göttlinger, H. Efficient HIV-1 replication can occur in the absence of the viral matrix protein. *EMBO J.* **17**, 2699–2708 (1998).

135. Limón, A., Devroe, E., Lu, R., Ghory, H. Z., Silver, P. A. & Engelman, A. Nuclear Localization of Human Immunodeficiency Virus Type 1 Preintegration Complexes (PICs): V165A and R166A Are Pleiotropic Integrase Mutants Primarily Defective for Integration, Not PIC Nuclear Import. *J. Virol.* **76**, 10598–10607 (2002).

136. Limón, A., Nakajima, N., Lu, R., Ghory, H. Z. & Engelman, A. Wild-Type Levels of Nuclear Localization and Human Immunodeficiency Virus Type 1 Replication in the Absence of the Central DNA Flap. *J. Virol.* **76**, 12078–12086 (2002).

137. Petit, C., Schwartz, O. & Mammano, F. The Karyophilic Properties of Human Immunodeficiency Virus Type 1 Integrase Are Not Required for Nuclear Import of Proviral DNA. *J. Virol.* **74**, 7119–7126 (2000).

138. Yamashita, M., Perez, O., Hope, T. J. & Emerman, M. Evidence for direct involvement of the capsid protein in HIV infection of nondividing cells. *PLoS Pathog.* **3**, 1502–1510 (2007).

139. Krishnan, L., Matreyek, K. A., Oztop, I., Lee, K., Tipper, C. H., Li, X., Dar, M. J., KewalRamani, V. N. & Engelman, A. The Requirement for Cellular Transportin 3 (TNPO3 or TRN-SR2) during Infection Maps to Human Immunodeficiency Virus Type 1 Capsid

and Not Integrase. *J. Virol.* **84**, 397–406 (2010).

140. Schaller, T., Ocwieja, K. E., Rasaiyaah, J., Price, A. J., Brady, T. L., Roth, S. L., Hué, S., Fletcher, A. J., Lee, K., KewalRamani, V. N., Noursadeghi, M., Jenner, R. G., James, L. C., Bushman, F. D. & Towers, G. J. HIV-1 Capsid-Cyclophilin Interactions Determine Nuclear Import Pathway, Integration Targeting and Replication Efficiency. *PLoS Pathog.* **7**, e1002439 (2011).

141. Lee, K. E., Ambrose, Z., Martin, T. D., Oztop, I., Mulky, A., Julias, J. G., Vandegraaff, N., Baumann, J. G., Wang, R., Yuen, W., Takemura, T., Shelton, K., Taniuchi, I., Li, Y., Sodroski, J., Littman, D. R., Coffin, J. M., Hughes, S. H., Unutmaz, D., *et al.* Flexible Use of Nuclear Import Pathways by HIV-1. *Cell Host Microbe* **7**, 221–233 (2010).

142. Ambrose, Z., Lee, K., Ndjomou, J., Xu, H., Oztop, I., Matous, J., Takemura, T., Unutmaz, D., Engelman, A., Hughes, S. H. & KewalRamani, V. N. Human Immunodeficiency Virus Type 1 Capsid Mutation N74D Alters Cyclophilin A Dependence and Impairs Macrophage Infection. *J. Virol.* **86**, 4708–4714 (2012).

143. Maertens, G. N., Cook, N. J., Wang, W., Hare, S., Gupta, S. S., Öztop, I., Lee, K. E., Pye, V. E., Cosnefroy, O., Snijders, A. P., Ramani, V. N. K., Fassati, A., Engelman, A. & Cherepanov, P. Structural basis for nuclear import of splicing factors by human Transportin 3. *Proc. Natl. Acad. Sci. U. S. A.* **111**, 2728–2733 (2014).

144. Price, A. J., Fletcher, A. J., Schaller, T., Elliott, T., Lee, K., KewalRamani, V. N., Chin, J. W., Towers, G. J. & James, L. C. CPSF6 Defines a Conserved Capsid Interface that Modulates HIV-1 Replication. *PLoS Pathog.* **8**, e1002896 (2012).

145. De Iaco, A., Santoni, F., Vannier, A., Guipponi, M., Antonarakis, S. & Luban, J. TNPO3 protects HIV-1 replication from CPSF6-mediated capsid stabilization in the host cell

cytoplasm. *Retrovirology* **10**, 20 (2013).

146. Saito, A., Henning, M. S., Serrao, E., Dubose, B. N., Teng, S., Huang, J., Li, X., Saito, N., Roy, S. P., Siddiqui, M. A., Ahn, J., Tsuji, M., Hatziioannou, T., Engelman, A. N. & Yamashita, M. Capsid-CPSF6 Interaction Is Dispensable for HIV-1 Replication in Primary Cells but Is Selected during Virus Passage In Vivo . *J. Virol.* **90**, 6918–6935 (2016).

147. Buffone, C., Martinez-Lopez, A., Fricke, T., Opp, S., Severgnini, M., Cifola, I., Petiti, L., Frabetti, S., Skorupka, K., Zadrozny, K. K., Ganser-Pornillos, B. K., Pornillos, O., Di Nunzio, F. & Diaz-Griffero, F. Nup153 Unlocks the Nuclear Pore Complex for HIV-1 Nuclear Translocation in Nondividing Cells. *J. Virol.* **92**, e00648-18 (2018).

148. Brown, P. O., Bowerman, B., Varmus, H. E. & Bishop, J. M. Correct integration of retroviral DNA in vitro. *Cell* **49**, 347–356 (1987).

149. Craigie, R., Fujiwara, T. & Bushman, F. The IN protein of Moloney murine leukemia virus processes the viral DNA ends and accomplishes their integration in vitro. *Cell* **62**, 829–837 (1990).

150. Engelman, A., Mizuuchi, K. & Craigie, R. HIV-1 DNA integration: Mechanism of viral DNA cleavage and DNA strand transfer. *Cell* **67**, 1211–1221 (1991).

151. Skalka, A. M. & Katz, R. A. Retroviral DNA integration and the DNA damage response. *Cell Death and Differentiation* vol. **12** 971–978 (2005).

152. Ciuffi, A., Llano, M., Poeschla, E., Hoffmann, C., Leipzig, J., Shinn, P., Ecker, J. R. & Bushman, F. A role for LEDGF/p75 in targeting HIV DNA integration. *Nat. Med.* **11**, 1287–1289 (2005).

153. Sowd, G. A., Serrao, E., Wang, H., Wang, W., Fadel, H. J., Poeschla, E. M. & Engelman, A. N. A critical role for alternative polyadenylation factor CPSF6 in targeting HIV-1

integration to transcriptionally active chromatin. *Proc. Natl. Acad. Sci.* **113**, E1054–E1063 (2016).

154. Llano, M., Delgado, S., Vanegas, M. & Poeschla, E. M. Lens epithelium-derived growth factor/p75 prevents proteasomal degradation of HIV-1 integrase. *J. Biol. Chem.* **279**, 55570–55577 (2004).

155. Jones, K. A. & Matija Peterlin, B. Control of RNA initiation and elongation at the HIV-1 promoter. *Annual Review of Biochemistry* vol. **63** 717–743 (1994).

156. Kao, S. Y., Calman, A. F., Luciw, P. A. & Peterlin, B. M. Anti-termination of transcription within the long terminal repeat of HIV-1 by tat gene product. *Nature* **330**, 489–493 (1987).

157. Vollenweider, F., Benjannet, S., Decroly, E., Savaria, D., Lazure, C., Thomas, G., Chrétien, M. & Seidah, N. G. Comparative cellular processing of the human immunodeficiency virus (HIV-1) envelope glycoprotein gp160 by the mammalian subtilisin/kexin-like convertases. *Biochem. J.* **314**, 521–532 (1996).

158. Giese, S. & Marsh, M. Cellular trafficking mechanisms in the assembly and release of HIV. in *Advances in HIV-1 Assembly and Release* 23–53 (2013).

159. Sundquist, W. I. & Kräusslich, H.-G. HIV-1 assembly, budding, and maturation. *Cold Spring Harb. Perspect. Med.* **2**, a006924 (2012).

160. Freed, E. O. HIV-1 assembly, release and maturation. *Nature Reviews Microbiology* vol. **13** 484–496 (2015).

161. Ono, A. Relationships between plasma membrane microdomains and HIV-1 assembly. *Biol. Cell* **102**, 335–350 (2010).

162. Morita, E., Sandrin, V., McCullough, J., Katsuyama, A., Baci Hamilton, I. & Sundquist, W. I. ESCRT-III Protein Requirements for HIV-1 Budding. *Cell Host Microbe* **9**, 235–242

(2011).

163. Colomer-Lluch, M., Ruiz, A., Moris, A. & Prado, J. G. Restriction Factors: From Intrinsic Viral Restriction to Shaping Cellular Immunity Against HIV-1. *Frontiers in immunology* vol. **9** 2876 (2018).

164. Harris, R. S., Sheehy, A. M., Craig, H. M., Malim, M. H. & Neuberger, M. S. DNA deamination: Not just a trigger for antibody diversification but also a mechanism for defense against retroviruses. *Nat. Immunol.* **4**, 641–643 (2003).

165. Sheehy, A. M., Gaddis, N. C. & Malim, M. H. The antiretroviral enzyme APOBEC3G is degraded by the proteasome in response to HIV-1 Vif. *Nat. Med.* **9**, 1404–1407 (2003).

166. Wiegand, H. L., Doehle, B. P., Bogerd, H. P. & Cullen, B. R. A second human antiretroviral factor, APOBEC3F, is suppressed by the HIV-1 and HIV-2 Vif proteins. *EMBO J.* **23**, 2451–2458 (2004).

167. Huthoff, H. & Malim, M. H. Identification of Amino Acid Residues in APOBEC3G Required for Regulation by Human Immunodeficiency Virus Type 1 Vif and Virion Encapsidation. *J. Virol.* **81**, 3807–3815 (2007).

168. Marin, M., Rose, K. M., Kozak, S. L. & Kabat, D. HIV-1 Vif protein binds the editing enzyme APOBEC3G and induces its degradation. *Nat. Med.* **9**, 1398–1403 (2003).

169. Lim, E. S., Fregoso, O. I., McCoy, C. O., Matsen, F. A., Malik, H. S. & Emerman, M. The ability of primate lentiviruses to degrade the monocyte restriction factor SAMHD1 preceded the birth of the viral accessory protein Vpx. *Cell Host Microbe* **11**, 194–204 (2012).

170. Goldstone, D. C., Ennis-Adeniran, V., Hedden, J. J., Groom, H. C. T., Rice, G. I., Christodoulou, E., Walker, P. A., Kelly, G., Haire, L. F., Yap, M. W., De Carvalho, L. P. S., Stoye, J. P., Crow, Y. J., Taylor, I. A. & Webb, M. HIV-1 restriction factor SAMHD1

is a deoxynucleoside triphosphate triphosphohydrolase. *Nature* **480**, 379–382 (2011).

171. Laguette, N., Sobhian, B., Casartelli, N., Ringeard, M., Chable-Bessia, C., Ségéral, E., Yatim, A., Emiliani, S., Schwartz, O. & Benkirane, M. SAMHD1 is the dendritic- and myeloid-cell-specific HIV-1 restriction factor counteracted by Vpx. *Nature* **474**, 654–657 (2011).

172. Hrecka, K., Hao, C., Gierszewska, M., Swanson, S. K., Kesik-Brodacka, M., Srivastava, S., Florens, L., Washburn, M. P. & Skowronski, J. Vpx relieves inhibition of HIV-1 infection of macrophages mediated by the SAMHD1 protein. *Nature* (2011) doi:10.1038/nature10195.

173. Neil, S. J. D., Zang, T. & Bieniasz, P. D. Tetherin inhibits retrovirus release and is antagonized by HIV-1 Vpu. *Nature* **451**, 425–430 (2008).

174. Perez-Caballero, D., Zang, T., Ebrahimi, A., McNatt, M. W., Gregory, D. A., Johnson, M. C. & Bieniasz, P. D. Tetherin Inhibits HIV-1 Release by Directly Tethering Virions to Cells. *Cell* **139**, 499–511 (2009).

175. Van Damme, N., Goff, D., Katsura, C., Jorgenson, R. L., Mitchell, R., Johnson, M. C., Stephens, E. B. & Guatelli, J. The Interferon-Induced Protein BST-2 Restricts HIV-1 Release and Is Downregulated from the Cell Surface by the Viral Vpu Protein. *Cell Host Microbe* **3**, 245–252 (2008).

176. Peng, H., Feldman, I. & Rauscher, F. J. Hetero-oligomerization among the TIF family of RBCC/TRIM domain-containing nuclear cofactors: A potential mechanism for regulating the switch between coactivation and corepression. *J. Mol. Biol.* **320**, 629–644 (2002).

177. Stremlau, M., Perron, M., Welikala, S. & Sodroski, J. Species-Specific Variation in the B30.2(SPRY) Domain of TRIM5α Determines the Potency of Human Immunodeficiency

Virus Restriction. *J. Virol.* (2005) doi:10.1128/jvi.79.5.3139-3145.2005.

178. Nakayama, E. E., Miyoshi, H., Nagai, Y. & Shioda, T. A Specific Region of 37 Amino Acid Residues in the SPRY (B30.2) Domain of African Green Monkey TRIM5α Determines Species-Specific Restriction of Simian Immunodeficiency Virus SIVmac Infection. *J. Virol.* (2005) doi:10.1128/jvi.79.14.8870-8877.2005.

179. Yang, H., Ji, X., Zhao, G., Ning, J., Zhao, Q., Aiken, C., Gronenborn, A. M., Zhang, P. & Xiong, Y. Structural insight into HIV-1 capsid recognition by rhesus TRIM5α. *Proc. Natl. Acad. Sci. U. S. A.* (2012) doi:10.1073/pnas.1210903109.

180. Lascano, J., Uchil, P. D., Mothes, W. & Luban, J. TRIM5 Retroviral Restriction Activity Correlates with the Ability To Induce Innate Immune Signaling. *J. Virol.* **90**, 308–316 (2016).

181. Stamnes, M. A., Rutherford, S. L. & Zuker, C. S. Cyclophilins: a new family of proteins involved in intracellular folding. *Trends Cell Biol.* **2**, 272–276 (1992).

182. Luban, J., Bossolt, K. L., Franke, E. K., Kalpana, G. V. & Goff, S. P. Human immunodeficiency virus type 1 Gag protein binds to cyclophilins A and B. *Cell* **73**, 1067–1078 (1993).

183. Bosco, D. A., Eisenmesser, E. Z., Pochapsky, S., Sundquist, W. I. & Kern, D. Catalysis of cis/trans isomerization in native HIV-1 capsid by human cyclophilin A. *Proc. Natl. Acad. Sci. U. S. A.* **99**, 5247–5252 (2002).

184. Kim, K., Dauphin, A., Komurlu, S., McCauley, S. M., Yurkovetskiy, L., Carbone, C., Diehl, W. E., Strambio-De-Castillia, C., Campbell, E. M. & Luban, J. Cyclophilin A protects HIV-1 from restriction by human TRIM5α. *Nature Microbiology* vol. **4** 2044–2051 (2019).

185. Selyutina, A., Persaud, M., Simons, L. M., Bulnes-Ramos, A., Buffone, C., Martinez-

Lopez, A., Scoca, V., Di Nunzio, F., Hiatt, J., Marson, A., Krogan, N. J., Hultquist, J. F. & Diaz-Griffero, F. Cyclophilin A Prevents HIV-1 Restriction in Lymphocytes by Blocking Human TRIM5α Binding to the Viral Core. *Cell Rep.* (2020) doi:10.1016/j.celrep.2020.02.100.

186. Tasnim, H., Fricke, G. M., Byrum, J. R., Sotiris, J. O., Cannon, J. L. & Moses, M. E. Quantitative Measurement of Naïve T Cell Association With Dendritic Cells, FRCs, and Blood Vessels in Lymph Nodes. *Front. Immunol.* **9**, (2018).

187. Guertin, D. A. & Sabatini, D. M. Cell Size Control. in *Encyclopedia of Life Sciences* (John Wiley & Sons, Ltd, 2006).

188. Luby-Phelps, K. Cytoarchitecture and physical properties of cytoplasm: Volume, viscosity, diffusion, intracellular surface area. *Int. Rev. Cytol.* **192**, 189–221 (1999).

189. Leopold, P. L. & Pfister, K. K. Viral strategies for intracellular trafficking: Motors and microtubules. *Traffic* vol. **7** 516–523 (2006).

190. Verhey, K. J. & Hammond, J. W. Traffic control: Regulation of kinesin motors. *Nature Reviews Molecular Cell Biology* vol. **10** 765–777 (2009).

191. McKenney, R. J., Huynh, W., Tanenbaum, M. E., Bhabha, G. & Vale, R. D. Activation of cytoplasmic dynein motility by dynactin-cargo adapter complexes. *Science (80-.).* **345**, 337–341 (2014).

192. Höök, P. & Vallee, R. B. The dynein family at a glance. *J. Cell Sci.* **119**, 4369–4371 (2006).

193. Hirokawa, N., Nitta, R. & Okada, Y. The mechanisms of kinesin motor motility: Lessons from the monomeric motor KIF1A. *Nature Reviews Molecular Cell Biology* vol. **10** 877–884 (2009).

194. Malikov, V., da Silva, E. S., Jovasevic, V., Bennett, G., de Souza Aranha Vieira, D. A.,

Schulte, B., Diaz-Griffero, F., Walsh, D. & Naghavi, M. H. HIV-1 capsids bind and exploit the kinesin-1 adaptor FEZ1 for inward movement to the nucleus. *Nat. Commun.* **6**, 6660 (2015).

195. Dharan, A., Opp, S., Abdel-Rahim, O., Keceli, S. K., Imam, S., Diaz-Griffero, F. & Campbell, E. M. Bicaudal D2 facilitates the cytoplasmic trafficking and nuclear import of HIV-1 genomes during infection. *Proc. Natl. Acad. Sci. U. S. A.* **114**, E10707–E10716 (2017).

196. Lukic, Z., Dharan, A., Fricke, T., Diaz-Griffero, F. & Campbell, E. M. HIV-1 Uncoating Is Facilitated by Dynein and Kinesin 1. *J. Virol.* **88**, 13613–13625 (2014).

197. Achuthan, V., Perreira, J. M., Sowd, G. A., Puray-Chavez, M., McDougall, W. M., Paulucci-Holthauzen, A., Wu, X., Fadel, H. J., Poeschla, E. M., Multani, A. S., Hughes, S. H., Sarafianos, S. G., Brass, A. L. & Engelman, A. N. Capsid-CPSF6 Interaction Licenses Nuclear HIV-1 Trafficking to Sites of Viral DNA Integration. *Cell Host Microbe* **24**, 392-404.e8 (2018).

198. Tian, B. & Manley, J. L. Alternative polyadenylation of mRNA precursors. *Nat. Rev. Mol. Cell Biol.* **18**, 18–30 (2017).

199. Hidalgo-Curtis, C., Chase, A., Drachenberg, M., Roberts, M. W., Finkelstein, J. Z., Mould, S., Oscier, D., Cross, N. C. P. & Grand, F. H. The t(1;9) (p34;q34) and t(8;12) (p11;q15) fuse pre-mRNA processing proteins SFPQ (PSF) and CPSF6 to ABL and FGFR1. *Genes, Chromosom. Cancer* **47**, 379–385 (2008).

200. Naumann, N., Schwaab, J., Metzgeroth, G., Jawhar, M., Haferlach, C., Göhring, G., Schlegelberger, B., Dietz, C. T., Schnittger, S., Lotfi, S., Gärtner, M., Dang, T.-A., Hofmann, W.-K., Cross, N. C. P., Reiter, A. & Fabarius, A. Fusion of PDGFRB to MPRIP,

CPSF6 , and GOLGB1 in three patients with eosinophilia-associated myeloproliferative neoplasms. *Genes, Chromosom. Cancer* **54**, 762–770 (2015).

201. Binothman, N., Hachim, I. Y., Lebrun, J.-J. & Ali, S. CPSF6 is a Clinically Relevant Breast Cancer Vulnerability Target. *EBioMedicine* **21**, 65–78 (2017).

202. Liu, T., Wen, L., Yuan, H., Wang, Y., Yao, L., Xu, Y., Cen, J., Ruan, C., Wu, D. & Chen, S. Identification of novel recurrent CPSF6-RARG fusions in acute myeloid leukemia resembling acute promyelocytic leukemia. *Blood* **131**, 1870–1873 (2018).

203. Qin, Y.-Z., Huang, X.-J. & Zhu, H.-H. Identification of a novel CPSF6-RARG fusion transcript in acute myeloid leukemia resembling acute promyelocytic leukemia. *Leukemia* **32**, 2285–2287 (2018).

204. Francis, A. & Melikyan, G. Live-Cell Imaging of Early Steps of Single HIV-1 Infection. *Viruses* **10**, 275 (2018).

205. Burdick, R. C., Hu, W.-S. & Pathak, V. K. Nuclear import of APOBEC3F-labeled HIV-1 preintegration complexes. *Proc. Natl. Acad. Sci.* **110**, E4780–E4789 (2013).

206. Mamede, J. I., Cianci, G. C., Anderson, M. R. & Hope, T. J. Early cytoplasmic uncoating is associated with infectivity of HIV-1. *Proc. Natl. Acad. Sci.* **114**, E7169–E7178 (2017).

207. Dobrucki, J. W. & Kubitscheck, U. Fluorescence Microscopy. in *Fluorescence Microscopy* 85–132 (Wiley-VCH Verlag GmbH & Co. KGaA, 2017).

208. Kulic, I. M., Brown, A. E. X., Kim, H., Kural, C., Blehm, B., Selvin, P. R., Nelson, P. C. & Gelfand, V. I. The role of microtubule movement in bidirectional organelle transport. *Proc. Natl. Acad. Sci.* **105**, 10011–10016 (2008).

209. Tokunaga, M., Imamoto, N. & Sakata-Sogawa, K. Highly inclined thin illumination enables clear single-molecule imaging in cells. *Nat. Methods* **5**, 159–161 (2008).

210. Funatsu, T., Harada, Y., Tokunaga, M., Saito, K. & Yanagida, T. Imaging of single fluorescent molecules and individual ATP turnovers by single myosin molecules in aqueous solution. *Nature* **374**, 555–559 (1995).

211. Tokunaga, M., Kitamura, K., Saito, K., Iwane, A. H. & Yanagida, T. Single Molecule Imaging of Fluorophores and Enzymatic Reactions Achieved by Objective-Type Total Internal Reflection Fluorescence Microscopy. *Biochem. Biophys. Res. Commun.* **235**, 47–53 (1997).

212. Axelrod, D. Cell-substrate contacts illuminated by total internal reflection fluorescence. *J. Cell Biol.* **89**, 141–145 (1981).

213. Fricke, T., Valle-Casuso, J. C., White, T. E., Brandariz-Nuñez, A., Bosche, W. J., Reszka, N., Gorelick, R. & Diaz-Griffero, F. The ability of TNPO3-depleted cells to inhibit HIV-1 infection requires CPSF6. *Retrovirology* **10**, 46 (2013).

214. Rüegsegger, U., Blank, D. & Keller, W. Human pre-mRNA cleavage factor Im Is related to spliceosomal SR proteins and can be reconstituted in vitro from recombinant subunits. *Mol. Cell* **1**, 243–253 (1998).

215. Merzlyak, E. M., Goedhart, J., Shcherbo, D., Bulina, M. E., Shcheglov, A. S., Fradkov, A. F., Gaintzeva, A., Lukyanov, K. A., Lukyanov, S., Gadella, T. W. J. & Chudakov, D. M. Bright monomeric red fluorescent protein with an extended fluorescence lifetime. *Nat. Methods* **4**, 555–557 (2007).

216. Bajar, B. T., Wang, E. S., Lam, A. J., Kim, B. B., Jacobs, C. L., Howe, E. S., Davidson, M. W., Lin, M. Z. & Chu, J. Improving brightness and photostability of green and red fluorescent proteins for live cell imaging and FRET reporting. *Sci. Rep.* **6**, 20889 (2016).

217. Wu, X., Liu, H., Xiao, H., Conway, J. A., Hunter, E. & Kappes, J. C. Functional RT and IN

incorporated into HIV-1 particles independently of the Gag/Pol precursor protein. *EMBO J.* **16**, 5113–5122 (1997).

218. Engelman, A., Englund, G., Orenstein, J. M., Martin, M. A. & Craigie, R. Multiple effects of mutations in human immunodeficiency virus type 1 integrase on viral replication. *J. Virol.* **69**, 2729–2736 (1995).

219. Dharan, A. & Campbell, E. M. Role of Microtubules and Microtubule-Associated Proteins in HIV-1 Infection. *J. Virol.* **92**, e00085-18 (2018).

220. Jang, S., Cook, N. J., Pye, V. E., Bedwell, G. J., Dudek, A. M., Singh, P. K., Cherepanov, P. & Engelman, A. N. Differential role for phosphorylation in alternative polyadenylation function versus nuclear import of SR-like protein CPSF6. *Nucleic Acids Res.* **47**, 4663–4683 (2019).

221. Caras, I. W. Probing the signal for glycophosphatidylinositol anchor attachment using decay accelerating factor as a model system. *Cell Biol. Int. Rep.* **15**, 815–826 (1991).

222. Szent-Gyorgyi, C., Schmidt, B. A., Creeger, Y., Fisher, G. W., Zakel, K. L., Adler, S., Fitzpatrick, J. A. J., Woolford, C. A., Yan, Q., Vasilev, K. V., Berget, P. B., Bruchez, M. P., Jarvik, J. W. & Waggoner, A. Fluorogen-activating single-chain antibodies for imaging cell surface proteins. *Nat. Biotechnol.* **26**, 235–240 (2008).

223. Lee, K., Mulky, A., Yuen, W., Martin, T. D., Meyerson, N. R., Choi, L., Yu, H., Sawyer, S. L. & KewalRamani, V. N. HIV-1 Capsid-Targeting Domain of Cleavage and Polyadenylation Specificity Factor 6. *J. Virol.* **86**, 3851–3860 (2012).

224. Yamashita, M. & Engelman, A. N. Capsid-Dependent Host Factors in HIV-1 Infection. *Trends in Microbiology* vol. **25** 741–755 (2017).

225. Stremlau, M., Perron, M., Lee, M., Li, Y., Song, B., Javanbakht, H., Diaz-Griffero, F.,

Anderson, D. J., Sundquist, W. I. & Sodroski, J. Specific recognition and accelerated uncoating of retroviral capsids by the TRIM5 restriction factor. *Proc. Natl. Acad. Sci.* **103**, 5514–5519 (2006).

226. Zhao, G., Ke, D., Vu, T., Ahn, J., Shah, V. B., Yang, R., Aiken, C., Charlton, L. M., Gronenborn, A. M. & Zhang, P. Rhesus TRIM5α Disrupts the HIV-1 Capsid at the Inter-Hexamer Interfaces. *PLoS Pathog.* **7**, e1002009 (2011).

227. Bejarano, D. A., Peng, K., Laketa, V., Börner, K., Jost, K. L., Lucic, B., Glass, B., Lusic, M., Müller, B. & Kräusslich, H.-G. HIV-1 nuclear import in macrophages is regulated by CPSF6-capsid interactions at the nuclear pore complex. *Elife* **8**, (2019).

228. Chin, C. R., Perreira, J. M., Savidis, G., Portmann, J. M., Aker, A. M., Feeley, E. M., Smith, M. C. & Brass, A. L. Direct Visualization of HIV-1 Replication Intermediates Shows that Capsid and CPSF6 Modulate HIV-1 Intra-nuclear Invasion and Integration. *Cell Rep.* **13**, 1717–1731 (2015).

229. Lee, P. P. & Linial, M. L. Efficient particle formation can occur if the matrix domain of human immunodeficiency virus type 1 Gag is substituted by a myristylation signal. *J. Virol.* **68**, 6644–6654 (1994).

230. Meng, X., Zhao, G., Yufenyuy, E., Ke, D., Ning, J., DeLucia, M., Ahn, J., Gronenborn, A. M., Aiken, C. & Zhang, P. Protease Cleavage Leads to Formation of Mature Trimer Interface in HIV-1 Capsid. *PLoS Pathog.* **8**, e1002886 (2012).

231. Ning, J., Erdemci-Tandogan, G., Yufenyuy, E. L., Wagner, J., Himes, B. A., Zhao, G., Aiken, C., Zandi, R. & Zhang, P. In vitro protease cleavage and computer simulations reveal the HIV-1 capsid maturation pathway. *Nat. Commun.* **7**, 13689 (2016).

232. Cecilia, D., KewalRamani, V. N., O'Leary, J., Volsky, B., Nyambi, P., Burda, S., Xu, S.,

Littman, D. R. & Zolla-Pazner, S. Neutralization Profiles of Primary Human Immunodeficiency Virus Type 1 Isolates in the Context of Coreceptor Usage. *J. Virol.* **72**, 6988–6996 (1998).

233. Perkins, L. A. & Bruchez, M. P. Fluorogen activating protein toolset for protein trafficking measurements. *Traffic* vol. **21** 333–348 (2020).

234. Pornillos, O., Ganser-Pornillos, B. K., Kelly, B. N., Hua, Y., Whitby, F. G., Stout, C. D., Sundquist, W. I., Hill, C. P. & Yeager, M. X-Ray Structures of the Hexameric Building Block of the HIV Capsid. *Cell* (2009) doi:10.1016/j.cell.2009.04.063.

235. Liu, P. T., Schenk, M., Walker, V. P., Dempsey, P. W., Kanchanapoomi, M., Wheelwright, M., Vazirnia, A., Zhang, X., Steinmeyer, A., Zügel, U., Hollis, B. W., Cheng, G. & Modlin, R. L. Convergence of IL-1β and VDR Activation Pathways in Human TLR2/1-Induced Antimicrobial Responses. *PLoS One* **4**, e5810 (2009).

236. Rasaiyaah, J., Tan, C. P., Fletcher, A. J., Price, A. J., Blondeau, C., Hilditch, L., Jacques, D. A., Selwood, D. L., James, L. C., Noursadeghi, M. & Towers, G. J. HIV-1 evades innate immune recognition through specific cofactor recruitment. *Nature* **503**, 402–405 (2013).

237. Li, Y.-L., Chandrasekaran, V., Carter, S. D., Woodward, C. L., Christensen, D. E., Dryden, K. A., Pornillos, O., Yeager, M., Ganser-Pornillos, B. K., Jensen, G. J. & Sundquist, W. I. Primate TRIM5 proteins form hexagonal nets on HIV-1 capsids. *Elife* **5**, (2016).

238. Alvarez, F. J. D., He, S., Perilla, J. R., Jang, S., Schulten, K., Engelman, A. N., Scheres, S. H. W. & Zhang, P. CryoEM structure of MxB reveals a novel oligomerization interface critical for HIV restriction. *Sci. Adv.* **3**, e1701264 (2017).

239. Liu, Z., Pan, Q., Ding, S., Qian, J., Xu, F., Zhou, J., Cen, S., Guo, F. & Liang, C. The Interferon-Inducible MxB Protein Inhibits HIV-1 Infection. *Cell Host Microbe* **14**, 398–410

(2013).

240. Price, A. J., Jacques, D. A., McEwan, W. A., Fletcher, A. J., Essig, S., Chin, J. W., Halambage, U. D., Aiken, C. & James, L. C. Host Cofactors and Pharmacologic Ligands Share an Essential Interface in HIV-1 Capsid That Is Lost upon Disassembly. *PLoS Pathog.* **10**, e1004459 (2014).

241. Dettwiler, S., Aringhieri, C., Cardinale, S., Keller, W. & Barabino, S. M. L. Distinct sequence motifs within the 68-kDa subunit of cleavage factor Im mediate RNA binding, protein-protein interactions, and subcellular localization. *J. Biol. Chem.* **279**, 35788–35797 (2004).

242. Ruepp, M. D., Aringhieri, C., Vivarelli, S., Cardinale, S., Paro, S., Schümperli, D. & Barabino, S. M. L. Mammalian pre-mRNA 3′ end processing factor CF Im68 functions in mRNA export. *Mol. Biol. Cell* **20**, 5211–5223 (2009).

243. Bhattacharya, A., Alam, S. L., Fricke, T., Zadrozny, K., Sedzicki, J., Taylor, A. B., Demeler, B., Pornillos, O., Ganser-Pornillos, B. K., Diaz-Griffero, F., Ivanov, D. N. & Yeager, M. Structural basis of HIV-1 capsid recognition by PF74 and CPSF6. *Proc. Natl. Acad. Sci. U. S. A.* **111**, 18625–18630 (2014).

244. Li, W., Singh, P. K., Sowd, G. A., Bedwell, G. J., Jang, S., Achuthan, V., Oleru, A. V., Wong, D., Fadel, H. J., Lee, K., KewalRamani, V. N., Poeschla, E. M., Herschhorn, A. & Engelman, A. N. CPSF6-Dependent Targeting of Speckle-Associated Domains Distinguishes Primate from Nonprimate Lentiviral Integration. *MBio* **11**, (2020).

245. Ylinen, L. M. J., Schaller, T., Price, A., Fletcher, A. J., Noursadeghi, M., James, L. C. & Towers, G. J. Cyclophilin A Levels Dictate Infection Efficiency of Human Immunodeficiency Virus Type 1 Capsid Escape Mutants A92E and G94D. *J. Virol.* **83**,

2044–2047 (2009).

246. Larocque, L., Bliu, A., Xu, R., Diress, A., Wang, J., Lin, R., He, R., Girard, M. & Li, X. Bioactivity Determination of Native and Variant Forms of Therapeutic Interferons. *J. Biomed. Biotechnol.* **2011**, 1–11 (2011).

247. Malikov, V. & Naghavi, M. H. Localized Phosphorylation of a Kinesin-1 Adaptor by a Capsid-Associated Kinase Regulates HIV-1 Motility and Uncoating. *Cell Rep.* **20**, 2792–2799 (2017).

248. Pawlica, P. & Berthoux, L. Cytoplasmic dynein promotes HIV-1 uncoating. *Viruses* **6**, 4195–4211 (2014).

249. Bukrinsky, M. I., Sharova, N., Dempsey, M. P., Stanwick, T. L., Bukrinskaya, A. G., Haggerty, S. & Stevenson, M. Active nuclear import of human immunodeficiency virus type 1 preintegration complexes. *Proc. Natl. Acad. Sci. U. S. A.* **89**, 6580–6584 (1992).

250. Arhel, N. J., Souquere-Besse, S., Munier, S., Souque, P., Guadagnini, S., Rutherford, S., Prévost, M. C., Allen, T. D. & Charneau, P. HIV-1 DNA Flap formation promotes uncoating of the pre-integration complex at the nuclear pore. *EMBO J.* **26**, 3025–3037 (2007).

251. Burdick, R. C., Delviks-Frankenberry, K. A., Chen, J., Janaka, S. K., Sastri, J., Hu, W.-S. & Pathak, V. K. Dynamics and regulation of nuclear import and nuclear movements of HIV-1 complexes. *PLOS Pathog.* **13**, e1006570 (2017).

252. Rihn, S. J., Wilson, S. J., Loman, N. J., Alim, M., Bakker, S. E., Bhella, D., Gifford, R. J., Rixon, F. J. & Bieniasz, P. D. Extreme Genetic Fragility of the HIV-1 Capsid. *PLoS Pathog.* **9**, e1003461 (2013).

253. von Schwedler, U. K., Stray, K. M., Garrus, J. E. & Sundquist, W. I. Functional Surfaces of the Human Immunodeficiency Virus Type 1 Capsid Protein. *J. Virol.* **77**, 5439–5450

(2003).

254. Gamble, T. R., Vajdos, F. F., Yoo, S., Worthylake, D. K., Houseweart, M., Sundquist, W. I. & Hill, C. P. Crystal structure of human cyclophilin A bound to the amino-terminal domain of HIV-1 capsid. *Cell* **87**, 1285–1294 (1996).

255. Koletsky, A. J., Harding, M. W. & Handschumacher, R. E. Cyclophilin: distribution and variant properties in normal and neoplastic tissues. *J. Immunol.* **137**, 1054–9 (1986).

256. Franke, E. K., Yuan, H. E. H. & Luban, J. Specific incorporation of cyclophilin a into HIV-1 virions. *Nature* **372**, 359–362 (1994).

257. Wiegers, K., Rutter, G., Schubert, U., Grättinger, M. & Kräusslich, H. G. Cyclophilin A incorporation is not required for human immunodeficiency virus type 1 particle maturation and does not destabilize the mature capsid. *Virology* **257**, 261–274 (1999).

258. Sokolskaja, E., Sayah, D. M. & Luban, J. Target Cell Cyclophilin A Modulates Human Immunodeficiency Virus Type 1 Infectivity. *J. Virol.* **78**, 12800–12808 (2004).

259. Braaten, D., Franke, E. K. & Luban, J. Cyclophilin A is required for an early step in the life cycle of human immunodeficiency virus type 1 before the initiation of reverse transcription. *J. Virol.* **70**, 3551–3560 (1996).

260. De Iaco, A. & Luban, J. Cyclophilin A promotes HIV-1 reverse transcription but its effect on transduction correlates best with its effect on nuclear entry of viral cDNA. *Retrovirology* **11**, 11 (2014).

261. Qi, M., Yang, R. & Aiken, C. Cyclophilin A-Dependent Restriction of Human Immunodeficiency Virus Type 1 Capsid Mutants for Infection of Nondividing Cells. *J. Virol.* **82**, 12001–12008 (2008).

262. Yamashita, M. & Emerman, M. Cellular Restriction Targeting Viral Capsids Perturbs

Human Immunodeficiency Virus Type 1 Infection of Nondividing Cells. *J. Virol.* **83**, 9835–9843 (2009).

263. Yant, S. R., Mulato, A., Hansen, D., Tse, W. C., Niedziela-Majka, A., Zhang, J. R., Stepan, G. J., Jin, D., Wong, M. H., Perreira, J. M., Singer, E., Papalia, G. A., Hu, E. Y., Zheng, J., Lu, B., Schroeder, S. D., Chou, K., Ahmadyar, S., Liclican, A., *et al.* A highly potent long-acting small-molecule HIV-1 capsid inhibitor with efficacy in a humanized mouse model. *Nat. Med.* **25**, 1377–1384 (2019).

264. Link, J. O., Rhee, M. S., Tse, W. C., Zheng, J., Somoza, J. R., Rowe, W., Begley, R., Chiu, A., Mulato, A., Hansen, D., Singer, E., Tsai, L. K., Bam, R. A., Chou, C. H., Canales, E., Brizgys, G., Zhang, J. R., Li, J., Graupe, M., *et al.* Clinical targeting of HIV capsid protein with a long-acting small molecule. *Nature* **584**, 614–618 (2020).

265. Ohainle, M., Kim, K., Komurlu Keceli, S., Felton, A., Campbell, E., Luban, J. & Emerman, M. TRIM34 restricts HIV-1 and SIV capsids in a TRIM5α-dependent manner. *PLOS Pathog.* **16**, e1008507 (2020).

266. Wang, R. & Brattain, M. G. The maximal size of protein to diffuse through the nuclear pore is larger than 60 kDa. *FEBS Lett.* **581**, 3164–3170 (2007).